THE UNIVERSITY OF OKLAHOMA

GRADUATE COLLEGE

ELECTROMAGNETIC INTERACTIONS OF 16.2 BeV NEGATIVE PIONS

A DISSERTATION

SUBMITTED TO THE GRADUATE FACULTY

in partial fulfillment of the requirements for the

degree of

DOCTOR OF PHILOSOPHY

BY

ROBERT LEE KINZER

Norman, Oklahoma

1967

ELECTROMAGNETIC INTERACTIONS OF 16.2 BeV NEGATIVE PIONS

A DISSERTATION

APPROVED FOR THE DEPARTMENT OF PHYSICS

APPROVED BY

DISSERTATION COMMITTEE

ACKNOWLEDGMENTS

The author would like to acknowledge his indebtedness and express his appreciation to Dr. James R. Burwell, who suggested this project and supervised it ably and diligently throughout the course of the experiment.

Sincere thanks are also given to Dr. Harald F. K. Zingl, Dr. Rudolf Rodenberg, and Dr. John M. Canfield for many helpful discussions concerning the theoretical problems involved in this work.

Thanks are also given to the Department of Health, Education, and Welfare for the authors support through an N.D.E.A. Title IV fellowship during the first part of this work, and to NASA for the fellowship which supported the latter part of the work.

Finally, the author is grateful to the several scanners who's many hours of diligent labor made this work possible.

TABLE OF CONTENTS

LIST OF TABLES

LIST OF ILLUSTRATIONS

LIST OF ILLUSTRATIONS (CONTINUED)

LIST OF ILLUSTRATIONS (CONTINUED)

CHAPTER I

INTRODUCTION

Since the time of their discovery in 1947, much work has gone into investigating the behavior of pions under strong interactions and weak (decay) interactions. Although the electrodynamic properties of the charged pions have been used in the ordinary ways for detection and for measurement of kinematical properties, very little has been done to investigate purely electromagnetic interactions as a method for studying the electromagnetic properties of these particles and for testing quantum electrodynamics in the extreme relativistic region. In order to test the validity of quantum electrodynamics in such experiments it is first necessary to have theoretical expressions for the cross sections involved which accurately represent the predictions of quantum electrodynamics. Otherwise, the experiments will merely be testing the validity of the approximations involved. Charge structure investigations are also dependent on the existence of accurate theoretical cross sections as predicted by quantum electrodynamics for the processes involved, with the particles considered as points, as well as upon the validity of quantum electrodynamics in the extreme relativistic region.

Types of collision experiments which can be used for such investigation are severely limited by the necessity, using present experimental techniques, of an essentially stable target particle. The short mean life of the pion ($2.55 \cdot 10^{-8}$ sec) prohibits its use as a target and hence forces experiments involving pions directly to be done by using pions as the incident particles. Thus, the ideal method for studying such electromagnetic properties, that of electron scattering from pions, is eliminated. This method has been used in most electromagnetic structure investigations of stable particles such as the nucleon. The most logical remaining method for accomplishing such investigations for the unstable pion is that of pion scattering by atomic electrons.

The cross section for pion-electron elastic scattering was calculated in the first Born approximation by Bhabha[1] and in the lowest order quantum electrodynamically using Feyman techniques by Salecker[2] with identical results. Since the lowest order in this process is only the second order in the electromagnetic field, it is possible to obtain a theoretical cross section which accurately represents the predictions of quantum electrodynamics in this order. At presently available energies a lowest order calculation is expected to give reliable results[2]

Pion-electron scattering has been studied experimentally by Allan et.al.,[3] in a bubble chamber experiment using 16 BeV pions. Agreement was found with the theoretical point particle predictions

at small momentum transfers, but at large momentum transfers the cross section was found to decrease from that predicted for point particles, as it should if the pion is an extended charge. However, small statistics at large momentum transfers prohibited definite conclusions about pion structure.

Electron-position pair production by high-energy pions provides one of the most direct methods for studying electromagnetic properties of pions. Unfortunately this process is fourth order in the electromagnetic field in the lowest order and hence cross section calculations are very complicated. Several attempts (4 thru 14) have been made to calculate this cross section, but all the calculations have employed approximate methods due to the complexity of the calculation. Murota et al. have made the most thorough calculation to date for spin ½ incident particles. Ternovskii has recalculated this cross section in a different manner than that used by Murota et al., considering both spin 0 and spin ½ particles. His is the only presently available calculation which considers spin 0 primary particles. The results of these two calculations give cross sections differing by only a few per cent at the energy of interest in this work. Due to the approximations made in calculation, these theoretical results are of questionable and unknown reliability in the energy regions which are of interest in this experiment. Thus experiments at present are more likely to be testing the calculational approximations rather than the underlying theory. It is of importance to know whether or not the present theoretical cross section

calculations are valid since no serious charge structure or quantum electrodynamics investigations at small distances can be made using this process until reliable calculations exist. The absence of experimental agreement would indicate the need for more accurate calculations.

The pair production process has been investigated experimentally in two separate nuclear emulsion experiments using 16 BeV primary pions[15, 16]. Results obtained are not in disagreement with Ternovskii's theoretical predictions, although small statistics are involved in each case. Definite conclusions about the validity of the theoretical results are not possible from these experiments.

In the present investigation the electromagnetic properties of pions are examined by studying electromagnetic interactions of 16.2 BeV pions in nuclear emulsion. Both elastic scattering of pions on electrons (knock-on electrons) and direct production of electron pairs by interaction of the pions with emulsion nuclei are considered. Comparison is made with available theoretical calculations. With the amount of data available in the present experiment it is not possible to draw definite conclusions about small cross section corrections such as charge structure effects. However, the accuracy is sufficiently good to permit a test of the overall cross section calculations. The theoretical differential cross sections for pion-electron scattering and direct pair production by pions are considered in detail. Approximations and methods of calculation used in the derivation of these cross sections are considered. The reliability of the theoretical results is discussed.

CHAPTER II

HIGH ENERGY PION-ELECTRON ELASTIC SCATTERING

Introduction

Pion-electron elastic scattering provides the most direct method for studying the electromagnetic properties of the pion as well as for testing quantum electrodynamics at small distances. Due to the large mass of the pion (273.26 times the mass of the electron) only a small fraction (≈1/273) of the pion lab energy is effective in the center of mass system. In addition, cross section measurements of pion-electron scattering in emulsion are hampered by difficulty in obtaining high efficiency in event location, especially at low energies (<150 MeV). Such difficulties can be partially overcome by careful scanning efficiency analysis. Higher energy interactions are located with better efficiency, but such interactions have very small cross sections.

Theoretical Calculations

Cross Sections

One of the first derivations of a differential cross section for the process of charged particle scattering on electrons was by Bhabha[1] in 1936. This calculation was carried out with both the

incident particle and electron considered as point particles. The expression which was obtained for the differential cross section for the production, by a high energy, charged, spin 0 particle, of an electron of energy E_e in the energy range corresponding to the interval dT_e between T_e and $T_e + dT_e$ is*

$$d\sigma = \frac{2\pi r_o^2 m_e}{m_\pi(\gamma-1)} \frac{\gamma^2}{\gamma^2-1}\left[1 - \frac{\gamma^2-1}{\gamma^2}\frac{T_e}{T_m} + \frac{\gamma-1}{\gamma^2}\frac{m_e}{m_\pi}\frac{T_e}{E_\pi - m_\pi}\right]\frac{(E_\pi - m_\pi)dT_e}{T_e^2}$$

where

e = charge of electron,
$r_o = e^2/m_e$, the classical electron radius,
E_π = total energy of incident particle,
T_e = kinetic energy of the scattered electron,
$\gamma = E_{\pi_o}/m_\pi$,
m_π = mass of incident particle (pion),
m_e = electron mass,
T_m = maximum kinetic energy which can be transferred to the free electron.

This expression can be integrated to obtain the total cross section for the production of scattered electrons with total energies between E_{min} and E_{max}, the upper and lower limits of the total electron energy region of interest ($T_e \simeq E_e$). The integrated result is

$$\sigma = \frac{2\pi r_o^2 m_e}{m_\pi(\gamma-1)} \frac{\gamma^2}{\gamma^2-1}\left\{(E_\pi - m_\pi)\left(\frac{1}{E_{min}} - \frac{1}{E_{max}}\right) + \left[\frac{\gamma-1}{\gamma^2}\frac{m_e}{m_\pi} - \frac{(\gamma^2-1)(E_\pi - m_\pi)}{\gamma^2 T_m}\right] \times \ln\left(\frac{E_{max}}{E_{min}}\right)\right\}$$

*A unit system is used throughout this work in which $\hbar = c = 1$.

The cross section for this process was later derived by Salecker[2] who, using the Feynman formulation of quantum electrodynamics, obtained results in excellent agreement with Bhabha's calculations. Following Salecker's treatment it is possible to derive the lowest order term for this cross section by considering the Feynman graph

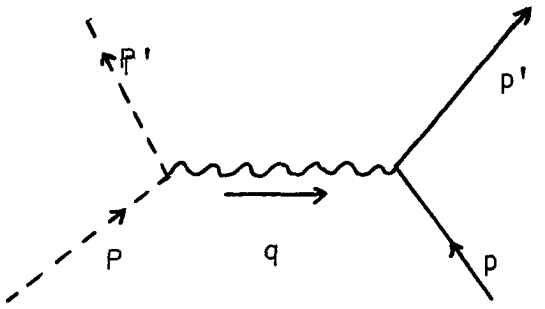

Fig. 1. Feynman diagram for pion-electron elastic scattering.

where

----- = pion line,

~~~ = photon line,

——— = electron line,

P, P' = initial, final four-momentum of the pion,

p, p' = initial, final four-momentum of the electron,

q = four-momentum transferred to the scattered electron,

= P - P' = p' - p.

Using the standard Feynman rules which can be found in texts on quantum field theory [17, 18], the matrix element for this diagram can be constructed. After integrating over q, the four-momentum of the transferred virtual photon, the matrix element becomes

$$\langle f|M|i\rangle = \pm\, ie^2 2\pi \frac{1}{q^2} (P + P')_\mu \bar{v}^{\beta,+}(\vec{p}')\gamma_\mu v^{\alpha,-}(\vec{p}) \ ,$$

where

$v^{\nu,+}(\vec{p})$ = Dirac spinor solution to Dirac equation with $E = \sqrt{|\vec{p}|^2 + m_e^2} > 0$, ν = general spin index = 1, 2 (α, β above),
~~~

$v^{\nu,-}(\vec{p})$ = Dirac spinor solution to Dirac equation with $E = \sqrt{|\vec{p}|^2 + m_e^2} < 0$,

$\bar{v} = v^{\dagger}\gamma_4$ = adjoint spinor, where $\dagger$ represents Hermitean conjugation,

$\gamma_\beta, \beta = 1,2,3,4$ = Dirac matrices (standard)

Thus, since

$$|M|^2 = \langle f|M|i\rangle\langle f|M|i\rangle^{\dagger},$$

then

$$|M|^2 = e^4(2\pi)^2(P + P')_\mu \frac{1}{q^4} \bar{v}^{\beta,+}(\vec{p}')\gamma_\mu v^{\alpha,-}(\vec{p})\bar{v}^{\alpha,+}(\vec{p})\gamma_\omega v^{\beta,-}(\vec{p}')(P + P')_\omega .$$

An average over the initial spins and a sum over the final spins (only the electrons have spins) leads to

$$|M|^2 = \frac{(2\pi)^2 e^4}{2} (P + P')_\mu \frac{1}{q^4} \frac{1}{m_e^2}$$

$$\times \mathrm{Tr}[\gamma_\mu \hat{p}\gamma_\omega \hat{p}' + m_e\gamma_\mu \hat{p}\gamma_\omega + m_e\gamma_\mu \hat{p}'\gamma_\omega + m_e^2\gamma_\mu\gamma_\omega](P + P')_\omega ,$$

where $\hat{p} = \gamma_\mu p^\mu$.

The application of several theorems (17, 18) concerning γ matrices, their products, and traces of products of γ matrices and hat vectors ($\hat{p}$, etc.), yields

$$|M|^2 = 16\pi^2 \frac{1}{q^4} r_o^2[(p'P)(pP) + (p'P)(pP') + (p'P')(pP)$$

$$+ (p'P')(pP') - (p'p)(P'P) - m_\pi^2 (p'p) + m_e^2(PP') + m_\pi^2 m_e^2],$$

where

$$(pP) = -\vec{p}\cdot\vec{P} + p_4P_4 \text{ (4-vector scalar product).}^* .$$

*The metric used is $g_{ii} = (-1, -1, -1, +1)$.

This quantity is related to the differential cross section for the process by

$$d\sigma = \frac{1}{|\vec{v}|}\left(\frac{1}{2E_\pi}\right)\left(\frac{m_e}{E_e}\right)|M|^2\frac{d^3P'}{2E_\pi'}\frac{m_e d^3p'}{E_e'}\delta^4(p + P - p' - P')$$

where

$|\vec{v}|$ = magnitude of relative velocity of incident and target particles,

$E_\pi = (|\vec{p}|^2 + m_\pi^2)^{\frac{1}{2}}$ (initial pion energy),

$E_\pi' = (|\vec{p}'|^2 + m_\pi^2)^{\frac{1}{2}}$ (final pion energy),

E_e' = energy of final electron,

E_e = energy of initial electron,

δ^4 = 4-dimensional delta function.

Using the kinematics of the scattering process, Salecker obtained the cross section

$$d\sigma = \frac{2\pi r_o^2 m_e}{m_\pi(\gamma^2-1)}\frac{\gamma^2}{\gamma^2-1}\left[1 - \frac{(\gamma-1)T_e}{\gamma(E_\pi-m_\pi)} - \frac{m_\pi}{m_e}\frac{\gamma-1}{2\gamma^2}\frac{T_e}{E_\pi+m_\pi}\right](E_\pi-m_\pi)\frac{dT_e}{T_e^2}$$

This is the differential cross section for production of knock-on electrons with a transfer of energy between T_e and $T_e + dT_e$, where

T_e = kinetic energy transferred in the process,

$E_\pi - m_\pi$ = kinetic energy of the incident particle (pion),

$\gamma = E_\pi/m_\pi$,

E_π, m_π = energy, rest mass of colliding particle in the lab frame (pion).

The four-momentum transfer for π - e scattering is

$$q^2 = (P - P')^2 = (p - p')^2 \ ,$$

$$P = (0, m_e) \equiv (\vec{P}, P_4) \text{(notation for 3-vector and fourth components of a 4-vector)} \ ,$$

$$P' = (\vec{p}', E_e) \ ,$$

$$q^2 = (\vec{p}', T_e)^2 \ ,$$

$$q^2 = \angle \vec{p}'^2 + T_e^2 \ ,$$

$$q^2 = - 2 m_e T_e \ .$$

The differential π - e scattering cross section as given by Salecker is plotted in Figure 2.

The integrated or total cross section for elastic pion-electron scattering with scattered electrons having total energies between E_{min} and E_{max} as obtained from Salecker's differential cross section is

$$\sigma = 2\pi \, r_o^2 m_e \left(\frac{\gamma^2}{\gamma^2 - 1}\right)\left[\frac{1}{E_{min}} - \frac{1}{E_{max}} + \left(\frac{1}{\gamma m_\pi} + \frac{1}{2\gamma^2 m_e}\right) \ln\left(\frac{E_{min}}{E_{max}}\right)\right].$$

A histogram for the integrated cross section is given in Figures 3 and 4.

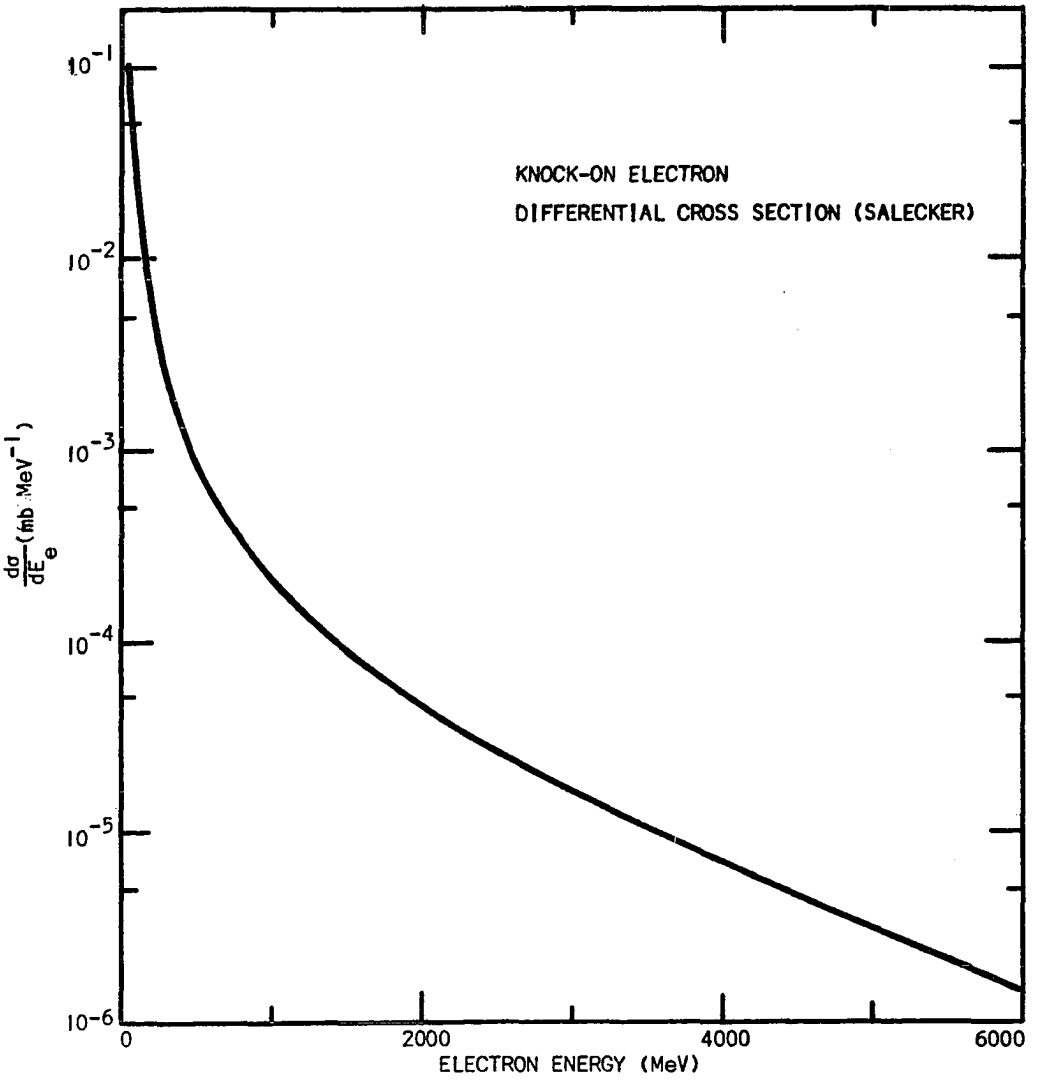

Fig. 2. Differential pion-electron elastic scattering cross section vs. electron energy.

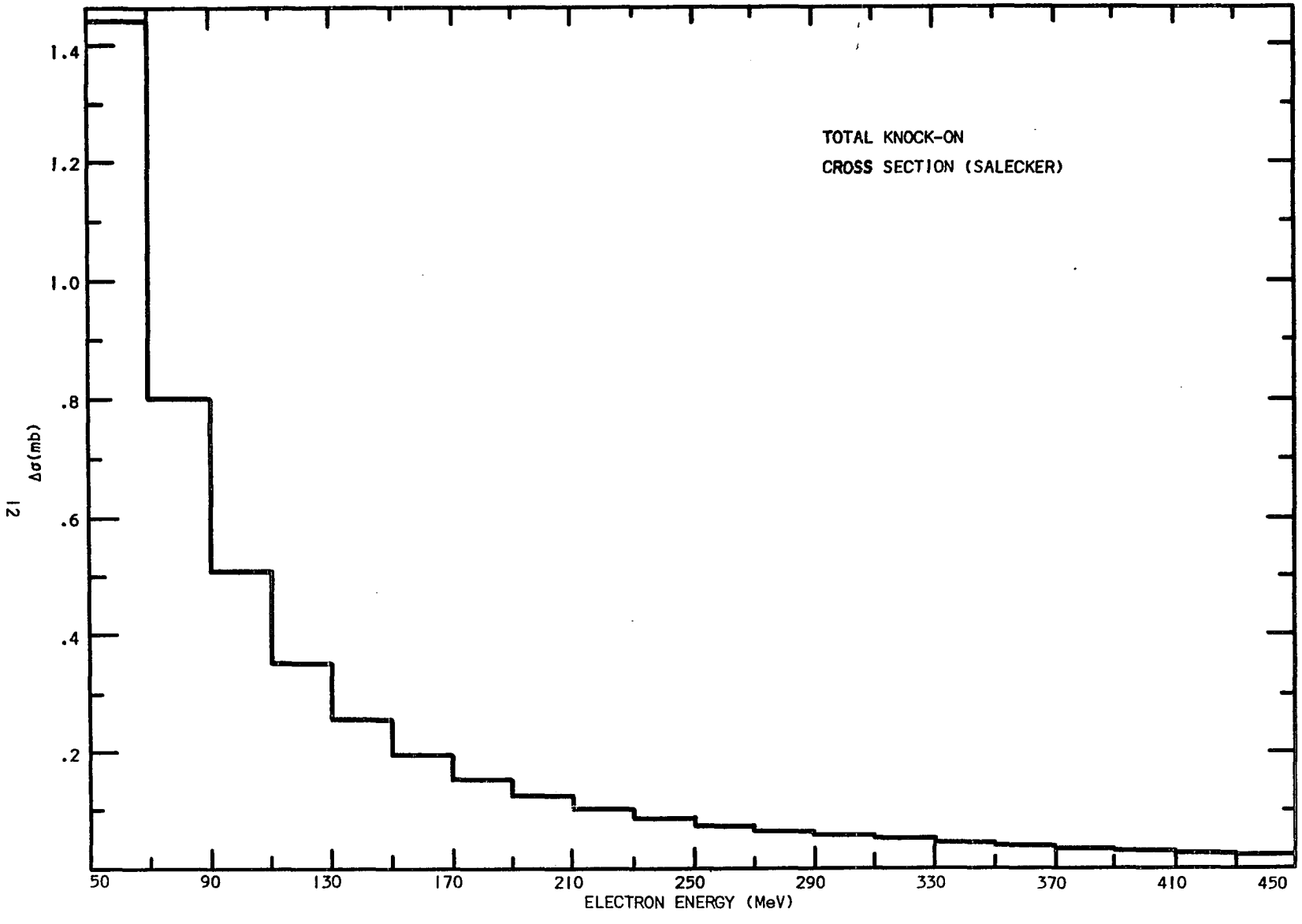

Fig. 3. Distribution of total pion-electron scattering cross section per 20 MeV electron energy interval.

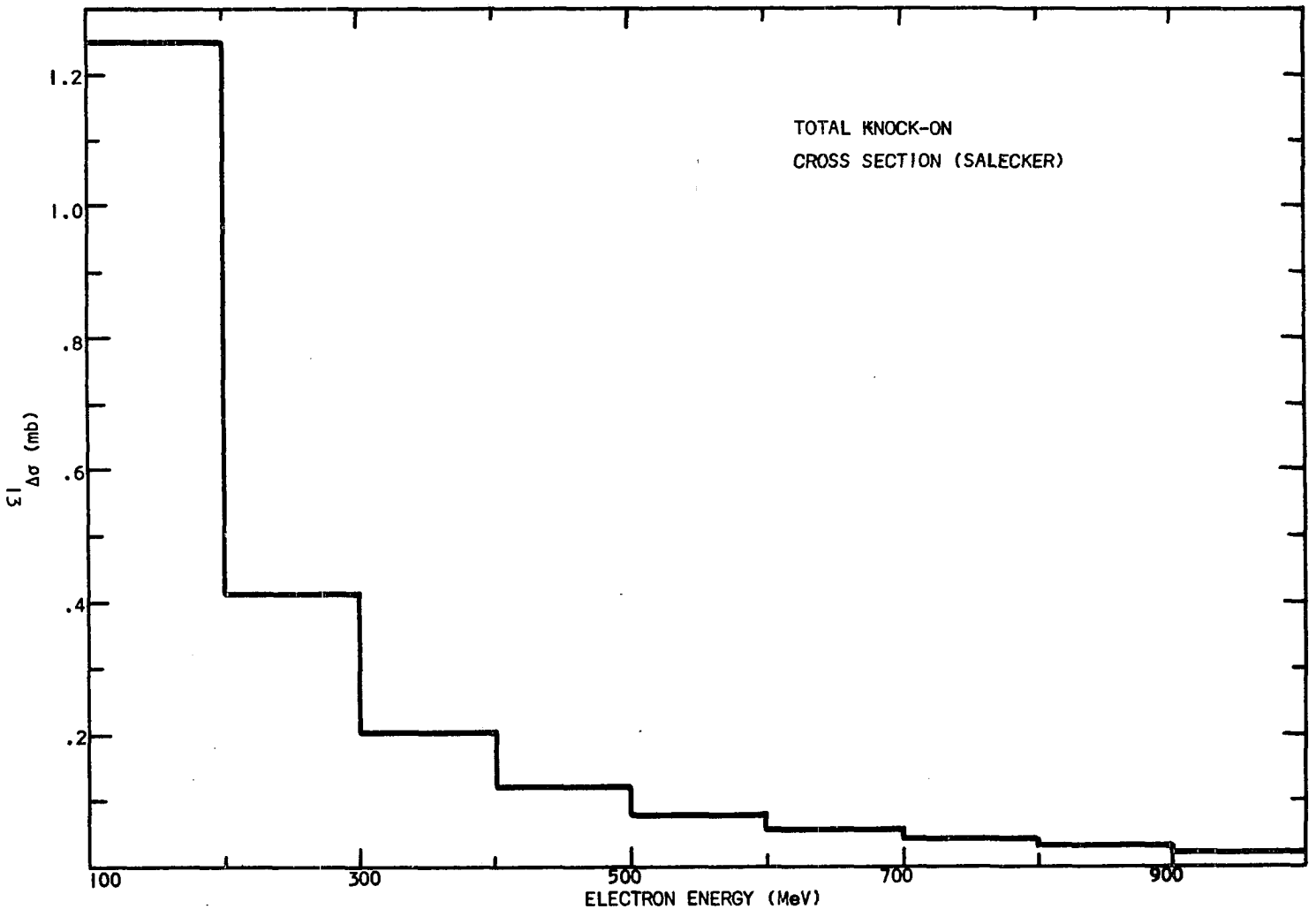

Fig. 4 . Total pion-electron scattering cross section distribution per 100 MeV electron energy interval.

General Experimental Procedure

Introduction

The experimental data for this investigation was obtained from a stack of fifty-five pellicles of Ilford K-5 nuclear emulsion, these pellicles being one-third of the $\mathcal{R}$ stack from the University of California at Berkeley. Each pellicle is 15 cm. long, 7.5 cm. wide, and had a thickness before processing of about 600 microns. The 16.2 BeV CERN pion beam is incident in the 15 cm. direction.

Before development of the stack a grid of 1 mm. squares with pairs of coordinate numbers was optically exposed on the bottom of each pellicle. Since this grid is in almost exactly the same position on every pellicle, it is possible to follow even minimum ionizing tracks from one pellicle to the next. Only the bottom layer of emulsion grains were blackened by the grid exposure, creating a minimum amount of obscuration of tracks by the grid.

This emulsion stack has a relatively small background due to random ionization. It exhibits very little distortion and few flaws.

The particle beam content is $\geq$90% negative pions, most of the remaining 10% being muons. For the interactions of thterest in this work, the behavior of the muon is not greatly different from that of the pion. Spin considerations produce only small differences.

Most of the difference occurs due to the mass difference, which is fractionally small in this case. Thus, the effect of this beam contamination should be small for our considerations.

Equipment

General purpose measurements and scattering measurements were done mostly on two microscopes which are a combination of commercial Leitz Wetzlar optics and a traveling stage built in the physics department machine shop at the University of Oklahoma. The optics include Ortholux binocular microscope heads. The stage on which the optics are mounted has two-dimensional motion in a plane perpendicular to the optic axis with travel of 18½ cm. in one direction and 14 cm. in a perpendicular direction. The emulsion plate holder is designed to allow rotation of the emulsion under the microscope. This feature simplifies and improves many measurements since any track can be aligned with either direction of travel of the stage.

The stages of these microscopes were carefully constructed to eliminate stage noise, i.e., to insure that motion in one direction is as nearly linear as possible. One microscope has sufficiently low stage noise to allow measurement of particle momenta in the BeV range by the multiple Coulomb scattering method. The low noise level was obtained by changing an ordinary dovetail way system to one in which sliding contact between ways was maintained on only one side, the contract being maintained by two spring-loaded teflon plugs sliding on the way on the other side. These ways were machined and lapped

with extreme precision. It was also found necessary to mount the drive screw in a manner such that it could impart no lateral motion to the stage.

Although the 1 mm. pitch screw drive is calibrated in microns, these microscopes are also equipped with precision micrometer dials (Ames gauges) to allow more accurate measurement of distances along the two directions of stage motion. The micrometers are calibrated in microns.

Vertical displacements are measured with the micrometer on the fine focus of the microscope (also calibrated in microns).

A commercial Leitz Wetzlar Ortholux binocular microscope with travelling stage is also available. Since this stage is inferior to those on the microscopes described above, this microscope was not used for general measurements. However, this microscope has excellent rigidity, which is desired in making fixed position measurements. Since the fine focus mechanism and vertical stage motion of this microscope are superior to those on the other microscopes, this microscope was used for all critical measurements in the vertical direction. Heat absorbing glass was placed between the emulsion and the light source when making such measurements to reduce thermal expansion of the emulsion.

A Spencer binocular microscope mounted on an ordinary dovetail stage is used for scanning. An electric motor drive has been attached to this microscope stage to allow uniform motion in one direction. This drive consists of a variable speed gear system with

a rubber belt drive attached to a 9.5 r.p.m. synchronous motor which developes a torque of 40 in. oz. This is a reversible system, with foot and hand controls, whose speed can be varied from one to ten r.p.m. (giving scanning speeds from 1 mm. to 1 cm. per minute).

All of the microscopes were mounted on a 30 ft. by 3 ft. by 3 in. concrete table supported by padded concrete blocks on a concrete floor on the basement of the physics building. This installation provides good stability against vibrations.

The room in which the emulsion work is done is kept at approximately 72°F. and 60% relative humidity, this condition being maintained by the use of an integrated cooling-heating-humidifying-dehumidifying system. These conditions were maintained to keep the emulsion at the same thickness and to keep the microscopes at constant temperature.

All measurements were done with blue filtered light. This gives the double advantage of visual comfort and a short wavelength of light for better resolution of small objects.

Leitz Wetzlar eyepieces and objectives were used with the microscopes for all critical measurements. Eyepieces used were Leitz periplan GF 10X, 16X, and 25X. Objectives used were Leitz 10X, numerical aperture 0.25, for general location work; Leitz 53X oil immersion, numerical aperature 0.95, 1000 micron working distance; Koristka 55X oil immersion, numerical aperture 0.90, working distance 3500 microns; Leitz 100X oil immersion fluorite apochromat, numerical aperture 1.32, 370 microns working distance; Leitz

plano 100X oil immersion apochromat, numerical aperture 1.32, 370 micron working distance; Koristka 100X oil immersion, numerical aperture 1.25, 530 micron working distance. Various other eyepieces and objectives were available but were used infrequently.

The 100X Leitz plano and fluorite objectives have an almost undetectable curvature of field while the similar Koristka 100X objective has a quite pronounced curvature of field. Thus, most critical measurements were made using the Leitz objectives in combination with the 10X eyepieces. With the inherent body-tube magnification of 1.25X, this gives a total magnification of 1250X, which is about the maximum usable magnification for optical microscopes. For less critical measurements, the 53X Leitz objective was used with 10X eyepieces. Most of the scanning work was done with Compens 15X eyepieces in combination with a 55X Koristka objective.

A Leitz Wetzlar screw-type eyepiece micrometer was used for measuring small distances with extreme accuracy. The measuring portion of the micrometer consists of a cross hair capable of motion along a scale with twelve divisions. This cross hair motion is controlled by a hand-operated drum, each complete turn of which moves the cross hair through one division on the scale. Inherent setting accuracy of the micrometer cross hair is $\pm$ 0.1 drum division, or $\pm$ 0.001 scale division. For measuring less critical distances in a fixed field of view, a calibrated eyepiece reticle was used.

An eyepiece goniometer, manufactured in the physics shop, was used for measuring angles. This instrument consists of a rotating

portion graduated in degrees and a fixed vernier which allows measurement to the nearest minute of arc. The rotating portion replaces the regular eyepiece tube on the microscope, allowing the eyepiece and cross hair to be rotated.

Scanning Procedure

In order to make cross section measurements on interactions in nuclear emulsion it is necessary to systematically locate the desired interactions. Since most analyses are statistical and hence dependent on large numbers of interactions of the same type, it is necessary to use a scanning method which insures that large numbers of events can be located in a manner to allow determination of the mean free path. In this experiment this was done by careful and systematic scanning along the tracks of many beam pions. The position in the emulsion of each beam track used in the analysis was carefully recorded in order to prevent duplicate scanning and to enable track relocation at any future time. These tracks were then followed until the particle either interacted or left the emulsion. Most of the tracks which did not interact traversed the entire length of the emulsion. The position and nature of each interaction was carefully recorded.

The scanning was done specifically to locate electromagnetic interactions. Since these interactions are usually of low energy relative to the energy of the incident particle, they are seldom accompanied by a noticeable direction change of the primary particle. This makes such interactions difficult to locate since their location is

entirely dependent upon seeing the minimum ionizing secondary tracks without the aid of a pion direction change. Due to the fact that most secondary tracks dip, i.e., they are not perpendicular to the line of sight, they will leave the focal plane shortly after the interaction point, and some of the events will escape detection. Scanning was therefore done at a slow rate in order to locate the maximum possible number of these events. The original scanning rate of about 14 cm. per hour was later increased to 22 cm. per hour.

A relatively low magnification of 825X was used for scanning (the inherent tube magnification of the Spencer scanning microscope is unity). This magnification is accompanied by a greater depth of field than the higher powers used for measuring, and hence provides an improved probability of finding electromagnetic interactions. Higher powers were tried with undesirable results, both in scanning efficiency and ease of scanning.

The average pion beam divergence in this stack is ± 5 minutes of arc at a given point of entrance of the beam into the emulsion. A divergence of approximately ± 8 minutes exists in the beam over the entire emulsion at the entrance point. Only tracks within this magnitude of divergence from the average beam direction were scanned. This method of beam track selection insures that, with a large probability, the tracks scanned are beam tracks.

Classical Scattering

Radiative corrections to the pion electron scattering process are negligible relative to experimental error[19] at our momentum

transfers. Pion-electron scattering can be treated as purely elastic scattering, within present experimental errors. All secondary particles in this process are charged and hence visible in emulsion, allowing the use of conservation of energy and momentum with measurable tracks only. The energy of an electron scattered elastically by a pion of known energy is completely determined by the angle the electron direction makes with the incident pion direction. This provides a very convenient and accurate method for measuring the energies of scattered electrons. Energies can be determined much more accurately by this method then by the only alternative method, that of multiple Coulomb scattering on the electron tracks. The relation between electron energy, E_e, and angle, ω, can be derived using conservation of energy and momentum (this is a planar process since it is a two body interaction).

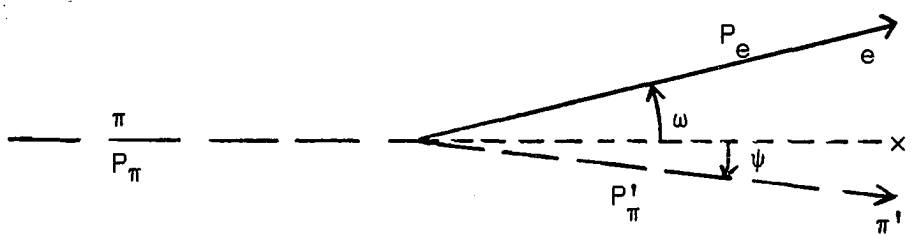

Figure 5

Using the energy-momentum conservation equations to eliminate ψ and P_π, the relation obtained is

$$E_e = \frac{m_e(E_\pi + m_e)^2 + m_e P_\pi^2 \cos^2\omega}{(E_\pi + m_e)^2 - P_\pi^2 \cos^2\omega}$$

where

P_π, E_π = incident pion momentum, energy,

P'_π, E'_π = scattered pion momentum, energy,

P_e, E_e = scattered electron momentum, energy,

m_e = electron mass,

$E = (p^2 + m^2)^{1/2}$

ω, ψ = angle of direction of final electron, pion relative to direction of the incident pion.

The graph of E_e versus ω is given in Figure 6. The maximum energy which can be transferred by a 16.2 BeV pion is seen to occur at $\omega = 0°$, and is equal to 7.4 BeV.

Using this equation for E_e it is possible to obtain the square of the four-momentum transfer to the electron as a function of ω using

$$q^2 = -2m_e(E_e - m_e) \quad .$$

This result is illustrated in Figure 7.

By eliminating ω and P'_π from the energy-momentum conservation equation, it is possible to determine ψ in terms of E_e as

$$\cos\psi = \frac{(m_e + E_\pi)^2 - m_\pi^2 + m_e^2 + E_e^2 - 2(m_e + E_\pi)E_e + P_\pi^2 - E_e^2}{2P_\pi\left[(m_e + E_\pi)^2 - 2(m_e + E_\pi)E_e - m_\pi^2 + E_e^2\right]^{1/2}} \quad .$$

The secondary pion angle is plotted versus the electron energy and the final pion energy in Figures 8 and 9. The maximum deflection of the pion occurs at $E_e = 4.8$ BeV and is 12.5 minutes.

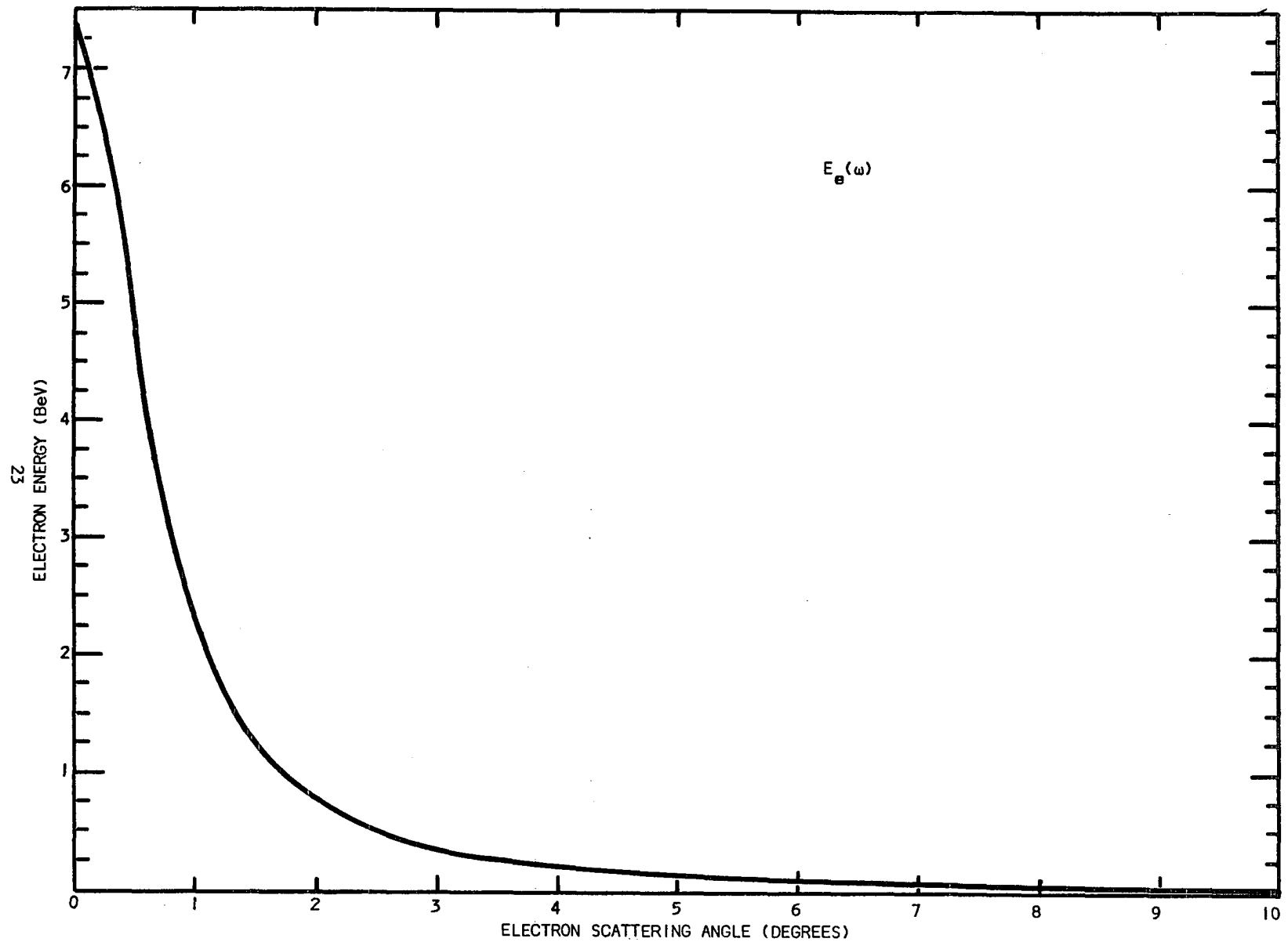

Fig. 6. Electron energy vs. electron scattering angle.

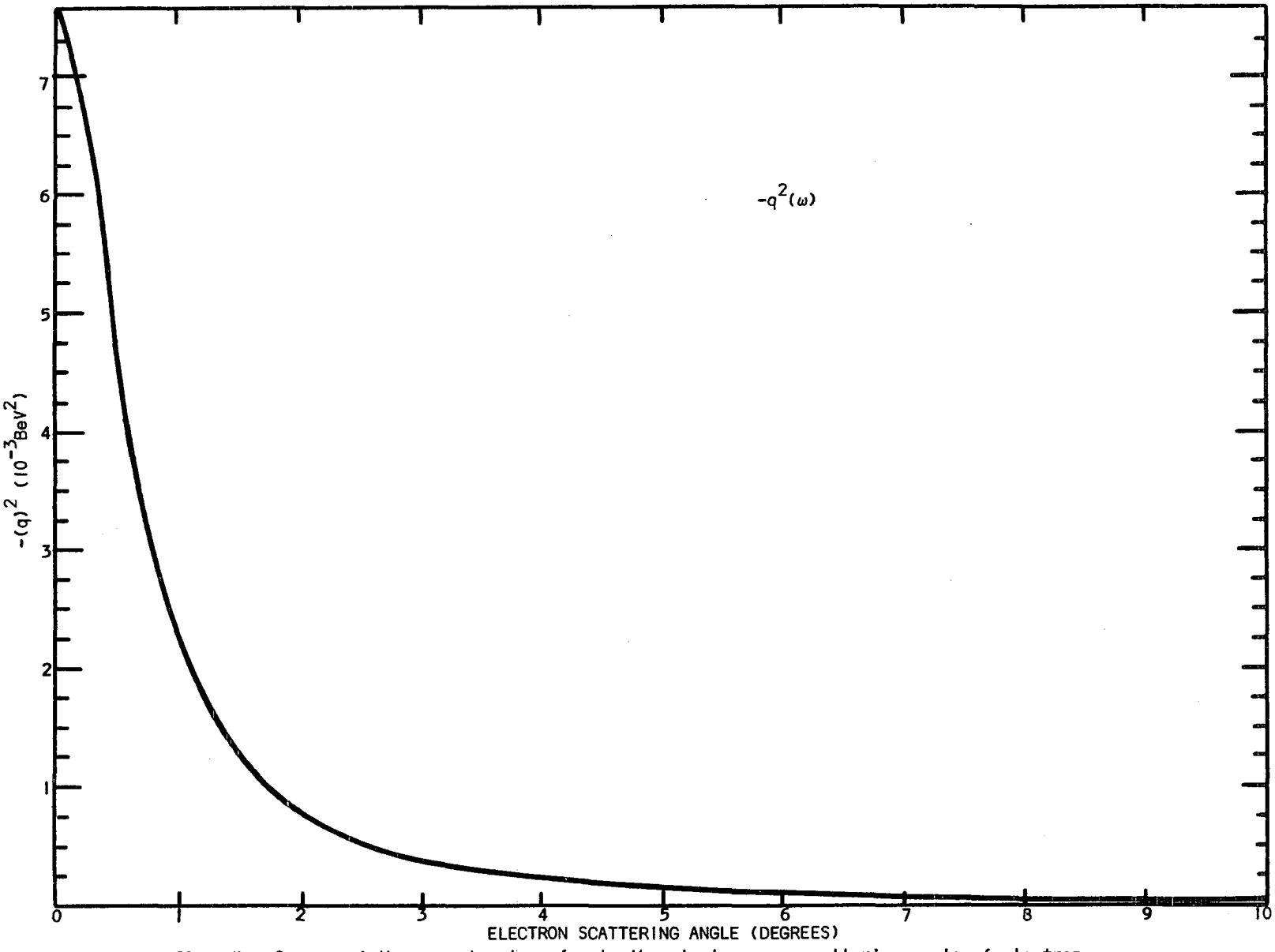

Fig. 7. Square of the momentum transfer to the electron vs. scattering angle of electron, ω.

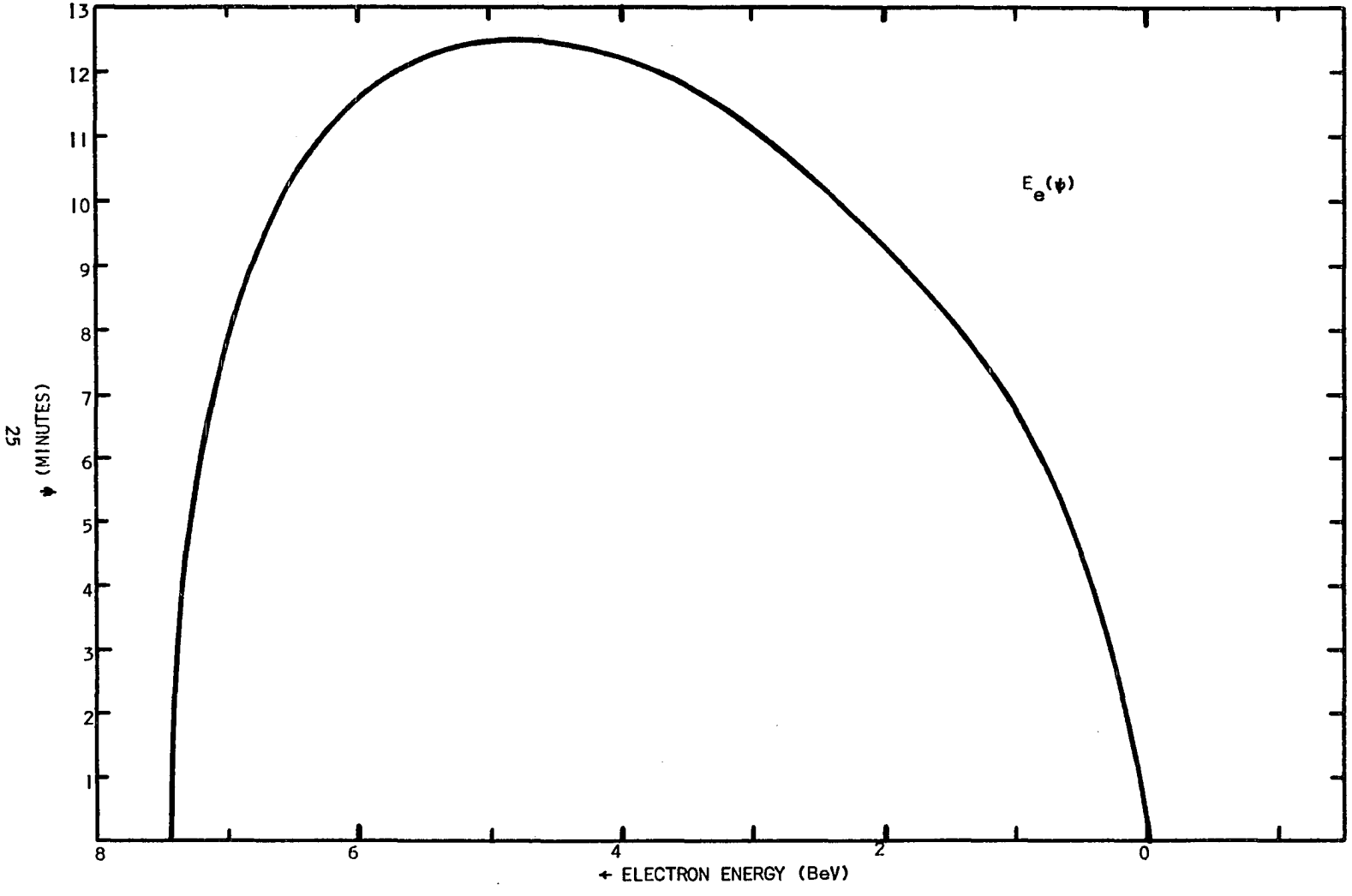

Fig. 8. Pion scattering angle vs. electron energy.

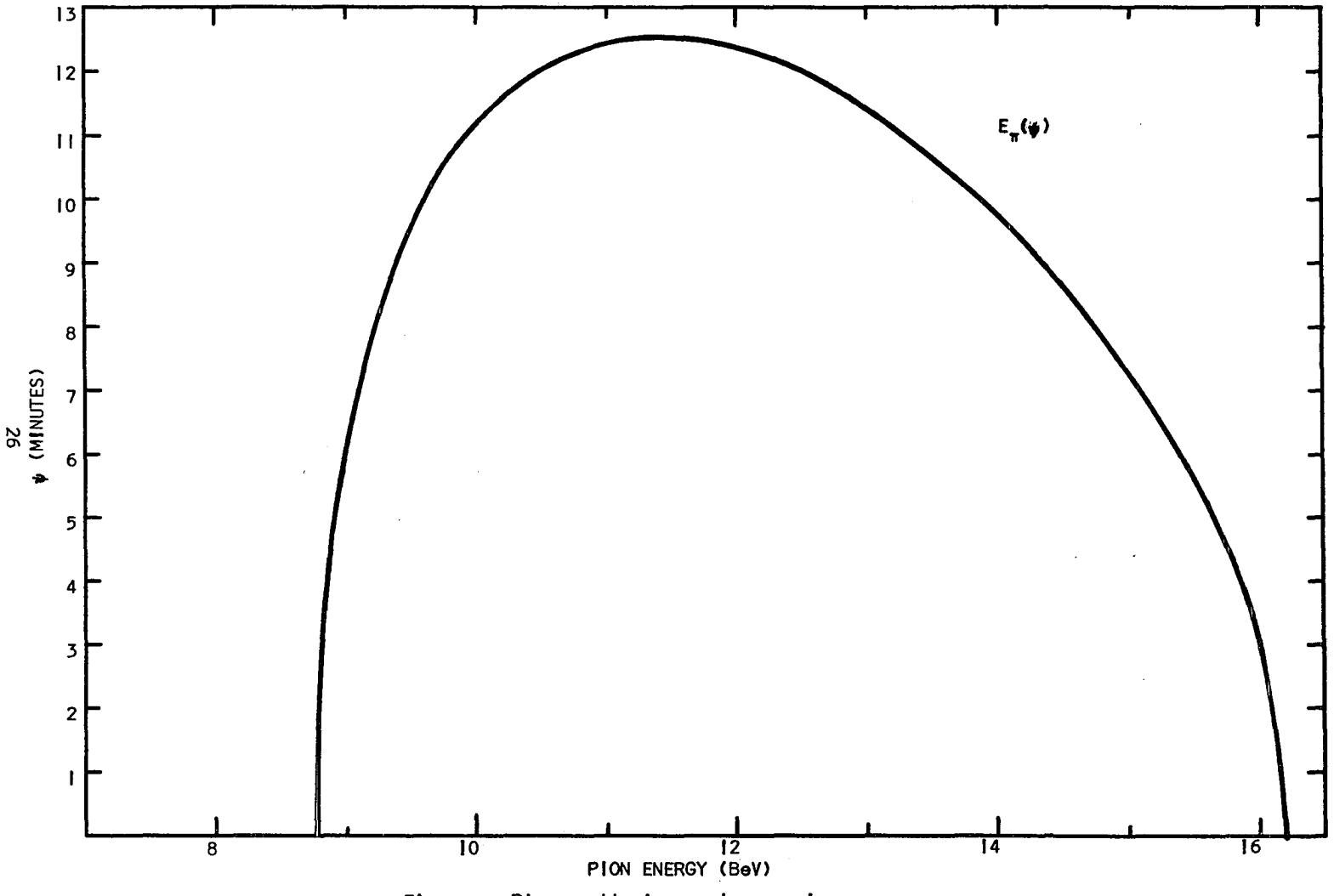

Fig. 9 . Pion scattering angle vs. pion energy.

Knock-on Electron Experimental Procedure

Event Location and Identification

Among the interactions located, while scanning 902.7 m. of pion beam track, 155 high energy ($\geq$50 MeV) elastic pion-electron scattering interactions (knock-on electrons) were found. These interactions have two minimum ionizing secondary tracks. Knock-on electrons are characterized by very slight primary pion deviations, with a maximum deflection of 12.5 minutes of arc occuring at a scattered electron energy of 4.8 BeV (Figure 8). Strong interactions with two minimum ionizing secondary tracks having the direction of one of the secondaries within 12.5' of the primary direction can be eliminated by comparing the energy measured for the secondary tracks with that predicted from energy-momentum conservation for elastic scattering. No such interactions were found. This is anticipated since only 5 strong interactions with two minimum secondary tracks were found in 514 m. of track, none of which had a pion deflection less than 1.3°. Due to the very small mass of electrons(.511 MeV), even the lowest energy electrons considered in this work are extremely relativistic and thus produce minimum (plateau)* ionizing tracks in emulsion. Electron tracks are distinguishable from those of other particles due to the very large fractional energy losses of electrons by radiation as compared to negligible radiation losses by heavier particles[20]. Electrons of any energy lose on the average >90% of

*In this work no distinction is made between minimum and plateau ionization.

their energy in one radiation length (3 cm. in emulsion), while the fractional energy losses in this distance for minimum ionizing heavier particles is very small. The electron and positron are the only charged particles which, when extremely relativistic, have a large probability of losing a significant fraction of their energy at one time while passing through matter and hence of changing direction noticeably. In fact, this characteristic energy loss and visible scattering for reasonably low energy (<600 MeV) electrons is so predictable that, after examining several electrons of known energy, it is possible for one to distinguish electron tracks from those of other particles in this energy region. This fact, and the knowledge (Figure 6) of the energy of a knock-on electron for a given angle of emission with respect to the primary pion direction, coupled with the requirement of essentially no pion direction change, enables an accurate selection of knock-on electron events. High energy (>600 MeV) knock-on electrons are easily recognized due to the very small electron angle (<2.25°). The only significant possibilities for confusion exist in the form of crossover tracks, or disconnected tracks which cross the pion by chance, which can usually be distinguished from knock-on electrons even if the crossed branch is not detectable, and high energy electron pairs created by the pion with one track escaping detection. For such electron pairs, four of which were found, the angle of the visible electron is such that the possibility of the event being a knock-on electron can be eliminated by measuring the energy of the electron by multiple Coulomb scattering

and comparing the result with that expected for a knock-on electrons with that angle.

Since low energy knock-on electrons are difficult to locate with an acceptable scanning efficiency, it was necessary to arbitrarily employ a lower cutoff of 50 MeV, corresponding to an electron angle of 8°. Lower cutoffs of 100 and 200 MeV are also discussed.

Three examples of the knock-on process are illustrated in the photomicrographs in Figure 10, which were taken with a Leica 35 mm. camera. Event 1419 has an electron angle of 6.01° and hence an energy of 91.5 MeV, event 1098 has an electron angle of 2.77° and an electron energy of 413 MeV, and event 1745 has an angle of 7.50° and an energy of 58.9 MeV.

Measurements

It was necessary to accurately measure the angle of each knock-on electron, thus indirectly measuring its energy. This is a more accurate method for measuring the energy than that of multiple Coulomb scattering, which is a method of determining particle momentum by measuring the deviations of the particle as it passes through the Coulomb fields in matter. The scattering method has an inherent measurement error which is coupled with an error introduced by the energy loss of the electron as it passes through matter. Since electrons, especially low energy ones, tend to change their direction of travel due to scattering, it is necessary to measure the angle using the blobs nearest the interaction. In order to measure the space angle, ω, it is necessary to measure the projected angle,

Event 1419

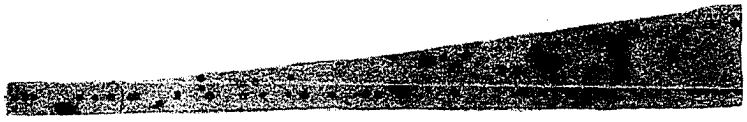

Event 1098

Event 1745

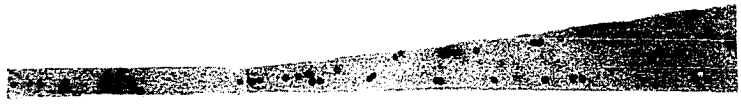

Fig. 10. Knock-on electron photomicrographs.

θ, in the x-y plane and the dip angle, ϕ (Figure 11, page 41).

The measurement of the projected angle θ is done most accurately by measuring the (x,y) coordinates of the first ten to fourteen blobs on each track (pion and electron) with the screw micrometer eyepiece. This measurement is performed by first positioning the event relative to the fixed micrometer eyepiece such that the pion makes an angle of about 45° with the axis of measurement of the micrometer, then measuring the x coordinates of the first few (ten to fourteen) blobs after the interaction on both the pion and the electron tracks. The micrometer eyepiece was then rotated through exactly 90° using a specially designed eyepiece holder, with the position of the eyepiece being locked at each extremity of the rotation. The measurement was then repeated for the same blobs, obtaining the y coordinates of the blobs. The method of least squares was applied to the x-y coordinate measurements to obtain the angle of each track with the x-y axes of the micrometer eyepiece. This gives, for the $i^{\underline{th}}$ track,

$$\tan \theta_i = \frac{(\overline{xy})_i - \overline{x}_i \overline{y}_i}{(\overline{x^2})_i - (\overline{x}_i)^2}$$

where the bar represents an average for the N measurements on a track. Since the micrometer eyepiece was fixed in space for the simultaneous measurement of the two track angles, the angle θ between the two tracks is

$$\theta = |\theta_\pi - \theta_e| \quad .$$

The error associated with the measurement of the angle for each track can be calculated by partial differentiation to be

$$\Delta\theta_i = \frac{\varepsilon\cos^2\theta_i}{\sqrt{N_i}} \frac{\{[(\overline{y^2})_i - (\overline{y})_i^2] + [(\overline{x^2})_i - (\overline{x})_i^2]\}}{[(\overline{x^2})_i - (\overline{x})_i^2]},$$

where ε = 0.03 microns (error associated with each measurement of blob position with the micrometer eyepiece at 100X12.5X1.25), and N_i = number of measurements. Thus, the total error associated with the projected angle measurement is

$$\Delta\theta = [(\Delta\theta_e)^2 + (\Delta\theta_\pi)^2]^{\frac{1}{2}}$$

This measurement is subject to small errors. Most of the measurements were repeated two or more times in order to insure reliability. For any given track in emulsion the developed blobs along the track are distributed randomly around the direction of the track. It is possible that a blob might be included which actually isn't on the track, or that the track might change direction at some point included in the measurement. These sources of error were reduced to a minimum by graphing the measured points on an expanded scale in order to see the relative blob positions. This approach also helps eliminate data recording errors. This plotting was done with an IBM 1620 computer and a "Cal Comp 563" 29 inch plotter.

The dip angle measurement is less accurate than the projected angle measurement since this measurement requires the measurement of vertical distances. Thus the measurement is necessarily

limited in accuracy to that of the fine focus micrometer, coupled with the ability to focus on a particular group of blobs, which is in turn limited by the depth of focus. This measurement was performed by measuring the difference in depth of focus of the secondary pion and the electron track at a distance of, on the average, about 250 microns from the interaction point. This value, as well as its error, was multiplied by S = 2.4, the average shrinkage factor for the emulsion. In order to decrease the error, the measurements were repeated several times and averaged, the error being given as the probable error in the measurements. Thus, ϕ and the error in ϕ are given by

$$\phi = \tan^{-1}\left[\frac{S\cdot\bar{z}}{x}\right] ,$$

$$\Delta\phi = \cos^2\phi\left[\left(\frac{S}{x}\right)^2(\Delta\bar{z})^2 + \left(\frac{S\cdot\bar{x}}{x^2}\right)^2(\Delta x)^2\right]^{\frac{1}{2}} ,$$

where

$\bar{z}$ = average difference in depth of pion and electron at the point of measurement,

x = distance from the point of interaction to the point of measurement,

$\Delta\bar{z} = 0.6745\ (\overline{z^2} - \bar{z}^2)^{\frac{1}{2}}$,

Δx = 1 micron.

The total angle, ω, between the two tracks is related to θ and ϕ, as can be seen by projecting a unit vector in the $\vec{R}$ direction on the y axis (Figure 11, page 41), by

$$\omega = \cos^{-1}(\cos\theta\cos\phi)$$

with a total error

$$\Delta\omega = \csc\omega\left[\cos^2\theta\sin^2\phi(\Delta\phi)^2 + \cos^2\phi\sin^2\theta(\Delta\theta)^2\right]^{\frac{1}{2}} .$$

However, this is not the true scattering angle of the electron, but the total angle between the final directions of the pion and the electron. The deflection of the pion must be subtracted from this in order to obtain the true scattering angle of the electron beacuse the pion always scatters away from the electron (the three tracks are coplanar), resulting in every case in a larger measured angle than the true electron scattering angle. Only at very high electron energies, or very small scattering angles, is this correction significant. It was necessary to calculate the pion deflection correction in an iterative manner. This process was perfromed by first calculating the pion angle by assuming the measured angle of the electron to be correct, correcting the measured electron angle with the result, then repeating the whole process to obtain a twice corrected electron angle and a twice corrected electron energy. That is, the answer was accepted as correct after two iterations. This is an excellent approximation since the error is slight in the beginning.

Data

The equation relating electron energy to angle is given above. Using this result, the error associated with E_e due to an error in the measurement of ω and to the error in the knowledge of the incident pion momentum can be obtained by partial differentiation to be

$$\Delta E_e = \frac{4m_e(E_{\pi_o} + m_e)P_{\pi_o}\cos\omega}{[(E_{\pi_o} + m_e)^2 - P_{\pi_o}^2\cos^2\omega]^2}$$

$$\times \{[(E_{\pi_o} - P_{\pi_o} + m_e)\cos\omega]^2 (\Delta P_{\pi_o})^2 + [P_{\pi_o}(E_\pi + m_e)\sin\omega]^2(\Delta\omega)^2\}^{\frac{1}{2}},$$

where

$$\Delta P_{\pi_o} = 0.64 \text{ BeV}.$$

Using the values of ω and $\Delta\omega$ obtained in the above manner, the energies and errors in energy for all the knock-on electrons considered were calculated. The values measured for the electron energy, errors in energy, space angle ω, projected angle, dip angle, and the square of the four momentum transfer for each knock-on electron considered is listed in Table I. Only interactions with electron energy greater than 50 MeV are included.

Scanning Efficiency

Since there is less than a unit probability of finding all knock-on electrons in scanning, no matter how careful the scanning process, the scanning efficiency must be investigated. One way of doing this is to investigate the distribution of the plane angle, ρ, (defined in Figure 11, p. 41) which is the angle between the plane formed by the electron and the pion trajectories and the x-y plane (plane of the emulsion).

Table 1. Knock-on Electron Data

Event	E_e(MeV)	ΔE_e	$-q^2$(MeV)^2	ω(°)	θ(°)	ϕ(°)
113	50.5	4.3	51.1	8.11	2.31	7.80
1608	51.1	1.5	51.7	8.06	7.14	3.80
915	51.1	2.3	51.7	8.06	5.71	5.74
1580	53.1	1.2	53.7	7.91	7.58	2.36
1660	53.4	1.8	54.0	7.89	7.63	2.10
2443	53.5	2.0	54.2	7.88	4.74	6.33
305	53.9	0.9	54.6	7.85	7.87	0.0
2495	55.6	1.64	56.3	7.73	5.82	5.13
688	56.4	0.8	57.2	7.67	7.63	1.04
2466	57.6	1.6	58.3	7.59	5.93	4.80
369	57.9	1.7	58.6	7.57	7.07	2.80
2524	58.5	1.3	59.3	7.53	6.91	3.08
1745	58.9	.8	59.7	7.50	7.53	0.0
2413	59.8	1.4	60.1	7.45	7.48	0.0
673	62.3	1.0	63.1	7.30	7.13	1.68
2964	63.0	1.8	63.9	7.25	6.26	3.72
1553	63.8	4.0	64.7	7.21	4.61	5.59
631	65.9	2.6	66.9	7.09	6.35	3.22
2729	66.1	1.4	67.0	7.08	6.54	2.80
1913	67.7	1.21	68.63	7.00	7.03	.16
1050	68.4	2.2	69.3	6.96	6.31	3.00
1652	69.1	1.0	70.1	6.93	6.95	0.0
*1009	72.9	1.5	73.9	6.74	6.65	1.28
6	73.3	6.0	74.4	6.72	1.87	6.49
701	73.9	4.8	75.0	6.70	3.86	5.51
1701	74.9	2.8	76.1	6.65	5.59	3.66
3292	75.0	1.40	76.2	6.64	6.60	.99
1753	76.64	1.62	77.8	6.57	6.21	2.25
878	77.8	4.5	79.0	6.52	3.04	5.81
381	77.8	1.6	79.0	6.52	6.33	1.69
2033	78.75	1.72	79.96	6.48	6.12	2.23

Table 1. (Continued)

Event	E_e(MeV)	ΔE_e	$-q^2$(MeV)^2	ω(°)	θ(°)	ϕ(°)
700	78.9	7.8	80.1	6.48	.93	6.44
3097	80.8	2.2	82.1	6.40	2.06	6.10
2911	81.0	4.0	82.4	6.39	0.0	6.49
1573	81.3	1.1	82.6	6.38	6.40	.37
2195	81.5	2.9	82.8	6.37	4.93	4.09
651	82.2	3.6	83.5	6.34	5.07	3.88
2122	84.7	2.8	86.1	6.25	5.8	2.41
140	86.4	2.8	87.7	6.19	5.82	2.20
2168	88.9	3.8	90.4	6.10	4.06	4.60
1619	89.6	4.7	91.0	6.08	4.86	3.71
2414	90.5	3.3	91.9	6.05	1.97	5.75
1419	91.5	1.4	93.0	6.01	6.04	0.0
2481	91.6	3.2	93.1	6.01	5.05	3.32
1559	92.3	2.5	93.8	5.99	5.69	1.96
2030	93.64	5.6	95.2	5.94	.97	5.90
913	93.9	3.9	95.5	5.93	5.43	2.49
850	94.1	10.2	95.6	5.96	0.76	5.91
81	96.2	5.6	97.8	5.86	4.23	4.11
2107	96.5	5.26	98.08	5.85	1.89	5.57
2320	96.6	1.6	98.3	5.85	5.88	0.0
104	99.8	8.9	101.5	5.75	4.63	3.48
2655	103.0	7.92	104.7	5.66	2.04	5.32
2144	103.2	3.2	105.0	5.66	5.12	2.49
1221	103.2	11.7	104.9	5.66	.71	5.65
1275	108.0	2.3	109.9	5.53	5.56	0
362	108.6	17.4	109.5	5.54	4.47	3.33
1603	108.6	2.5	110.4	5.51	5.23	1.85
485	111.4	4.6	113.3	5.44	4.74	2.75
2544	113.3	2.9	115.3	5.4	3.07	4.48
1841	117.9	4.3	119.9	5.29	4.13	3.36
2448	119.6	3.5	121.7	5.25	3.52	3.95
2097	120.2	3.9	122.3	5.23	4.12	3.28

Table 1. (Continued)

Event	E_e(MeV)	ΔE_e	$-q^2$(MeV)^2	ω(°)	θ(°)	ϕ(°)
3262	120.6	27	122.7	5.22	5.24	.521
2408	121.8	4.5	124	5.20	1.79	4.93
2923	123.0	2.3	125.2	5.18	4.58	2.5
426	123.3	9.2	125.5	5.17	3.85	3.52
1428	126.7	9.1	129.0	5.14	.525	5.11
1965	127.6	5.29	129.9	5.08	3.02	4.1
1408	130.2	6.5	132.5	5.03	2.80	4.22
1232	133.5	9.9	135.9	4.96	1.60	4.74
431	133.5	5.3	135.9	4.96	4.61	1.94
2975	134.2	4.4	136.7	4.95	2.70	4.20
164	140.6	12.8	143.4	4.83	3.25	3.63
2228	141.3	5.9	143.9	4.82	3.94	2.85
709	142.3	4.8	144.9	4.81	4.55	1.66
23	145.8	3.3	148.5	4.75	4.79	0.0
3228	148.8	3.4	151.5	4.7	4.69	.68
3044	150.0	2.5	152.8	4.68	4.69	.47
1169	156.6	3.3	159.5	4.58	4.62	0.0
1451	156.8	13.9	159.7	4.57	2.98	3.53
1371	157.5	7.4	160.5	4.56	1.16	4.46
1298	158.9	18.1	161.9	4.54	.69	4.54
1490	159.7	5.8	162.7	4.53	4.29	1.58
1130	160.0	5.15	163.0	4.53	4.08	2.05
2117	162.8	4.9	165.9	4.49	3.25	3.16
248	162.9	24.6	166.0	4.49	2.97	3.42
2948	163.0	4.9	166.1	4.48	4.48	0.0
2240	163.6	3.9	166.7	4.47	4.52	0.0
399	169.6	4.3	172.8	4.40	4.44	0.0
1427	171.0	13.5	174.2	4.38	1.36	4.21
1993	171.1	10.8	174.3	4.37	2.81	3.41
1731	171.6	7.6	174.8	4.37	2.92	3.31
2420	179.9	6.4	183.4	4.26	4.10	1.34
*1010	182.6	5.0	186.1	4.23	4.28	0.0

Table 1. (Continued)

Event	E_e(MeV)	ΔE_e	$-q^2$(MeV)^2	ω(°)	θ(°)	ϕ(°)
2270	185.6	8.4	189.1	4.19	3.55	2.32
1237	188.6	4.7	192.2	4.16	4.11	.93
62	188.8	4.7	192.4	4.16	4.17	.55
2073	196.1	7.0	193.9	4.08	2.3	3.40
1350	196.2	28.6	200.2	4.08	1.94	3.64
811	201.1	12.8	205.0	4.03	1.14	3.92
168	203.3	35.1	207.3	4.00	2.22	3.39
3043	213.4	9.2	217.6	3.91	3.03	2.54
12	215.1	17.1	219.3	3.89	1.51	3.64
398	215.9	29.0	220.2	3.88	1.84	3.48
2242	216.3	7.6	220.5	3.88	3.18	2.31
1223	217.9	24.2	222.2	3.86	2.41	3.09
1936	219.0	17.15	223.29	3.85	.89	3.81
2109	225.4	33.3	229.9	3.8	1.69	3.46
126	231.7	7.8	236.3	3.74	3.59	1.24
2013	242.9	15.7	247.7	3.65	.53	3.67
1320	245.7	8.0	250.6	3.63	3.52	1.11
1407	248.2	8.4	253.1	3.61	3.67	0.0
1909	259.8	10.94	265.0	3.53	2.35	2.71
1923	262.8	8.11	268.04	3.51	2.37	2.61
109	269.3	14.2	274.7	3.46	3.12	1.63
1498	285.0	35.1	290.3	3.40	3.34	.50
2307	286.9	27.0	292.7	3.35	1.88	2.85
1163	299.8	39.7	305.9	3.28	1.69	2.89
857	307.7	20.3	314.0	3.23	2.76	1.80
1882	308.1	31.7	314.4	3.30	.87	3.17
170	311.9	20.8	318.2	3.21	2.84	1.63
1423	321.8	17.6	328.4	3.16	2.38	2.18
823	330.8	29.7	337.6	3.11	2.61	1.81
2985	333.1	12	339.9	3.10	2.62	1.79
1692	333.7	19.5	340.5	3.10	1.99	2.46
2743	336.1	12.9	343	3.09	3.0	.95
1067	342.2	9.3	349.2	3.06	3.09	.48

Table 1. (Continued)

Event	E_e(MeV)	ΔE_e	$-q^2$(MeV)^2	ω(°)	θ(°)	ϕ(°)
1982	348.4	22	355.5	3.03	.89	2.96
2111	350.0	22.0	357.0	3.11	3.11	0.0
1630	366.0	11.1	312.2	3.24	3.30	0.0
1836	374.2	11.74	381.9	2.92	2.98	0.0
166	385.6	23.9	393.6	2.87	2.55	1.47
171	405.0	13.6	413.4	2.80	2.83	.45
1175	405.4	37.9	413.8	2.80	1.89	2.16
1098	413.0	10.8	421.6	2.77	2.78	.58
3191	441.5	15.8	450.7	2.67	2.37	1.39
2442	474.9	31.5	484.9	2.57	1.68	2.04
1174	502.1	16.9	512.7	2.50	2.57	0.0
1758	510.0	90.7	520.7	2.47	1.05	2.33
169	521.9	28.3	532.9	2.44	.14	2.52
82	558.0	29.2	569.7	2.36	.346	2.42
3275	595.5	27.6	608.1	2.27	1.33	1.95
727	611.4	38.8	624.3	2.24	2.04	1.14
3265	642.1	27.8	655.7	2.18	1.10	1.98
1935	658.3	30.07	672.2	2.15	1.34	1.80
2709	669.5	34.8	683.7	2.34	2.16	3.54
408	669.7	46.4	683.9	2.13	2.06	.84
2670	687.9	33.6	702.4	2.10	1.91	1.08
3210	708.4	30.3	723.5	2.07	2.05	.67
*1008	762.9	42.2	779.2	1.99	1.94	.74
3080	799.4	35.3	816.5	1.94	2.03	.15
354	870.0	169.3	879.4	1.86	1.28	1.48
322	891.3	141.6	910.4	1.82	.824	1.74
525	986.7	64.1	1007.9	1.72	1.83	0.0
302	1259.6	158.7	1286.8	1.49	.89	1.34
142	1290.6	282.9	1318.5	1.47	.88	1.33
544	2300.9	177.5	2351.0	1.003	1.17	0.0
2005	2430.9	182.2	2483.8	.96	.96	.60
1776	2852.8	234	2915.1	.851	.95	.40
1005	3577.9	385.5	3656.1	.697	.522	.724
2932	3581.6	271.9	3659.8	.696	.826	.338

*Events not used in cross section calculation.

It will be helpful at this point to describe the orientation of the emulsion pellicles during measurement. Let y denote the direction parallel to that of the incident pion, x the 7½ cm. direction (perpendicular to y), and z the 600 micron direction. The x-y plane is defined as the plane of the emulsion and is the same as the focal plane of the microscopes. Any plane containing the z axis is called a vertical plane.

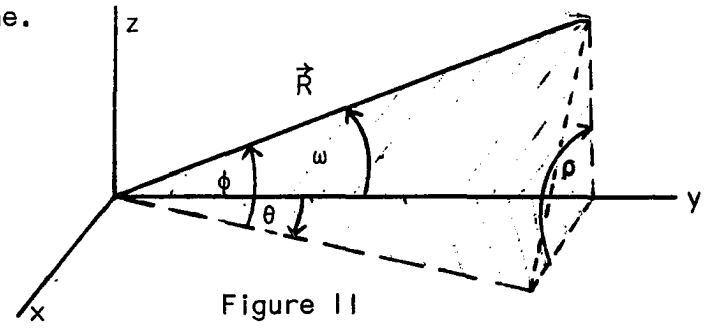

Figure 11

The relation between ρ, where $\sin\rho = \cos\alpha$ or $\rho + \alpha = 90°$, and the measurable quantities, θ and ϕ (and hence ω), is obtained by the vector relation

$$\cos\alpha = \frac{\vec{i} \cdot \vec{j} \times \tilde{R}}{|\vec{j} \times \tilde{R}|} \quad ,$$

where

$\vec{i}$ = unit vector in x direction,

$\vec{j}$ = unit vector in y direction,

$\tilde{R}$ = unit vector along $\vec{R}$,

α = angle between the normal to the plane formed by the y axis and $\vec{R}$ and the plane of the emulsion,

ρ = angle between this plane and the plane of emulsion.

Thus,

$$\sin\rho = \frac{\sin\phi}{(1 - \cos^2\phi\cos^2\theta)^{\frac{1}{2}}} \quad .$$

The relation between ω, θ, and ϕ is shown above to be

$$\cos\omega = \cos\theta\cos\phi \quad .$$

Hence

$$\sin\rho = \frac{\sin\phi}{(1 - \cos^2\omega)^{\frac{1}{2}}} \quad ,$$

or

$$\sin\rho = \frac{\sin\phi}{\sin\omega} \quad ,$$

where

θ = projected angle of the electron with respect to the incident pion direction,

ϕ = dip angle (angle between electron and its projection in the xy plane),

ω = total space angle between pion and electron,

$0 \leq \rho \leq 90°$.

Since the knock-on electrons should have an isotropic ρ distribution, it is possible to determine whether or not the knock-on events found were biased towards those having a small dip angle, (i.e., those which are in the plane of the emulsion for some distance--commonly known as "flat tracks"). Electron tracks with large dip angles are, in general, much more difficult to locate than "flat" tracks because only the first few, at most, of the blobs of their tracks are in focus when focusing on the pion track, making it relatively more difficult to find such interactions using standard scanning techniques. If electrons with different dip angles have

different probabilities of being located in scanning, then the distribution of the plane angle ρ should be anisotropic, the degree of anisotropy indicating the percentage of events missed. This angle ρ has been calculated for each event and its distribution is plotted in Figure 12 for the events found by all scanners in the energy intervals $100 \leq E_e \leq 200$ MeV and $E_e > 200$ MeV. A cutoff of 100 MeV electron energy is arbitrarily employed due to the apparent poor scanning efficiency for knock-on electrons below this energy. This can be seen in the Histograms of the experimental results in Figures 13 - 14. Salecker's predicted results are superposed.

From Figure 12 it is seen that fewer events were found with plane angles between 60° and 90° than between 0° and 30° or between 30° and 60°. Statistical errors cause the use of this anisotropy in the plane angle distribution to predict a definite scanning efficiency to be of questionable reliability. However, since there is a definite decrease in scanning efficiency at large dip angles as indicated in this figure, it is necessary to make a quantitative estimate of loss of efficiency in order to correct the experimental results for this loss. This is done by determining the number of events needed to make the distributions isotropic. In this manner a scanning efficiency of approximately 85% for locating events with all dip angles is determined from these results.

It is probable that the scanning efficiency is also dependent on the particular scanner. For this reason it is necessary to investigate the relative scanning efficiency of different scanners.

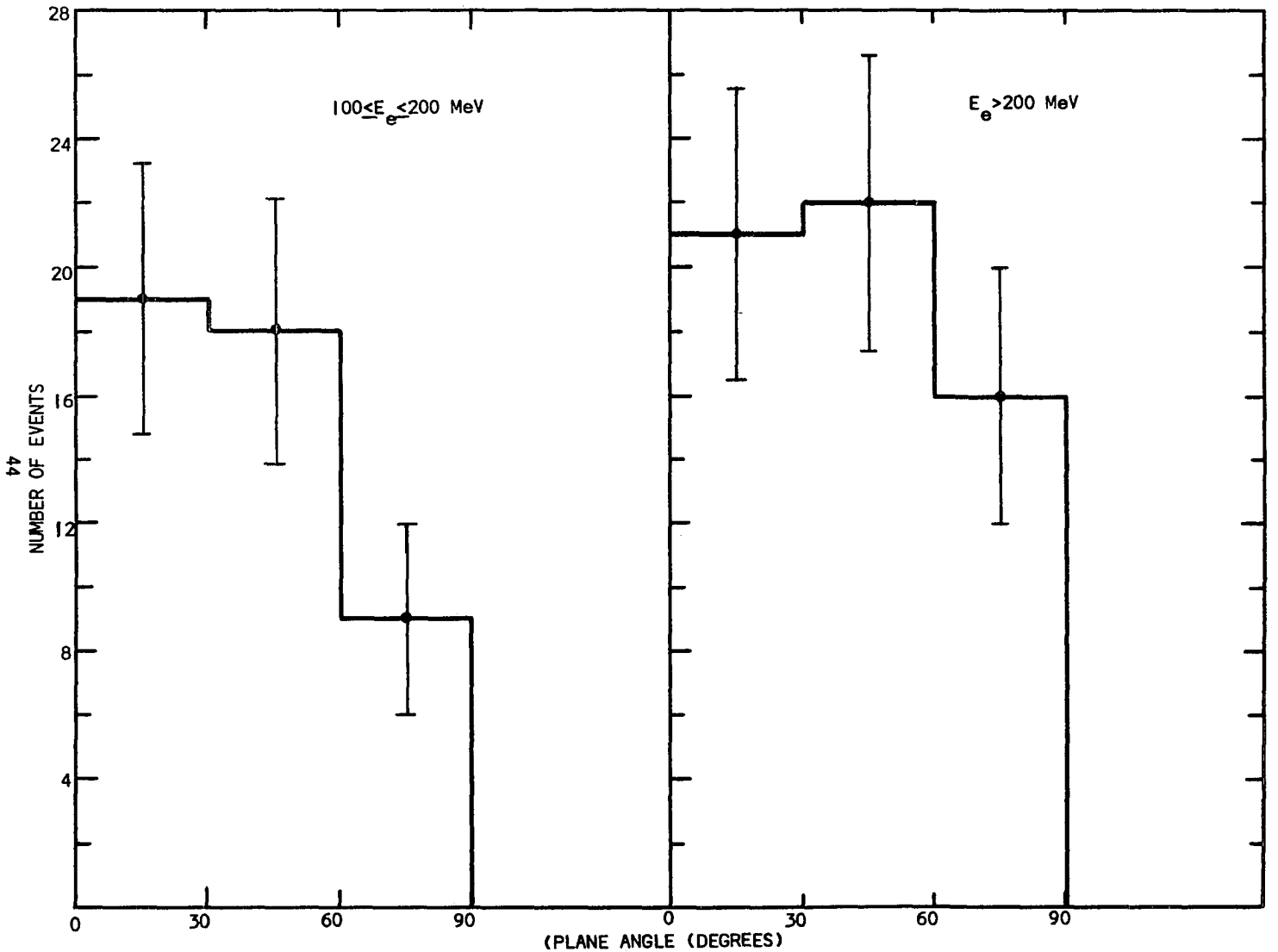

Fig. 12 Plane angle distribution for all knock-on events with energy greater than 100 MeV (902 m. of track).

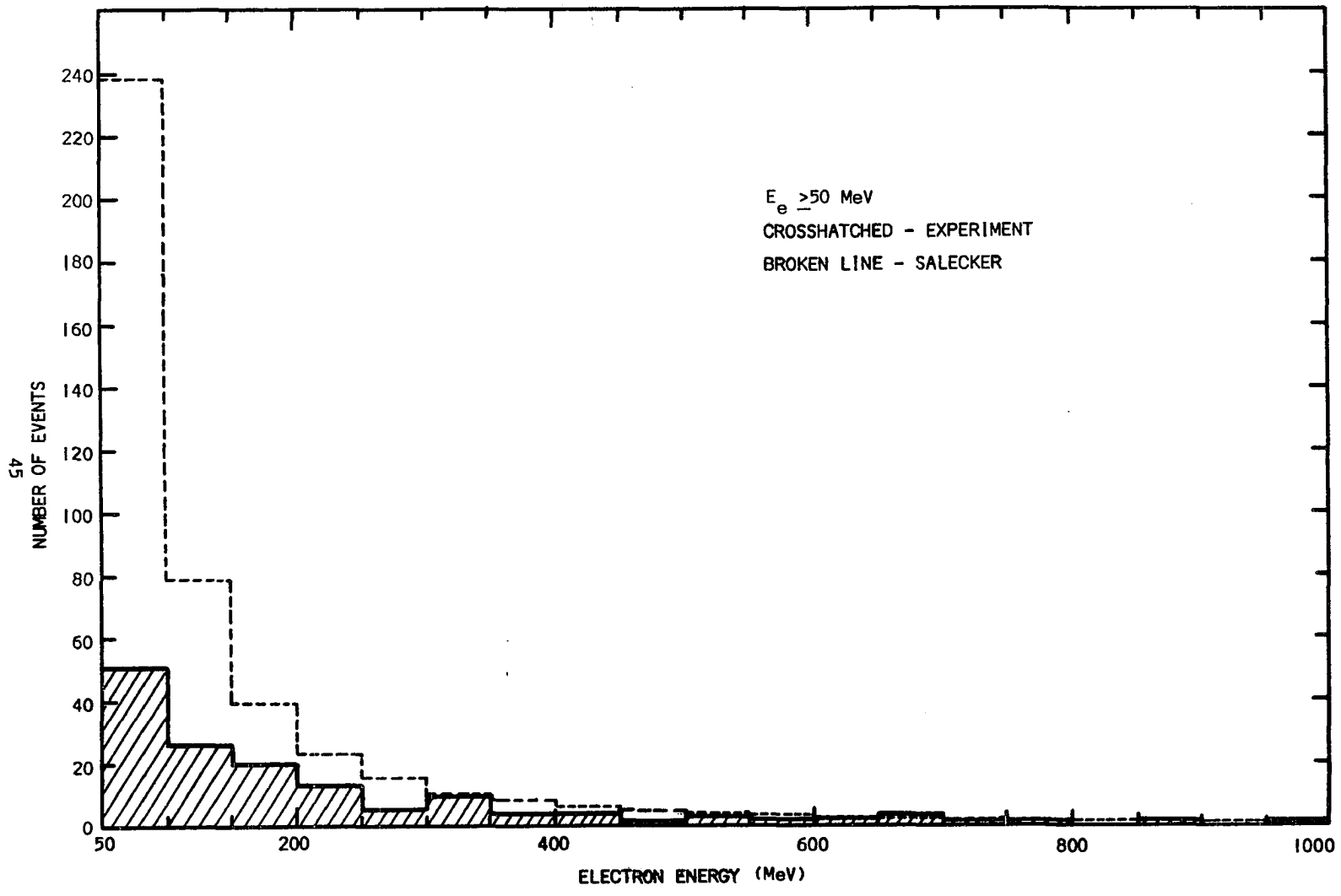

Fig. 13. Distribution of knock-on electrons per 50 MeV interval, with the number predicted by Salecker superposed.

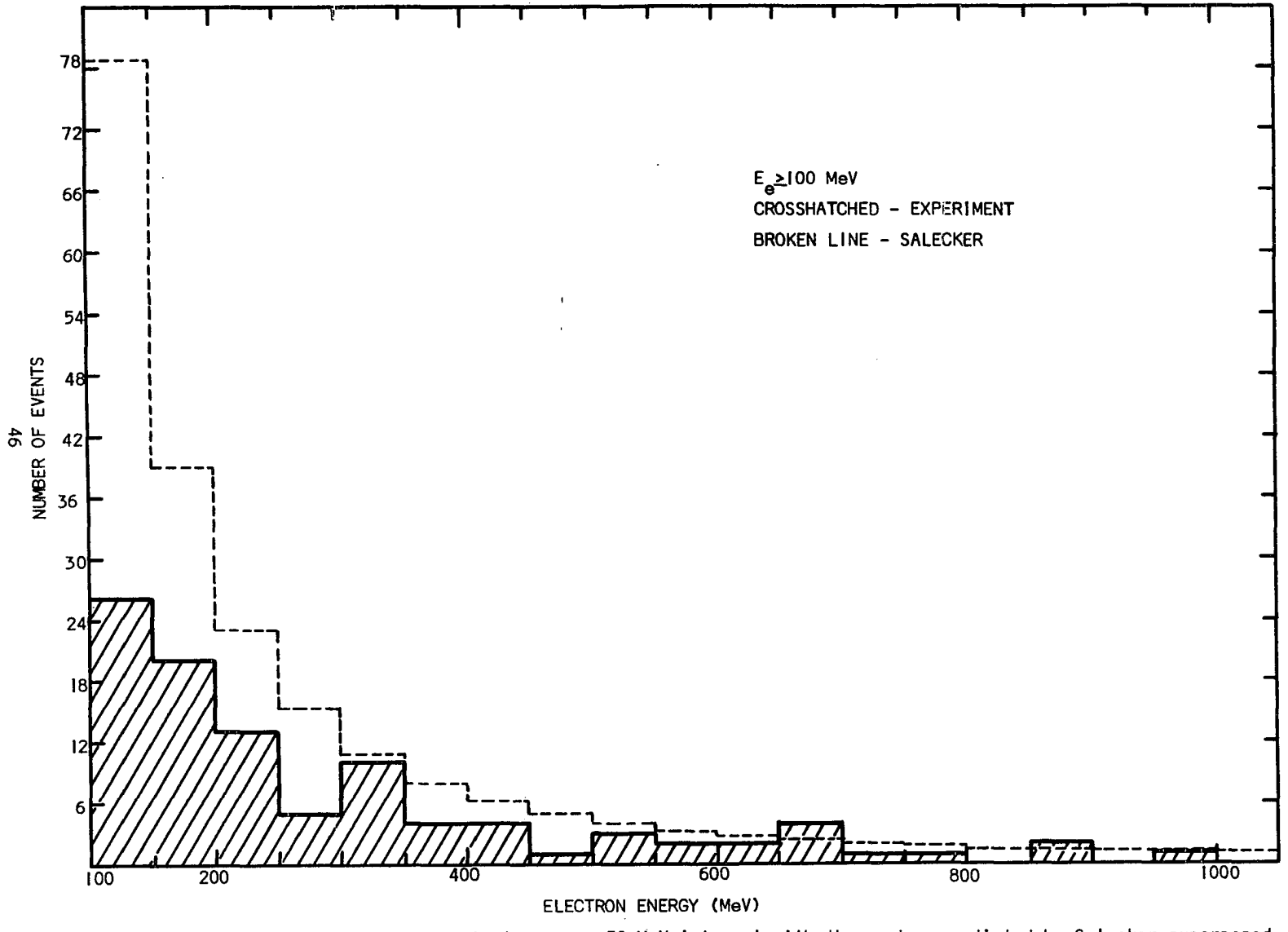

Fig. 14. Distribution of knock-on electrons per 50 MeV interval with the number predicted by Salecker superposed.

The distribution of plane angles for the events found by each scanner gives a good indication of the relative scanning efficiencies. It was possible to select a group of three of the nine scanners whose events showed plane angle distributions which were the most isotropic. Hence the scanning efficiencies of these scanners were the highest. Indeed, the mean free path for knock-on electrons with energy >50 MeV as found by these scanners is $4.7 \pm .55$ m. in a total track length of 345 m. as compared to a mean free path of $5.8 \pm .46$ m. in 902.7 m. of track for all the scanners combined. The plane angle distribution for the events with energies >100 MeV found by these three scanners is given in Figure 15 for two energy regions. This can be compared to the same distribution for the events from all scanners given in Figure 12 and seen to be a considerably more isotropic distribution. Thus, the results of this group of scanners ("best") will be investigated separately. A histogram of the total cross section for events found by these scanners is plotted in Figure 16 with the result predicted by Salecker superposed. From the plane angle distributions it can be concluded that the results of these scanners are not significantly biased toward flat events.

In order to further check the scanning efficiency for locating knock-on electrons, a procedure of rescanning was used which checked the individual scanner's probability for locating all knock-on electrons. The data collected in this experiment was obtained by nine different scanners. Consistent results, within

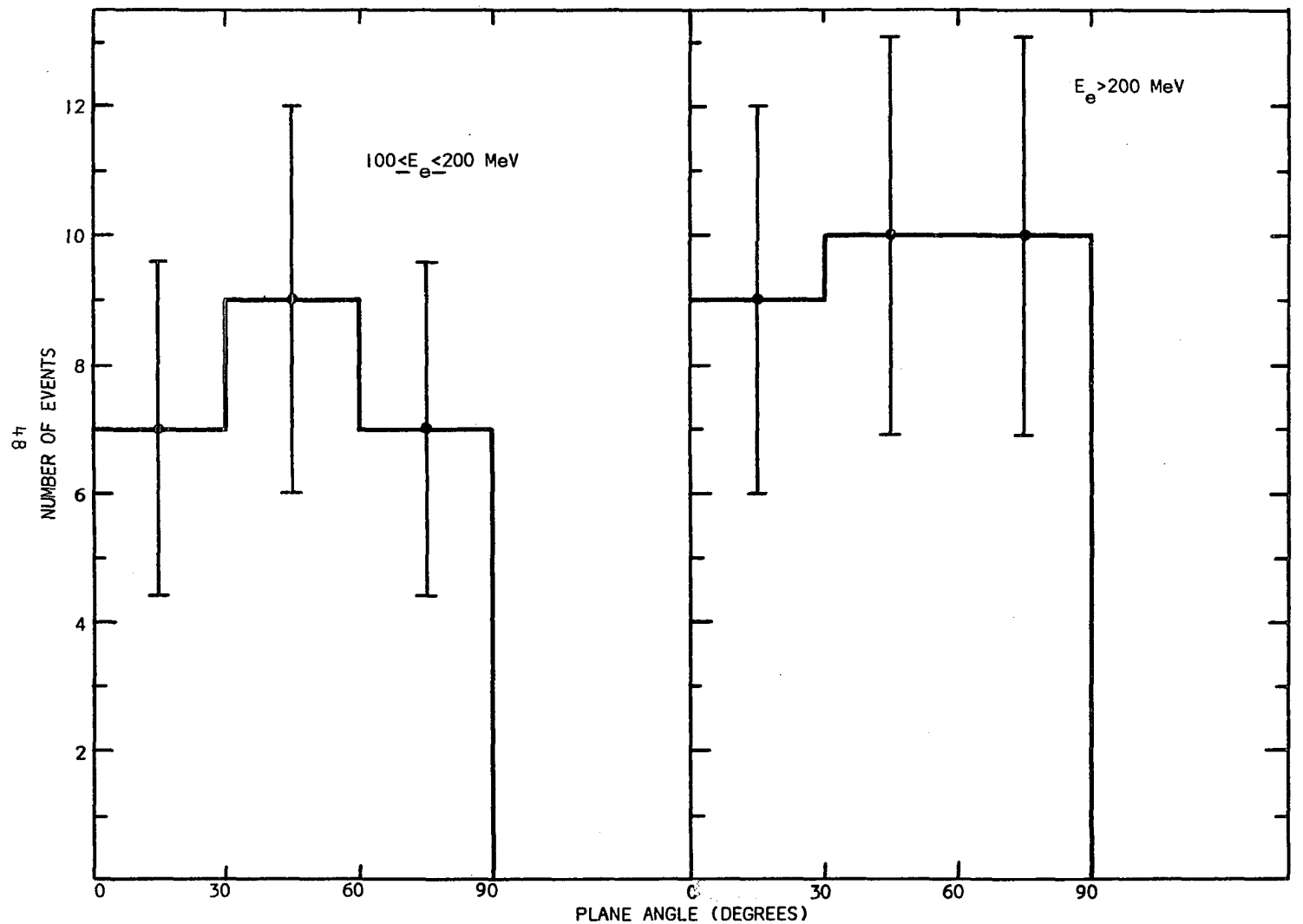

Fig. 15. Plane angle distribution for the portion of the knock-on events found by those scanners with the highest scanning efficiency (345 m.)

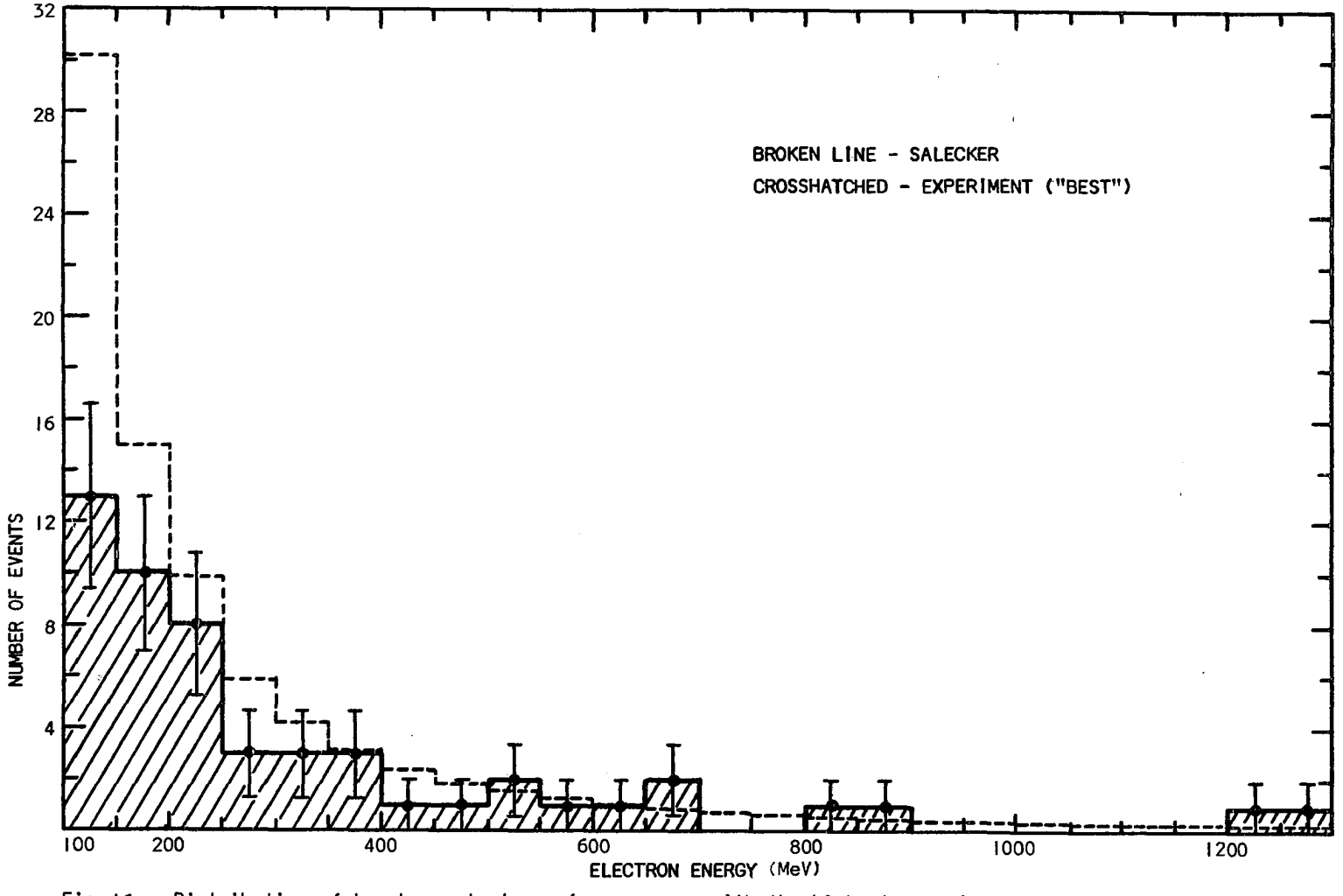

Fig. 16. Distribution of knock-on electrons for scanners with the highest scanning efficiency, at intervals of 50 MeV, for 345 m, of track. Salecker's theoretical results are superposed.

statistical error, were obtained by each scanner. The rescanning procedure entailed requiring each scanner to scan tracks which had been previously scanned. The same group of tracks were rescanned by each scanner. Knock-on electrons had been found on ¼ of the tracks rescanned. On the average, scanners missed ≈16% of the knock-on electrons in rescanning. These results indicate that there is approximately 84% scanning efficiency for relocating knock-on interactions with energy >100 MeV. One knock-on interaction was found in rescanning which was missed in the original scanning, indicating a still lower scanning efficiency. This additional loss is estimated as 4%. Overall, it is estimated that there is approximately 80% scanning efficiency in locating general knock-on interactions of the type recorded in Table I.

This 20% loss in scanning efficiency should be coupled with the 15% loss due to missing interactions with large dip angles. Thus, the final scanning efficiency is estimated to be 65% for location of knock-on electrons with energy $\geq$100 MeV by all scanners.

Histograms of the experimental total cross section, corrected for scanning efficiency, are given in Figures 17 and 18, with the results of Salecker superposed.

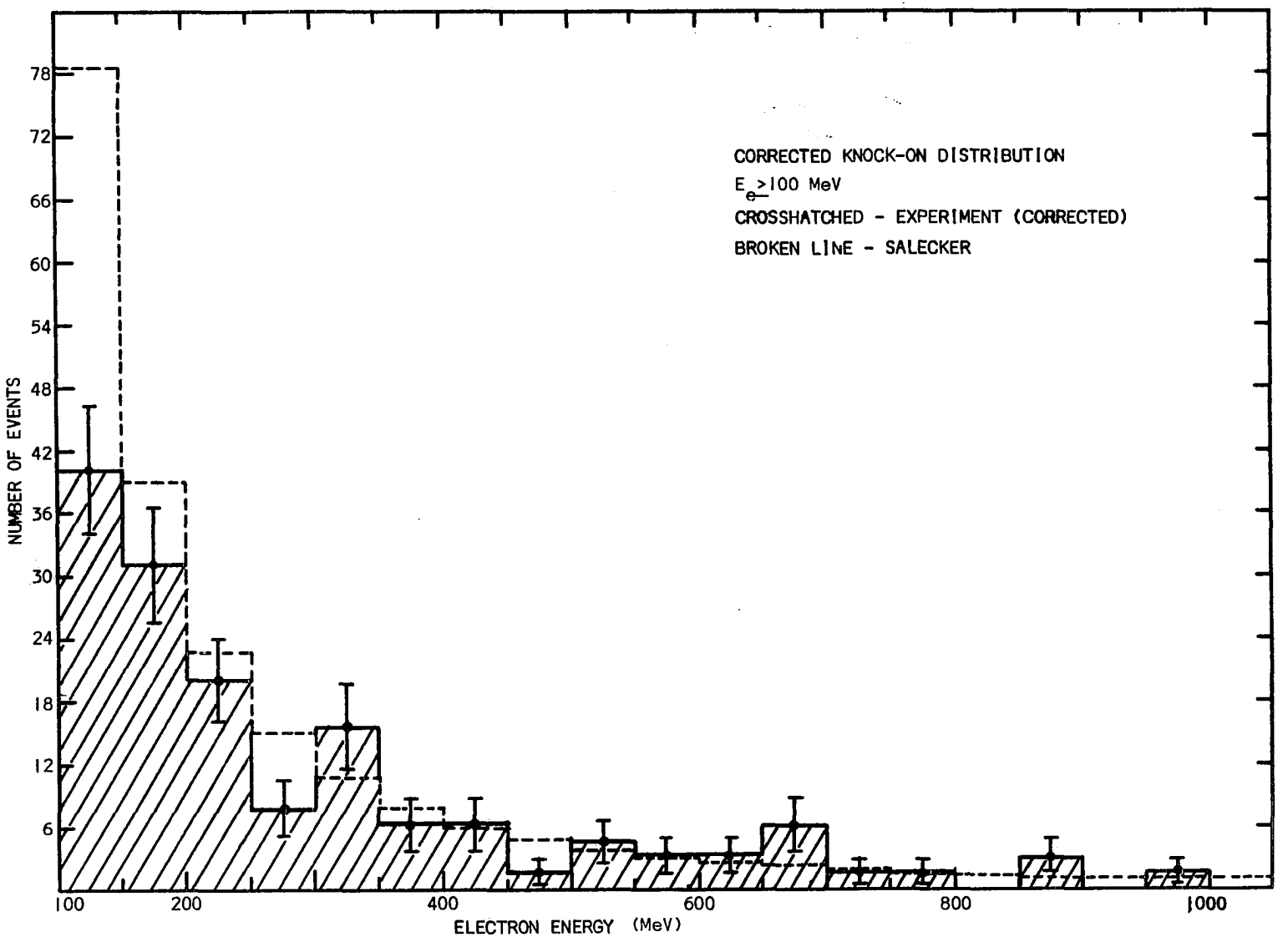

Fig. 17. Distribution of knock-on electrons, corrected for the scanning efficiency, per 50 MeV interval, with the number predicted by Salecker superposed.

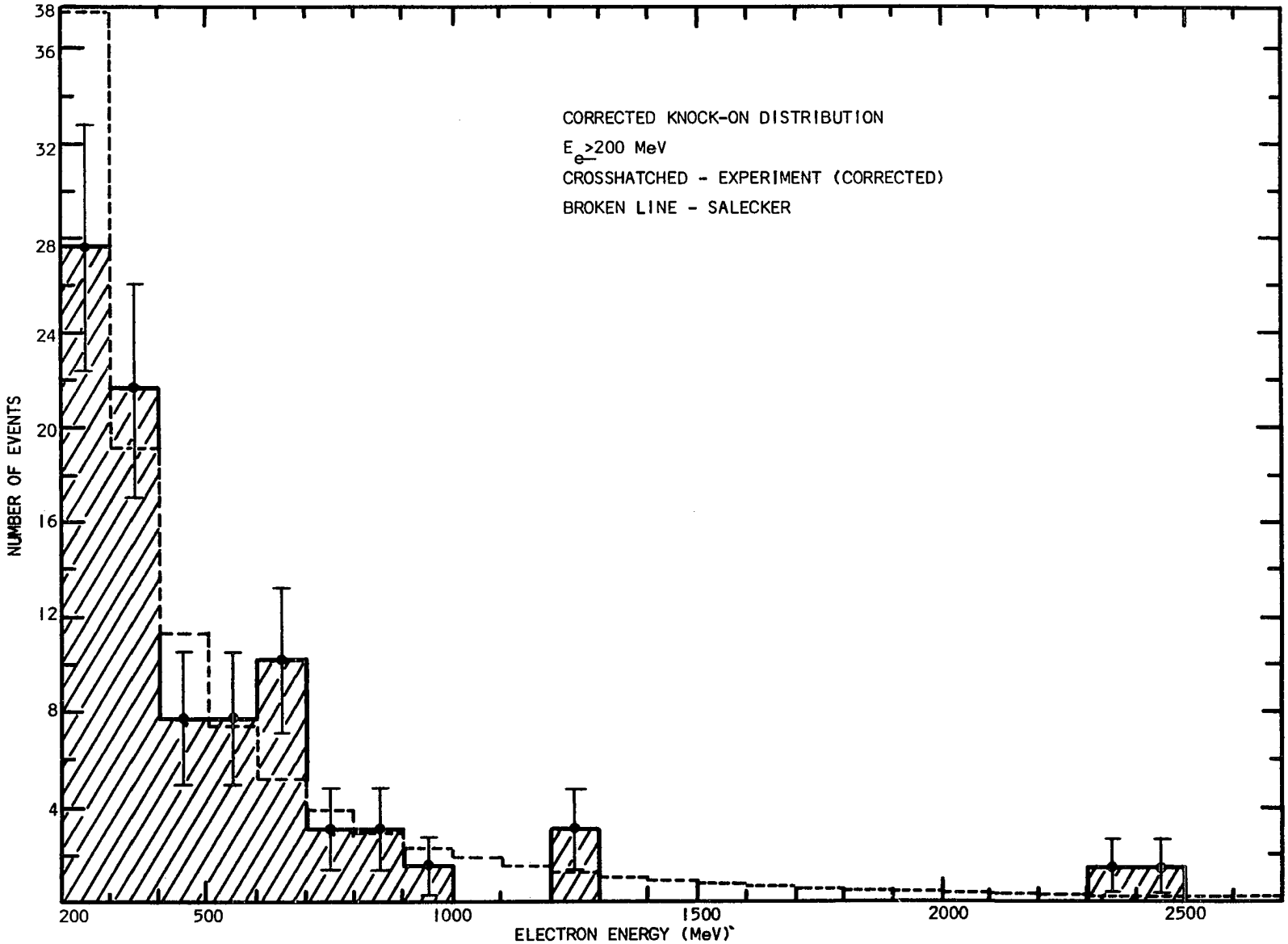

Fig. 18. Distribution of the number of knock-on electrons, corrected for scanning efficiency and cut off at 200 MeV, per 100 MeV interval with the number predicted by Salecker superposed.

Conclusions

From Figures 13, 14, 17, and 18 it can be seen that pion-electron elastic scattering experiments in emulsion are difficult to perform below about 200 MeV electron energy. This statement is based on the relatively large fractional difference between experiment and theory below this energy, which is the energy region where the theory is expected to be most reliable. A previous bubble chamber experiment by Allan et.al.[3], involving large statistics in this low energy region, found good agreement between Salecker's result and their experimental results. As a result, the differences between theory and experiment below ≈200 MeV must be attributed to low scanning efficiency. With statistics much larger than were obtained in this experiment it would be possible to accurately correct for this error.

Above 150 MeV electron energy, experiment and theory are in reasonable agreement, within statistical error, as is seen in Figures 17 and 18. Due to the small statistics obtained at high energies, no strong conclusions can be drawn concerning the reliability of the theoretical results. Within the accuracy of this experiment, Salecker's result for the production of knock-on electrons by 16 BeV pions is correct.

Any emulsion experiment involving elastic scattering of pions on electrons as a test of quantum electrodynamics or charge structure will require many times as much data as was obtained in this work. This illustrates one of the chief disadvantages of emulsion work, namely that of requiring very large amounts of time and labor to examine interactions with small cross sections.

CHAPTER III

DIRECT PRODUCTION OF HIGH ENERGY ELECTRON PAIRS BY PIONS

Introduction

High energy electron pair production by pions is of interest in that it provides one of the most direct methods presently available for investigating particle structure and quantum electrodynamics at small distances. This process has the advantage that, since the collision is with a nucleus (mass $\geq$ mass of the proton--no pairs produced in pion-electron interactions were observed), the energy in the center of mass system is quite large, in contradistinction to the pion-electron scattering process where only a small fraction of the incident energy is effective in the collision. Since direct electron pair production is an electromagnetic process, quantum electrodynamics should provide the correct method for calculating the cross section if quantum electrodynamics is valid at high energies.

Theoretical Calculations

Introduction

Several attempts have been made to calculate the electron pair production cross section for charged particles passing through matter. These attempts have met with only limited success due to

the use of approximations, even in the calculations of the lowest order quantum electrodynamical process, which are necessary in order to obtain a closed form expression for the cross section.

In any calculation of this cross section, the matrix elements corresponding to the Feynman graphs given in Figure 19, as well as cross terms between these graphs, should be considered. For incident pions, the matrix elements corresponding to diagrams A and A' are expected to give the main contribution to the cross section since the differential cross section contribution from these graphs contain a term $(e/m_e)^2$ whereas the contribution from B and B' contains instead the factor $(e/m_\pi)^2$. Contributions from cross terms between A and A' and B and B' thus contain the factor $(e/m_e)(e/m_\pi)$. Hence, unless there is a large resonance effect in the matrix element B + B', the contributions from B and B' are negligible for incident pions. The cross terms are more likely to be non-negligible, but again their effect should be much smaller than the A + A' contributions due to the smaller coefficient given above. Due to the difficulty of calculating the cross term contributions, their effect has been considered only very approximately, or neglected completely, in all calculations of this cross section.

The earliest attempts to calculate theoretical cross sections for charged particle pair production were by Landau and Lifshitz[4] in 1934 and by Bhabha[5] in 1935. Other early calculations for the process were made by Williams[6] (1935), Nishina et al.[7] (1935), Stueckelberg[8] (1935), Racah[9] (1937), and Block et al.,[10] (1954).

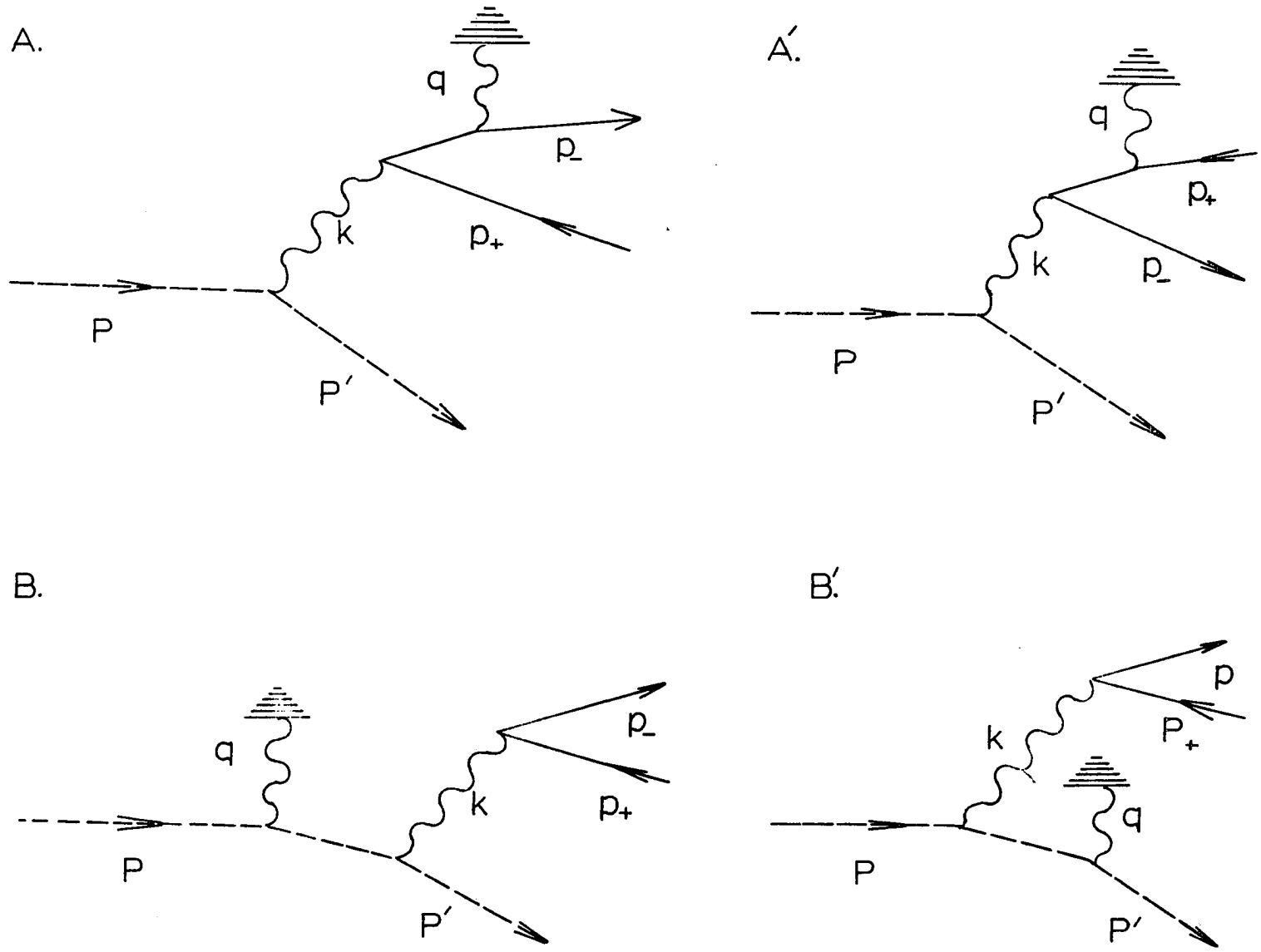

Fig. 19. Feynman Diagrams for Electron Pair Production.

Development of high energy particle accelerators with monoenergetic beams made possible a more direct test of the theoretical predictions through experiment. Previously, only the total cross section as a function of incident energy was measured, whereas monoenergetic beams made possible differential cross section measurements at a fixed incident energy. Disagreement between experiment and existing theories indicated a need for more exact calculations[21].

Attempts to calculate the pair production cross section in a more exact fashion were made by Murota et al.[11] in 1956, by Ternovskii[13] in 1959, and by Zapolsky[14] in 1962.

Calculations

The work of Ternovskii is the only one to date which considers spin 0 primary particles and therefore will be treated in considerable detail here.

Ternovskii considered two types of pair production processes: processes of the first type, where the pair particles are considered free, corresponding to diagrams B and B'; processes of the second type, where the parent particle is considered free, corresponding to diagrams A add A'. By a particle being free it is meant that the particle undergoes interaction with only one electromagnetic field, as can be seen in Figure 19. Cross section contributions from the diagrams A + A' are expected to be dominant in the region $K<<m_e \frac{E}{m}$ (region I), while the contributions from B + B' are expected to be dominant in the region $K>>\frac{m_e E}{m}$ (region II), where K ≐ sum of electron and positron energies and E, m = incident

particle energy and mass respectively. Between these two regions lies a large and very important energy region, including the region where it is presently possible to test quantum electrodynamics and investigate charge structure. Processes of the second type make the main contribution to the total cross section, as was discussed above, and will thus be considered in detail. Processes of the first type are shown to be much less important at total pair energies obtainable from 16 BeV incident pions, but they will also be considered below. Ternovskii's calculations, as well as each of the other cross section calculations to date, considers the nucleus in the static field approximation in which momentum, but no energy, is transferred to the nucleus. This is a good approximation for small momentum transfers to the nucleus.

Using the standard Feynman rules (17 and 18) it is possible to construct the matrix element M for the scattering process represented by the graphs A + A' (second type) to be

$$M = e^2 \frac{(P + P')_\mu}{k^2} \{\bar{v}^{\sigma,+}(\vec{p}_-)[i \frac{\gamma_4[(\hat{k} - \hat{p}_+) - m_e]\gamma_\mu}{(\vec{k} - \vec{p}_+)^2 + m_e^2}$$

$$+ \frac{i\gamma_\mu[(\hat{p}_- - \hat{k}) - m_e]\gamma_4}{(\vec{p}_- - \vec{k})^2 + m_e^2}] v^{\delta,+}(\vec{p}_+)\} V_q$$

where

P, P' = initial, final pion four-momentum,

p_+, p_- = positron, electron four-momentum,

k = four-momentum transfer from the pion to the pair and nucleus,

$\vec{k}$ = vector momentum transferred to the pair and nucleus,

$V_q = Ze^2/(|\vec{q}|^2 + |\vec{q}_o|^2)$ = factor connecting the nucleus to the matrix element in the static field approximation,

$\vec{q}$ = momentum transfer to the nucleus,
$= \vec{p} - \vec{p}' - \vec{p}_+ - \vec{p}_- = \vec{k} - \vec{p}_+ - \vec{p}_-$,
$|\vec{q}_o|$ = $Z^{1/3}m_e/137$ = inverse Thomas-Fermi radius (minimum momentum transferrable to the nucleus in the Thomas-Fermi model for the screened atom),
Z = charge of the nucleus.

Using this matrix element, the differential cross section is

$$d\sigma = \overline{|M|^2} \frac{\delta(E - E' - \omega)d^3P'd^3p_+d^3p_-}{2\sqrt{EE'}\,(2\pi)^8(|\vec{P}|/E)}$$

where

$$\vec{k} = \vec{P} - \vec{P}',$$
$$\omega = E_+ + E_-,$$
$$E_\pm = (|\vec{p}_\pm|^2 + m_e^2)\,,$$
$$E = (|\vec{P}|^2 + m^2)^{1/2},$$
$$E' = (|\vec{P}'|^2 + m_\pi^2)^{1/2},$$
m_π = mass of incident particle (pion).

The bar over $|M|^2$ indicates an average over the initial spins and summation over the final spins. The approximation $k^2 = |\vec{k}|^2 - \omega^2$ is now made (following Ternovskii).

The calculation was done in the lab system with the z axis directed along the direction $\tilde{n} = \vec{k}/|\vec{k}|$ of the total momentum transfer from the incident particle. Small angle approximations, which were used throughout the calculation, appear to be valid approximations since the angles involved are small (discussed experimentally below). That is, for all angles θ_i used in the calculation,

$$\theta_i \text{ replaces } \sin\theta_i$$

and

$$(1 - \tfrac{1}{2}\theta_i^2) \text{ replaces } \cos\theta_i.$$

By calculating the value of the matrix elements, and dropping the cross

terms which average to zero under angle integration, Ternovskii determined the differential cross section to be

$$d\sigma = \frac{e^4}{k^2(m_\pi^2 + P^2\theta'^2)/P(P-k)} \left[\tfrac{1}{2}\{4[\frac{1}{H^2 + p_+^2\theta_+'^2} - \frac{1}{H^2 + p_-^2\theta_-'^2}]^2 \right.$$

$$+ \frac{p_+^2 + p_-^2}{k^2}[\frac{p_+\theta_+'}{H^2 + p_+^2\theta_+'^2} - \frac{p_-\theta_-'}{H^2 + p_-^2\theta_-'^2}]^2\}|V_q|^2 \frac{P^2\theta'^2}{P(P-k)}$$

$$\left. + (1 - \omega^2/k^2)^2 \frac{8p_+^2p_-^2}{k^2}[\frac{1}{H^2 + p_+^2\theta_+'^2} - \frac{1}{H^2 + p_-^2\theta_-'^2}]^2 \frac{(P - k/2)^2}{P(P-k)}|V_q|^2 \right]$$

$$\times \frac{1}{2\sqrt{EE'}\,(2\pi)^8(P/E)} k^2 d\theta' p_+^2 d\theta_+' dp_+ p_-^2 d\theta_-' dp_-,$$

where

$$\vec{p}_\pm = \tilde{n}p_\pm(1 - \tfrac{1}{2}\theta_\pm'^2) + \tilde{T}_\pm p_\pm\theta_\pm' ,$$

$$\vec{P} = \tilde{n}P(1 - \tfrac{1}{2}\theta'^2) + \tilde{T}_\pi P\theta' ,$$

$$\vec{P}' = \tilde{n}(P - k - \tfrac{1}{2}P\theta'^2) + \tilde{T}_{\pi'}P\theta' ,$$

$$\tilde{n} = \vec{k}/|\vec{k}| ,$$

$\tilde{T}_i$ = unit vector perpendicular to $\tilde{n}$ in the plane of $\vec{P}_i$ and $\vec{k}$,

$$H^2 = m_e^2 + p_+p_-(m_\pi^2 + P^2\theta'^2)/P(P-k)$$

θ_-' = angle of the electron to $\tilde{n}$,

θ_+' = angle of the positron to $\tilde{n}$,

θ' = angle of primary pion to $\tilde{n}$.

All momentum symbols in this equation represent the scalar values of the corresponding vector quantities. Integration over the angles θ_+' and θ_-' was effected by replacing θ_+' and θ_-' by the two variables

$$x = (|\vec{p}_+|\theta_+' - |\vec{p}_-|\theta_-')/2H$$

$$y = (|\vec{p}_+|\theta_+' + |\vec{p}_-|\theta_-')/2H$$

then integrating over x and y. Integration over x was done directly, but integration over y was done by approximating the integral as a

logarithm in the manner

$$\int_{y_{min}}^{y_{max}} f(y)dy = C\ln\left(\frac{y_{max}}{y_{min}}\right)$$

[$C \neq C(y)$]. This procedure was justified by the fact that the range of y involved is limited to small values ($\lesssim 1$) by physical arguments.

The upper and lower limits, y_{max} and y_{min}, can be determined from physical arguments since

$$2Hy = |\vec{p}_+|\theta'_+ + |\vec{p}_-|\theta'_-$$

is greater than or equal to the transverse (to $\tilde{n}$) momentum transferred to the nucleus, $q_\perp$ (equal when $\tilde{T}_+ = \tilde{T}_-$). If the approximation

$$q_\perp \simeq |\vec{q}| \ ,$$

is made, then

$$2Hy \geq q$$

and

$$2Hy_{min} \geq q_{min} \ .$$

But the minimum momentum transferred to the nucleus in pair production as determined by Murota *et.al.*,[11], and by Ternovskii is

$$|\vec{q}|_{min} = \frac{kH^2}{2p_+p_-} \ .$$

This result, without H^2 which is approximately equal to unity for small p_+ and p_-, was also obtained by Bhabha[5]. However, in the Thomas-Fermi model of the screened atom, the minimum momentum that can be transferred to the nucleus, which is determined by the inverse Thomas-Fermi radius of the atom through the uncertainty principle, $\Delta q \Delta r \simeq 1$, is

$$|\vec{q}_o| = Z^{1/3}m_e/137 \ .$$

Hence, the minimum momentum transferred to the nucleus in pair production is determined approximately by the maximum of these two values.

$|\vec{q}_o|$ or $|\vec{q}_{min}|$, since the larger of the two serves as a lower limit to the momentum which can be transferred. For the energy range of interest in this experiment,

$$|\vec{q}_{min}| > |\vec{q}_o| \ .$$

Hence,

$$y_{min} = \frac{kH}{4p_+p_-} \ .$$

The upper limit, y_{max}, was determined by physical arguments concerning the size of y, to be

$$y_{max} \simeq 1 \ .$$

Using the above method and integrating over x and y, Ternovskii found the differential cross section for pair production by spin 0 incident particles to be

$$\frac{d^2\sigma_o(E_+,E_-)}{dE_+dE_-} = \frac{4\alpha^2Z^2r_o^2}{3\pi} \frac{1}{k^2} \ln\left(\frac{y_{max}}{y_{min}}\right)\left\{\frac{P-k}{P}\left[A(z) + \frac{2(E_+^2 + E_-^2)}{k^2} B(z)\right]\right.$$

$$\left. + \left(\frac{4E_+E_-}{k^2}\right) \frac{(P - k/2)^2}{P^2(1 + z)} \right\}$$

where

$$z = \frac{m_\pi^2 E_+ E_-}{P(P - k)m_e^2} \ ,$$

$$k \simeq p_+ + p_- \simeq E_+ + E_- \ ,$$

$$A(z) = (1 + 2z)\ln\left(1 + \frac{1}{z}\right) - 2,$$

$$B(z) = (1 + z)\ln\left(1 + \frac{1}{z}\right) - 1,$$

$r_o = e^2/m_e$ = classical radius of the electron,

α = fine structure constant.

For 16 BeV incident particles, Ternovskii suggested the use of the limits

$$y_{max} = 1 \ ,$$

$$y_{min} = \frac{kH}{p_+p_-}$$

(note the difference of a factor of 4 in y_{min} from the derived result above). In order to effect a useful comparison with experiment it is helpful to express the cross section in terms of a new pair of variables, K and μ, where

$$K = p_+ + p_- \simeq E_+ + E_- ,$$

$$\mu = |p_+ - p_-|/(p_+ + p_-) \simeq \frac{|E_+ - E_-|}{E_+ + E_-} ,$$

$$p_+ = \sqrt{E_+^2 - m_e^2} \simeq E_+ ,$$

$$p_- = \sqrt{E_-^2 - m_e^2} \simeq E_- .$$

In terms of these variables the above differential cross section becomes

$$\frac{d^2\sigma_o(\mu,K)}{d\mu dK} = \frac{4\alpha^2 Z^2 r_o^2}{3\pi} \frac{1}{K^2} \ln\left[\frac{\frac{1}{4}K^2(1-\mu^2)D}{m_e K\sqrt{1+z}}\right]\left\{\left(\frac{P-k}{P}\right)\left[A(z) + \frac{K^2(1+\mu^2)}{K^2}B(z)\right]\right.$$

$$\left. + \frac{K^2(1-\mu^2)}{K^2}\frac{(P-K/2)^2}{P^2(1+z)}\right\}\frac{K}{2}$$

where

$$|\vec{k}| \simeq K.$$

The logarithm argument has been expressed in terms of the usual variables, with an extra factor D multiplying it. By varying D it is possible to vary the value given y_{min}. D = 1 for Ternovskii's choice of y_{min}. That such an arbitrary factor should be present can be seen from the theoretical results of Bhabha and of Murota et al.. Each contains a term similar to

$$\ln\left[\frac{\frac{1}{4}K^2(1-\mu^2)}{m_e K\sqrt{1+z}}\right]$$

(Bhabha's result doesn't contain $\sqrt{1+z}$ which is ≃ 1 at low energies and Murota's result has an extra factor of 2 and no θ' dependence in z)

)

except that their results contain an arbitrary parameter α of order of magnitude unity as a result of cutoffs employed in angle integrations. Since Ternovskii's result for this term is obtained using similar angle approximations, it is logical that his result should also contain an arbitrary factor. μ represents the disparity in the pair particle energies and has an integration range from 0.0 to 1.0.

$d\sigma_o/dK$ was obtained by integrating numerically over the pair energy disparity for different values of the total pair energy K. The resulting differential cross section is plotted in Figure 20. The value used for the average square of the nuclear charge in emulsion is $\langle Z^2 \rangle = 459.01$, as given recently by Barkas[22] for standard Ilford K-5 emulsion. It should be noted that the standard value used in previous works is $\langle Z^2 \rangle = 488.4$, which gives a difference of approximately 6.5% in cross section results from our value.

It is also of interest to investigate the total cross section expected per total pair energy interval. The relation for the total cross section, σ_K, for the production of pairs with total energy between K and K + ΔK is

$$\sigma_K = \int_K^{K+\Delta K} \left(\frac{d\sigma}{dK}\right) dK \ .$$

Average curves for σ_K are plotted versus K in Figure 21 for D = $4\sqrt{2}$, 4, $\sqrt{2}$, and 1. Histograms of the total cross section contributions, σ_{o_K}, are given in Figures 22 and 23.

From Figure 21 it is seen that large differences occur in the cross section for different limits in the y integration at small total pair energies (<100 MeV). However, the cross section is affected to a lesser extent at larger total pair energies. Thus, the limits of the y integration can be considered as parameters which can be adjusted to fit experimental results at low pair energies.

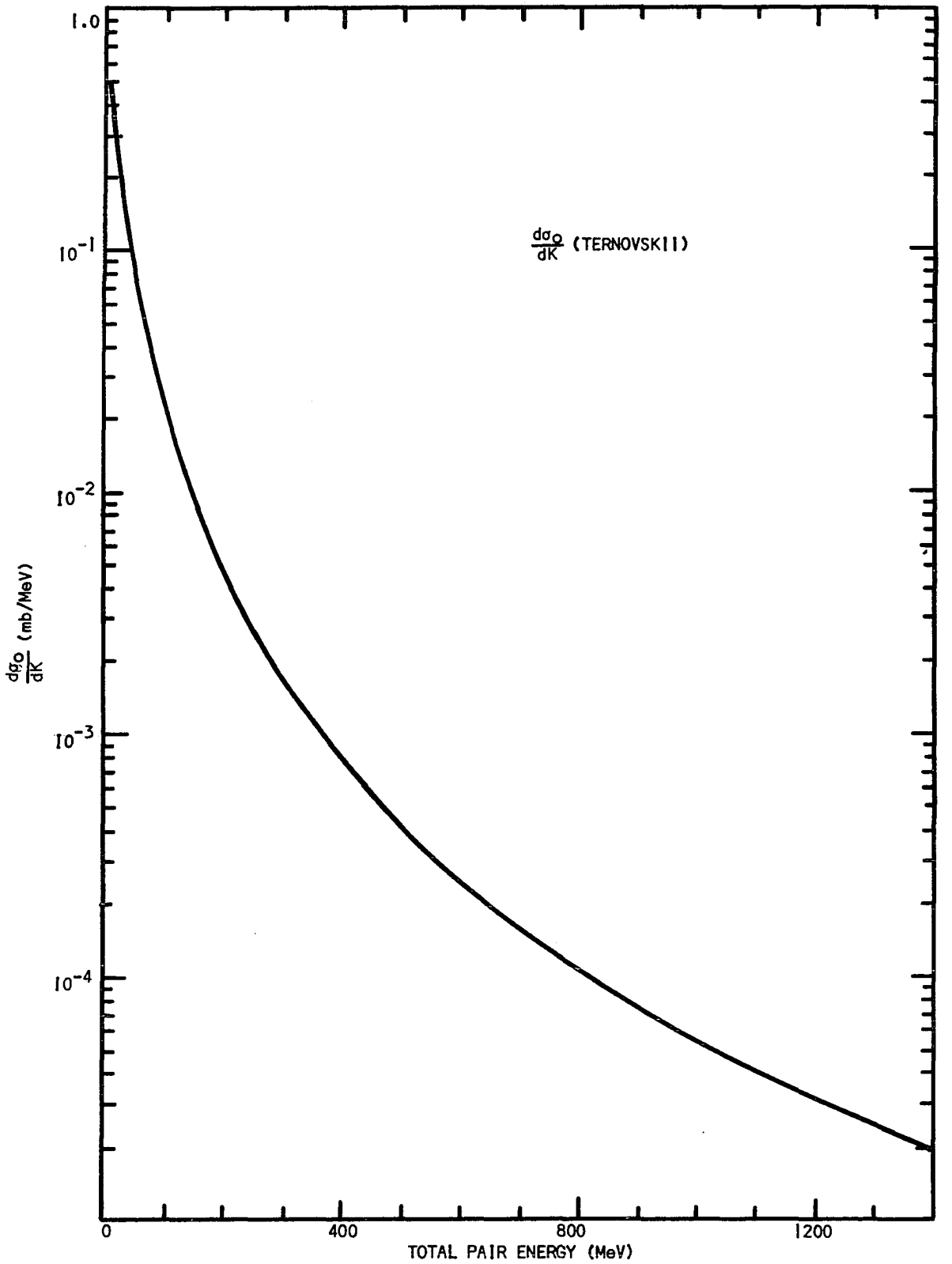

Fig. 20. Ternovskii cross section, differential in K, for pion pair production plotted against the total pair energy, K.

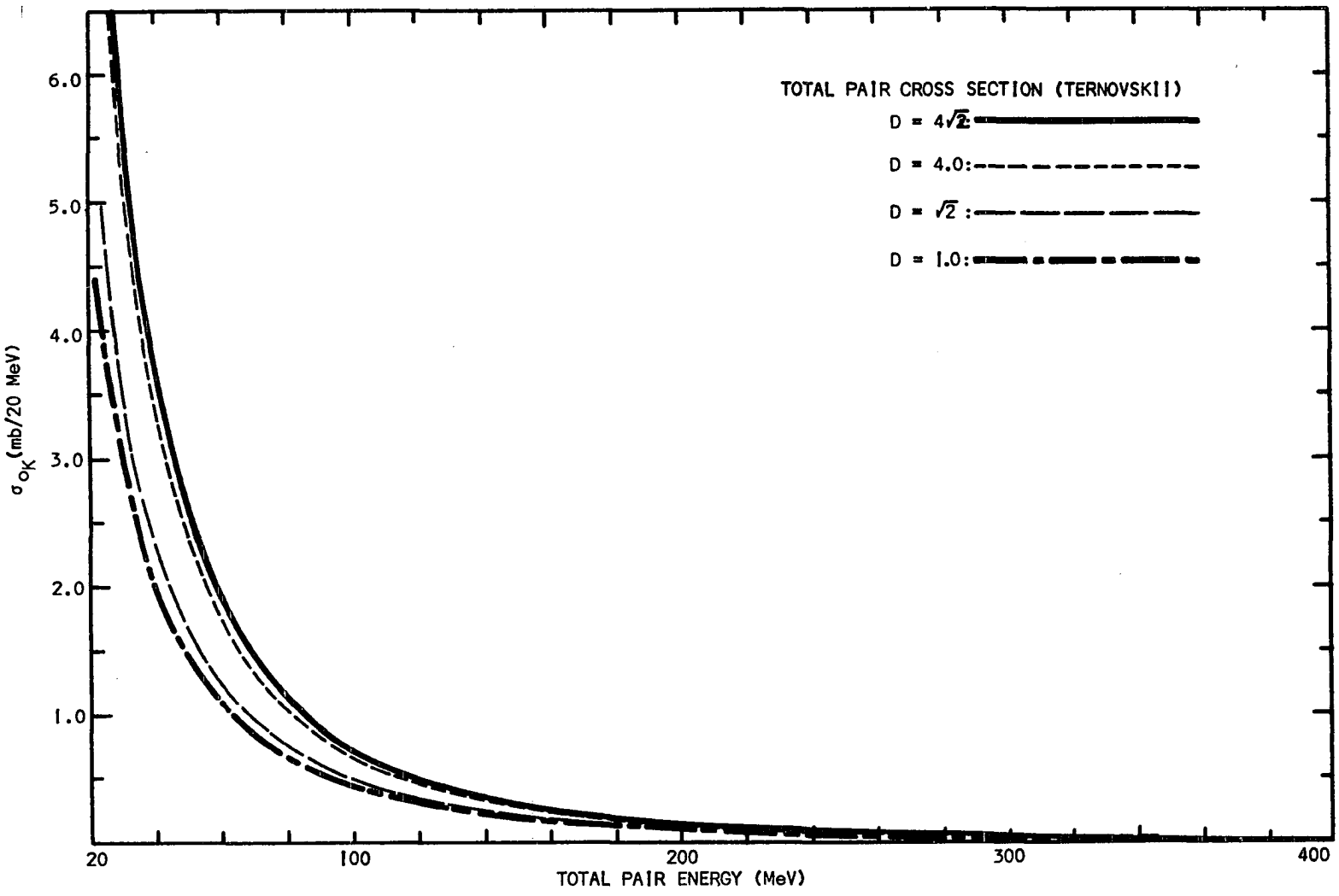

Fig. 21. Average total pair production cross section per 20 MeV interval for four values of the constant D which was inserted in Ternovskii's cross section.

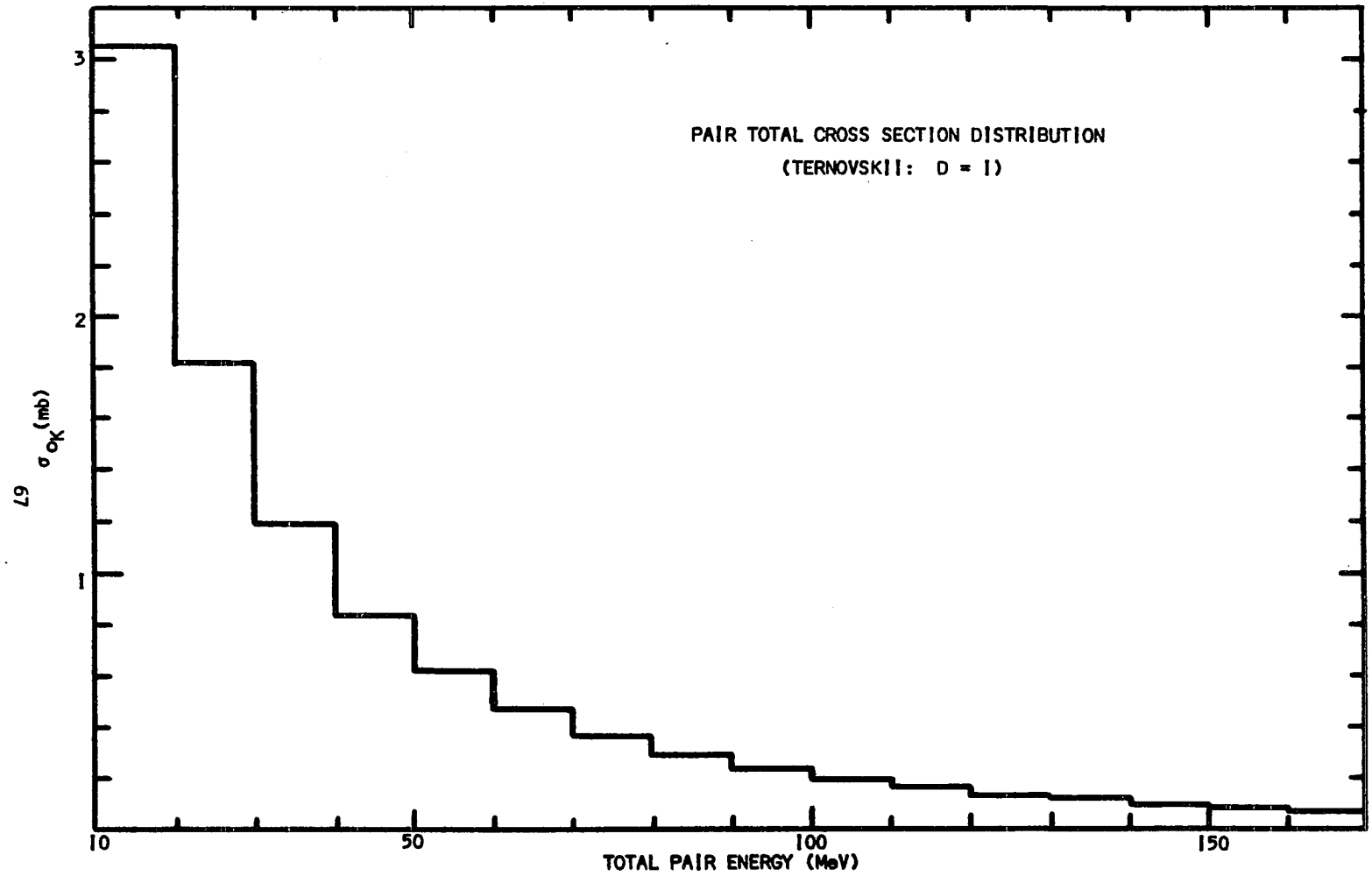

Fig. 22. Distribution of the total cross section, per 10 MeV total pair energy interval, for the production of electron pairs by 16 BeV pions, as predicted by Ternovskii's σ_p cross section term.

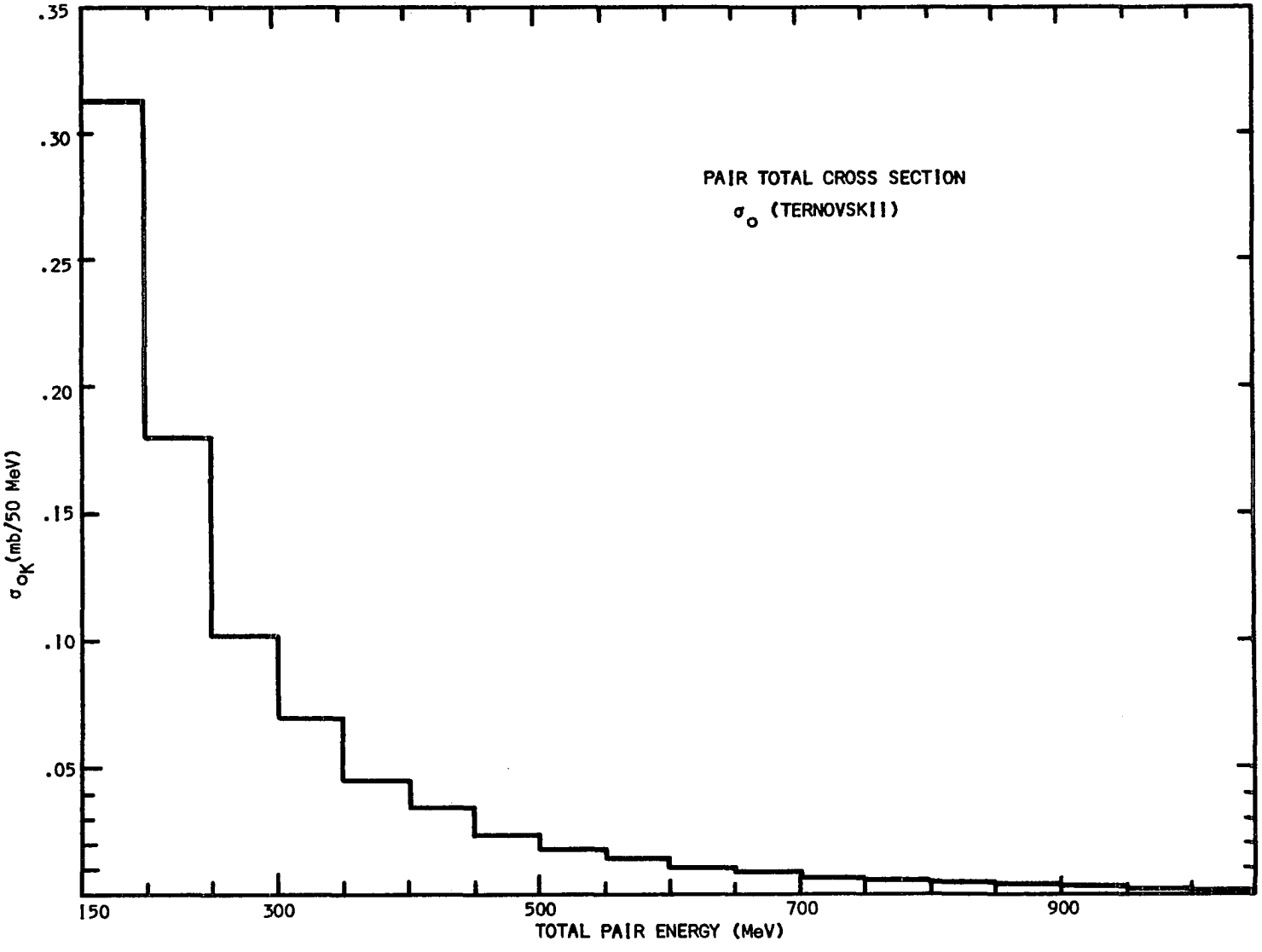

Fig. 23. Distribution of the total cross section for pair production by pions per 50 MeV total pair energy interval as given by Ternovskii's σ_o.

At this point it is convenient to give the corresponding result for spin ½ particles as obtained by Ternovskii in the same manner as above. Using the variables defined above, this result is

$$\frac{d^2\sigma_{\frac{1}{2}}(E_+,E_-)}{dE_+dE_-} = \frac{2\alpha^2Z^2r_o^2}{3\pi K^2}\ln\left(\frac{E_+E_-}{m_eKH}\right)\left\{\frac{P^2+(P-K)^2}{P^2}\left[A(z) + \frac{2(E_+^2+E_-^2)}{K^2}B(z)\right]\right.$$

$$\left. + \frac{K^2}{P^2}\left[C(z) + \frac{2(E_+^2+E_-^2)}{K^2}D(z)\right] + \frac{8p_+p_-}{K^2}\frac{(P-K)}{P(1+z)}\right\} .$$

Changing variables to μ and K, and introducing an arbitrary factor, D, as above, to allow the possibility of varying the limit of integration, y_{min}, the expression becomes

$$\frac{d^2\sigma_{\frac{1}{2}}(\mu,K)}{d\mu dK} = \frac{2\alpha^2Z^2r_o^2}{3\pi K^2}\ln\left[\frac{\frac{1}{2}K^2(1-\mu^2)D}{m_eK\sqrt{1+z}}\right]$$

$$\times\left\{\frac{P^2+(P-K)^2}{P^2}\left[A(z) + \frac{K^2(1+\mu^2)}{K^2}B(z)\right]\right.$$

$$+ \frac{K^2}{P}\left[C(z) + \frac{K^2(1+\mu^2)}{K^2}D(z)\right]$$

$$\left. + 2(1-\nu^2)\frac{(P-K)}{P(1+z)}\right\}\frac{K}{2} .$$

where

$$C(z) = \left(\frac{1+2z}{1+z}\right) - 2z\ln\left(1+\frac{1}{z}\right) ,$$

$$D(z) = 1 - z\ln\left(1+\frac{1}{z}\right) .$$

All of the integrals were evaluated numerically using the method of Gaussian quadrature. The computations were performed on IBM 1410 and 7040 computers and on the OSAGE computer.

The cross section terms for the diagrams B and B' are also calculated by Ternovskii in a manner similar to that described above for the terms corresponding to A and A', but considering the nucleus through a diffraction approximation[23]. These contributions (first type) were broken into two parts, the "Coulomb" terms ($d\sigma_c$) and the "Diffraction" terms ($d\sigma_d$). Contributions from these terms were calculated for the region

$$x = \frac{m_\pi^2 p_+ p_+}{m_e^2 P(P-K)} >> 1 \ .$$

This "Coulomb" contribution for incident pions is

$$\frac{d^2\sigma_c(E_+,E_-)}{dE_+dE_-} = \frac{8\alpha^2 r_o^2 Z^2 m_e^2}{3\pi m_\pi^2} \frac{1}{k^2} \left(\frac{P-k}{P}\right)\left(\frac{E_+^2 + E_-^2}{k^2}\right) \ln\left[\frac{m_\pi^2 E_+ E_-}{m_e^2 P(P-k)}\right]$$

$$\times \ln\left[\frac{2\pi P(P-k)}{R_o k m_\pi^2}\right]$$

The "diffraction" term for spin 0 incident particles is

$$\frac{d^2\sigma_d(E_+,E_-)}{dE_+dE_-} = \frac{2\alpha^2 R_o^2}{\pi} \left(\frac{P-k}{Pk^4}\right) \ln\left(\frac{m_\pi^2 E_+ E_-}{m_e^2 P(P-k)}\right)$$

$$\times \left[(E_+^2 + E_-^2) I_1 + \frac{2E_+E_-(P-k/2)^2}{P(P-k)} I_2\right]$$

where

$$I_1 = \int_o^\infty \left[-\frac{1}{q} + \left(\frac{2q^2+1}{q^2\sqrt{1+q^2}}\right) \ln\left(q + \sqrt{1+q^2}\right)\right] J_1^2(2m_\pi R_o q)\, dq \ ,$$

$$I_2 = \int_o^\infty \left[\frac{1}{q} - \left(\frac{2q^2+1}{q^2\sqrt{1+q^2}}\right)\ln(q + \sqrt{1+q^2})\right] J_1^2(2m_\pi R_o q)dq \quad ,$$

$R_o = .5\, r_o Z^{1/3}$ = nuclear radius as defined by Ternovskii,

J_1 = first order Bessel function,

$\langle Z^{1/3} \rangle = 1.927$ for emulsion,

$\langle Z^{2/3} \rangle = 4.658$ for emulsion[22].

Numerical integration yeilded the values

$$I_1 = 0.127 \quad ,$$

$$I_2 = 0.0424 \quad .$$

A change of integration variables to K and μ gives the differential cross section terms the forms

$$\frac{d^2\sigma_c(\mu,K)}{d\mu dK} = \frac{8\alpha^2 r_o^2 Z^2 m_e^2}{3\pi m_\pi^2 K^2}\left(\frac{P-K}{P}\right)\left(\frac{1+\mu^2}{2}\right)\ln\left[\frac{\frac{1}{4}m_\pi^2 K^2(1-\mu^2)}{P(P-K)m_e^2}\right]$$

$$\times \ln\left[\frac{2\pi P(P-K)}{R_o K m_\pi^2}\right]\frac{K}{2}$$

$$\frac{d^2\sigma_d(\mu,K)}{d\mu dK} = \frac{2\alpha^2 R_o^2}{\pi}\left(\frac{P-K}{PK^4}\right)\ln\left[\frac{\frac{1}{4}m_\pi^2 K^2(1-\mu^2)}{m_e^2 P(P-K)}\right]\left[\tfrac{1}{2}K^2(1+\mu^2)I_1\right.$$

$$\left. + \frac{\frac{1}{2}K^2(1-\mu^2)(P-K/2)^2}{P(P-K)} I_2\right]\frac{K}{2} \quad .$$

Contributions, σ_k, of these terms to the cross section per 20 MeV energy interval for 16.2 BeV incident pions were calculated in a manner analagous to that used for $d\sigma_o$. The resulting histograms are plotted for $d\sigma_c$ in Figure 24, and for $d\sigma_d$ in Figure 25. K>>1600 MeV is the approximate region of validity. These contributions can be seen to be negligible compared to the contributions from $d\sigma_o$ (Figures 20, 22 and 23) for K<1400 MeV.

Although all the cross section calculations except that of Ternovskii considered only spin ½ particles, it will be of interest to consider the results of the more noteworthy of the calculations, namely those of Bhabha, Murota et.al., and Zapolsky. Spin ½ cross sections differ negligibly from spin 0 cross sections, at least within the approximations made by Ternovskii. The ratio of the numerical values for Ternovskii's spin 0 and spin ½ cross sections at a given energy is unity for all energies of interest.

Bhabha's result was obtained by making a perturbation theory treatment corresponding to the cross section contributions from the Feynman graphs A and A' (Figure 19). The incident particle was considered to be moving along a straight line with uniform velocity throughout the interaction. Two arbitrary constants (of order of magnitude unity) occur in this cross section due to the use of cutoffs in angle integrations to avoid divergences. These constants must be determined experimentally, but in most experimental comparisons they have been set equal to unity. Bhabha's cross section, differential in final electron and positron energies, for the production of an

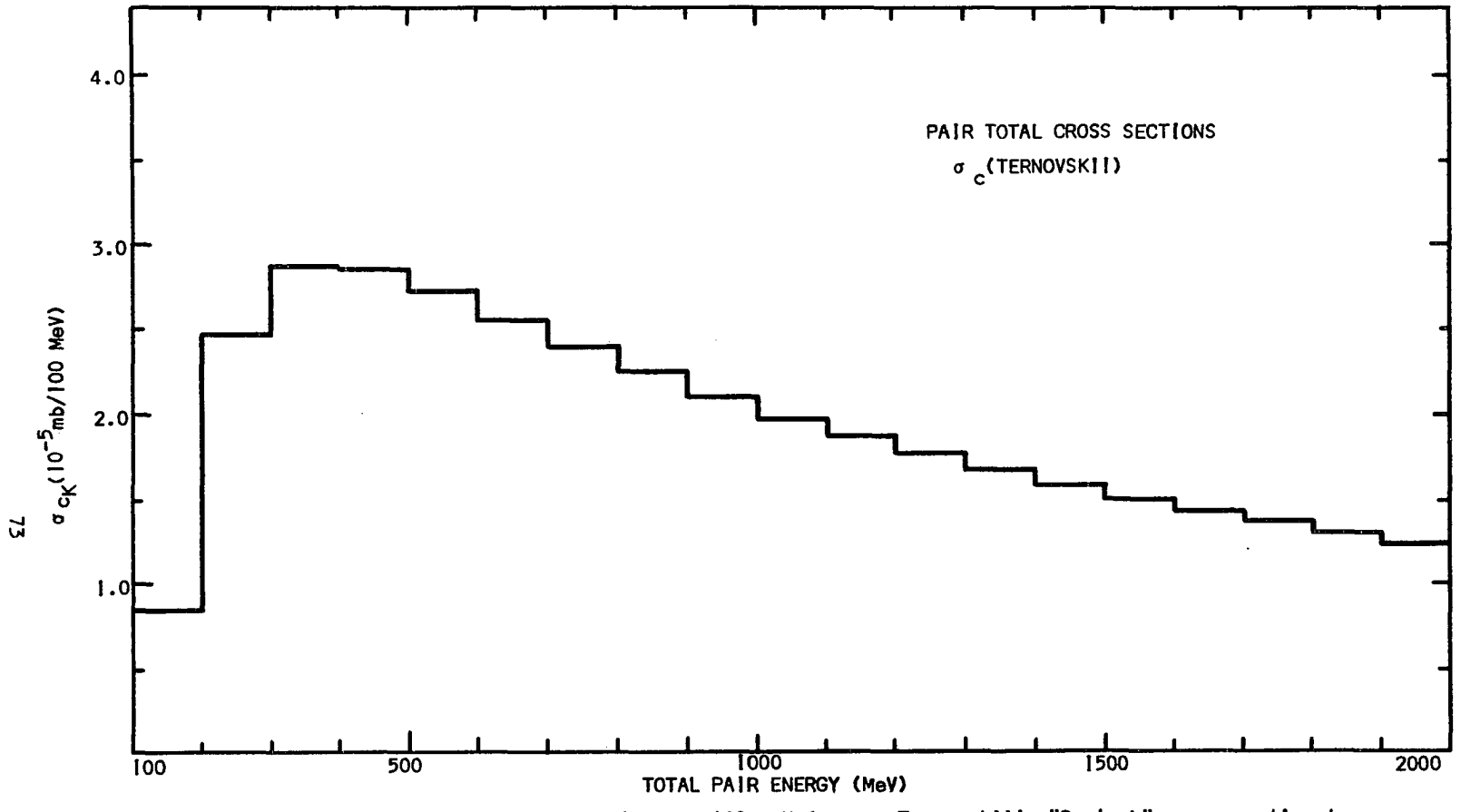

Fig. 24 . Distribution of total cross section per 100 MeV for σ_c, Ternovskii's "Coulomb" cross section term.

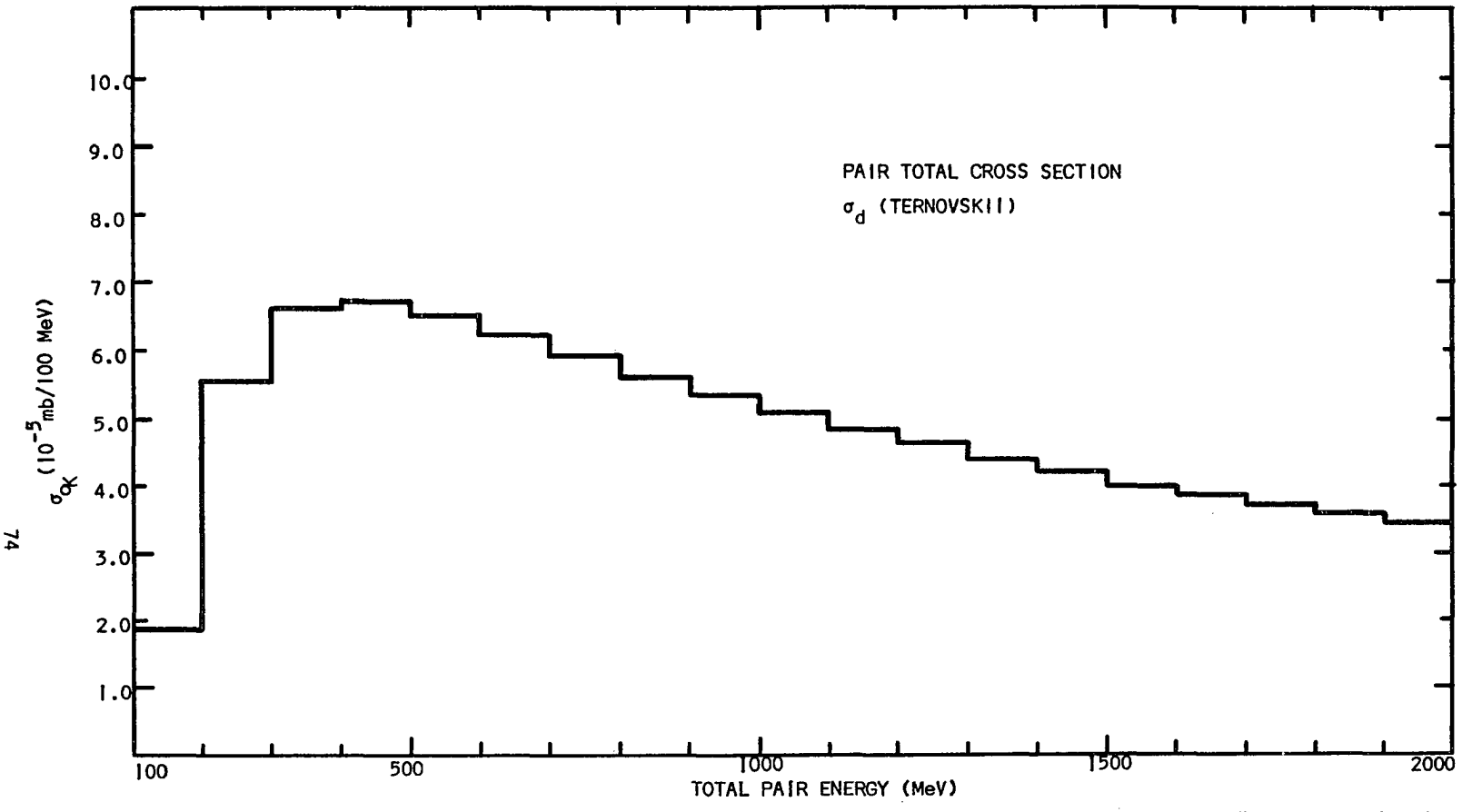

Fig. 25. Distribution of the total cross section per 100 MeV for σ_d, Ternovskii's "diffraction" cross section term.

an electron-positron pair by a relativistic charged fermion of mass m_π is

$$\frac{d^2\sigma_B(E_+,E_-)}{dE_+dE_-} = \frac{8}{\pi}\left(\frac{r_o Z^{22}}{137}\right)\left[\frac{E_+^2 + E_-^2 + \frac{2}{3}E_+E_-}{(E_+ + E_-)^4}\right]\ln\left(\frac{\alpha_B E_+E_-}{m_e(E_+ + E_-)}\right)\ln\left(\frac{\alpha'\gamma m_e}{(E_+ + E_-)}\right),$$

where

$\gamma = E/m_\pi$,

E_+, E_- = pair electron positron energies,

r_o = classical electron radius,

Z = nuclear charge,

α_B, α' = arbitrary constants of order unity,

$E_+, E_- >> m_e$,

$E_+, E_- << \gamma m_e$,

m_π = primary particle mass (pion),

E = primary particle energy.

This cross section is valid in the low energy region, as is seen by the limits placed on E_+, E_-.

For the higher energy region Bhabha obtained the approximate equation

$$\frac{d^2\sigma_B(E_+,E_-)}{dE_+dE_-} = \frac{8}{\pi}\left(\frac{r_o Z}{137}\right)^2 \frac{m_e^2\gamma^2}{(E_+ + E_-)^4}\ln(2\alpha\gamma),$$

where

$$E_+, E_- >> m_e\gamma \ ,$$

$$E_+, E_- << \gamma m \ ,$$

$$|E_+ - E_-| << E_+ + E_+ \ .$$

For 16.2 BeV primary particles it is possible to join these two cross sections at K = 60 MeV $\approx \gamma m_e$, although neither cross section is strictly valid near this energy. At approximately this energy the two terms become of the same magnitude.

In order to make a more meaningful comparison with experiment it is desirable to change to the variables μ and K as was done above. The above cross sections become

$$\frac{d^2\sigma_B(\mu,K)}{d\mu dK} = \frac{4}{3\pi}\left(\frac{r_o Z}{137}\right)^2 \left[\frac{2+\mu^2}{K}\right] \ln\left[\frac{\alpha_B K(1-\mu^2)}{4m_e}\right] \ln\left[\frac{\alpha'\gamma m_e}{K}\right]$$

$$\frac{d^2\sigma_B(\mu,K)}{d\mu dK} = \frac{4}{\pi}\left(\frac{r_o Z}{137}\right)^2 \frac{m_e^2\gamma^2}{K^3} \ln(2\alpha_B\gamma).$$

Now it is desirable to apply these cross sections to the case of 16 BeV pion primary particles. The pair energy disparity, μ, can be removed by integrating numerically from μ = 0.0 to μ = 1.0. The cross section, $\frac{d\sigma}{dK}$, thus obtained is plotted in Figure 26, with the above cross sections smoothly joined at K = 60 MeV.

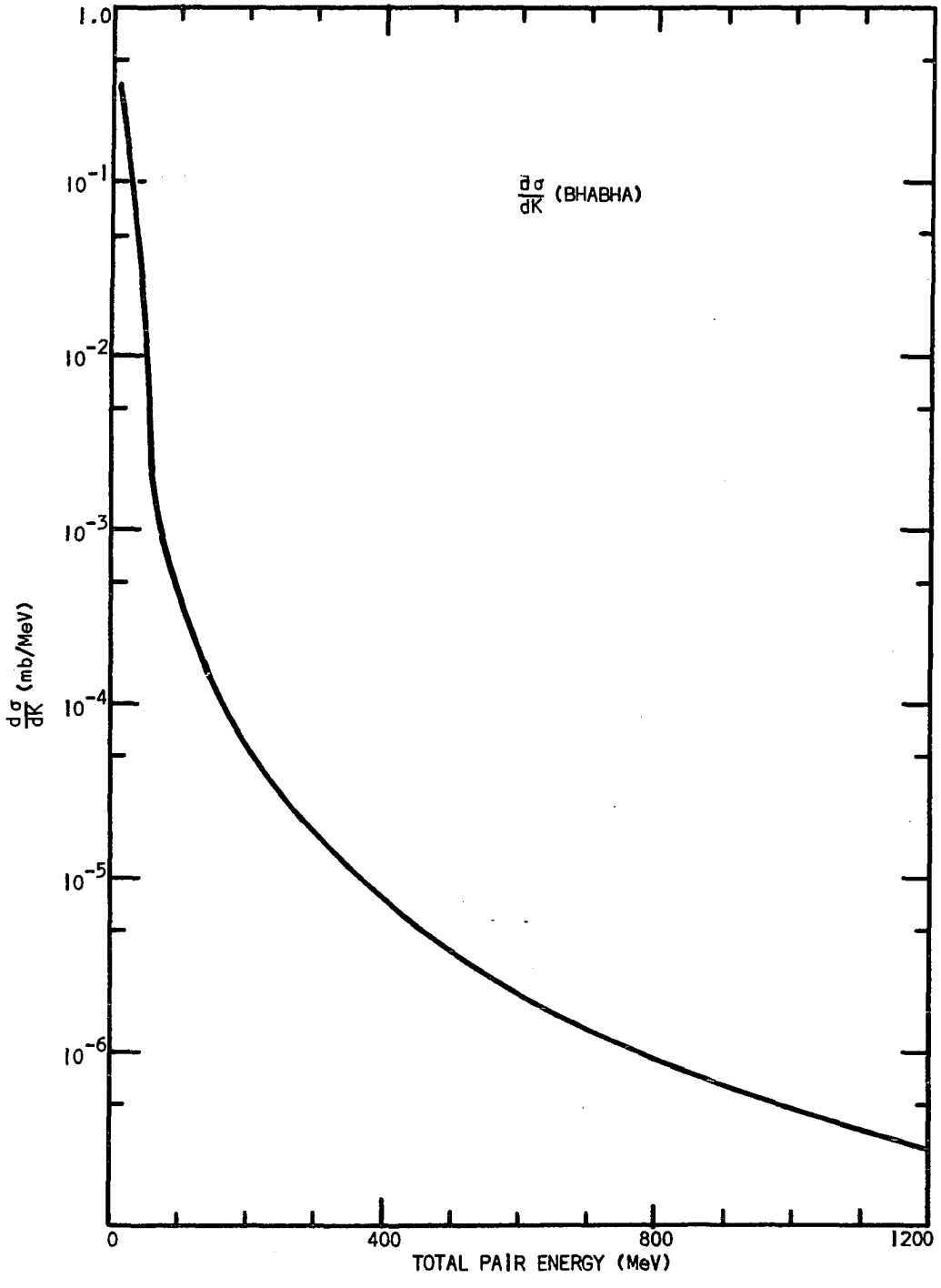

Fig. 26. Bhabha's cross section, differential in K, for the production of electron pairs by pions vs. the total pair energy.

In Figure 27 the total cross section per 20 MeV total pair energy is plotted. Numerical integration was again used to obtain the total cross section. In the above results, α_B is set equal unity.

In the cross section calculation of Murota et al, the Feynman-Dyson formulation of quantum electrodynamics was used to determine the cross section contributions from diagrams A and A' as well as from B and B' for pair production by high energy charged ferminons. The contributions from B and B' are shown by Murota to be negligible for heavy incident particles ($m>>m_e$), although their contributions are important for primary electrons. Cross terms between A + A' and B + B' were shown to be unimportant by calculating an upper limit to their contributions for heavy primary particles. An expression is obtained for the differential cross section which, for heavy incident particles, is valid as long as the participating particles have relativistic energies. The expression for the non-screened cross section, which also contains an arbitrary constant α_m of magnitude unity as a result of a cutoff employed in the angle integrations, is

$$\frac{d^2\sigma(E_+,E_-)}{dE_+dE_-} = \frac{2}{\pi}(Ze^2)^2\left(\frac{e^2}{m_e}\right)^2\left[\ln\left(2\,\frac{\alpha_m E_+E_-}{kH'}\right)-1\right]$$

$$\times\left[\left\{\frac{E_+^2+E_-^2}{k^4}\left[\left(1+\frac{4}{3}z\right)\log\left(1+\frac{1}{z}\right)-\frac{4}{3}\right]\right.\right.$$

$$+\frac{2}{3}\frac{E_+E_-}{k^4}\left[(1+2z)\log\left(1+\frac{1}{z}\right)-2\right]\Bigg\}\frac{E^2+E'^2}{E^2}$$

$$+\frac{8}{3}\frac{E_+E_-}{k^4}\frac{1}{1+z}\frac{E'}{E}$$

$$\left.+\left\{\frac{E_+^2+E_-^2}{k^4}\left[\frac{1}{3(1+z)}+\frac{1}{z}-\frac{4}{3}\log\left(1+\frac{1}{z}\right)\right]+\frac{2}{3}\frac{E_+E_-}{k^4}\left[\frac{1}{1+z}+\frac{1}{z}-2\log\left(1+\frac{1}{z}\right)\right]\right\}\right.$$

$$\left.\times\frac{zk^2}{E^2}\right],$$

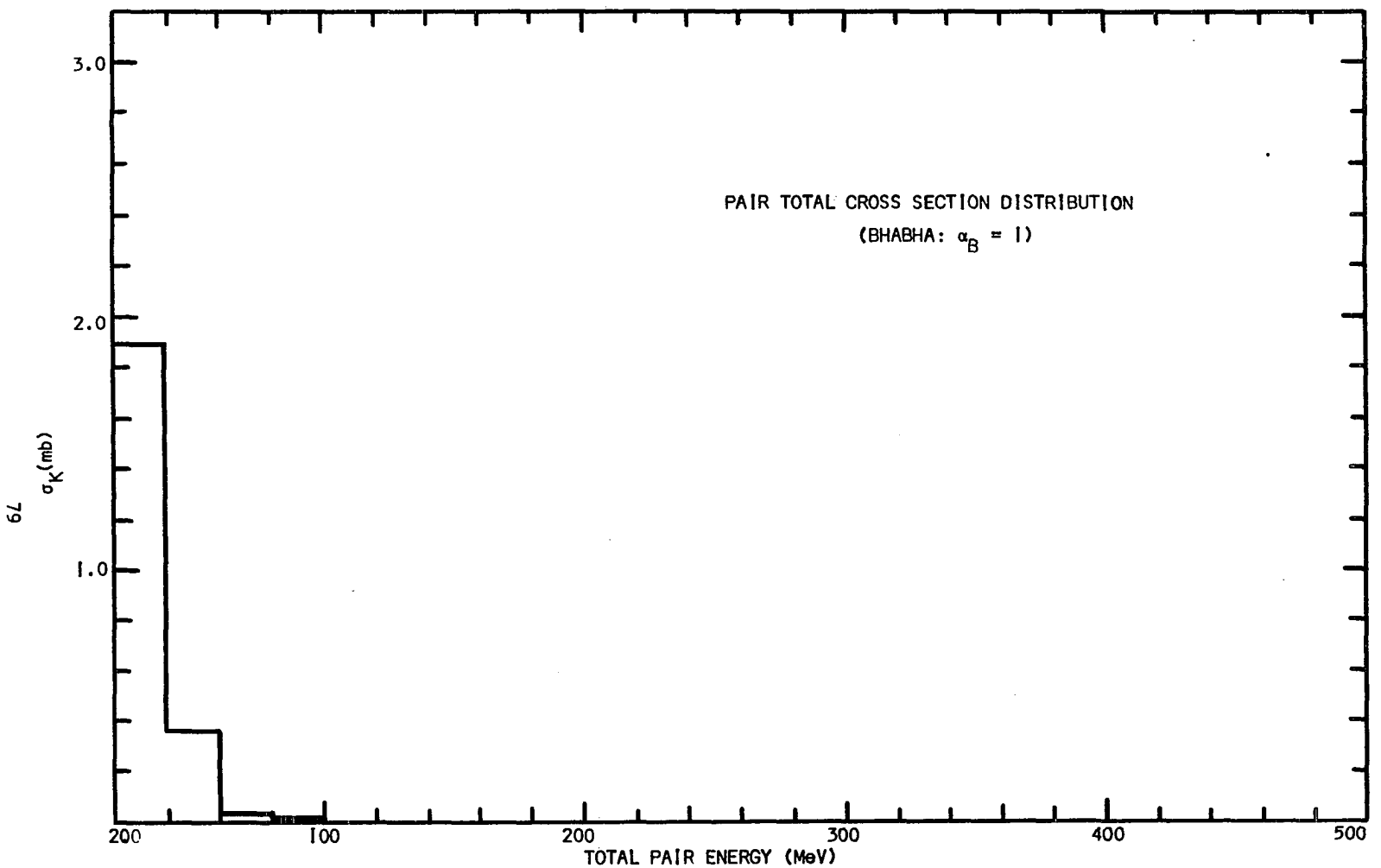

Fig. 27. Distribution of Bhabha's total cross section for pair production by 16BeV pions, per 20 MeV energy interval

where

$$k = P - P' \simeq E_+ + E_- ,$$

$$z' = \frac{m_\pi^2 E_+ E_-}{m_e^2 E E'} ,$$

E = energy of incident particle,

$E' = E - E_+ - E_-$ = energy of scattered particle,

m_π = mass of incident particle,

$$H' = [m_e^2 + m_\pi^2 E_+ E_- / E E']^{\frac{1}{2}} = m_e \sqrt{1 + z'} .$$

Changing variables to μ and K as in the two previous cases, this cross section becomes

$$\frac{d^2\sigma(\mu,K)}{dK d\mu} = \frac{1}{\pi} (Z_e^2)^2 \left(\frac{e^2}{m_\pi}\right)^2 \left[\ln\left(\frac{\alpha_m K(1-\mu^2)}{2H'}\right) - 1\right]$$

$$\times \left[\left\{ \frac{1+\mu^2}{2K}\left[\left(1 + \frac{4}{3}z\right)\ln\left(1 + \frac{1}{z}\right) - \frac{4}{3}\right] + \frac{1-\mu^2}{6K}\left[(1 + 2z)\ln\left(1 + \frac{1}{z}\right) - 2\right]\right\}\left[\frac{E^2 + (E-K)^2}{E^2}\right] \right.$$

$$+ \frac{2(1-\mu^2)(E-K)}{3K(1+z)E}$$

$$\left. + \left\{ \frac{1+\mu^2}{2K}\left[\frac{1}{3(1+z)} + \frac{1}{z} - \frac{4}{3}\ln\left(1 + \frac{1}{z}\right)\right] + \frac{1-\mu^2}{6K}\left[\frac{1}{1+z} + \frac{1}{z} - 2\ln\left(1 + \frac{1}{z}\right)\right]\right\} \frac{zK^2}{E^2} \right]$$

where

$$z = \frac{m_\pi^2 K^2 (1-\mu^2)}{4 m_e^2 E E'} .$$

This cross section can now be evaluated for 16 BeV incident fermions with pion mass. $\frac{d\sigma}{dK}$ is obtained in the same manner as above, and is plotted in Figure 28. The total cross section per 20 MeV total pair energy interval is plotted in Figure 29. For these results, α_m equals unity.

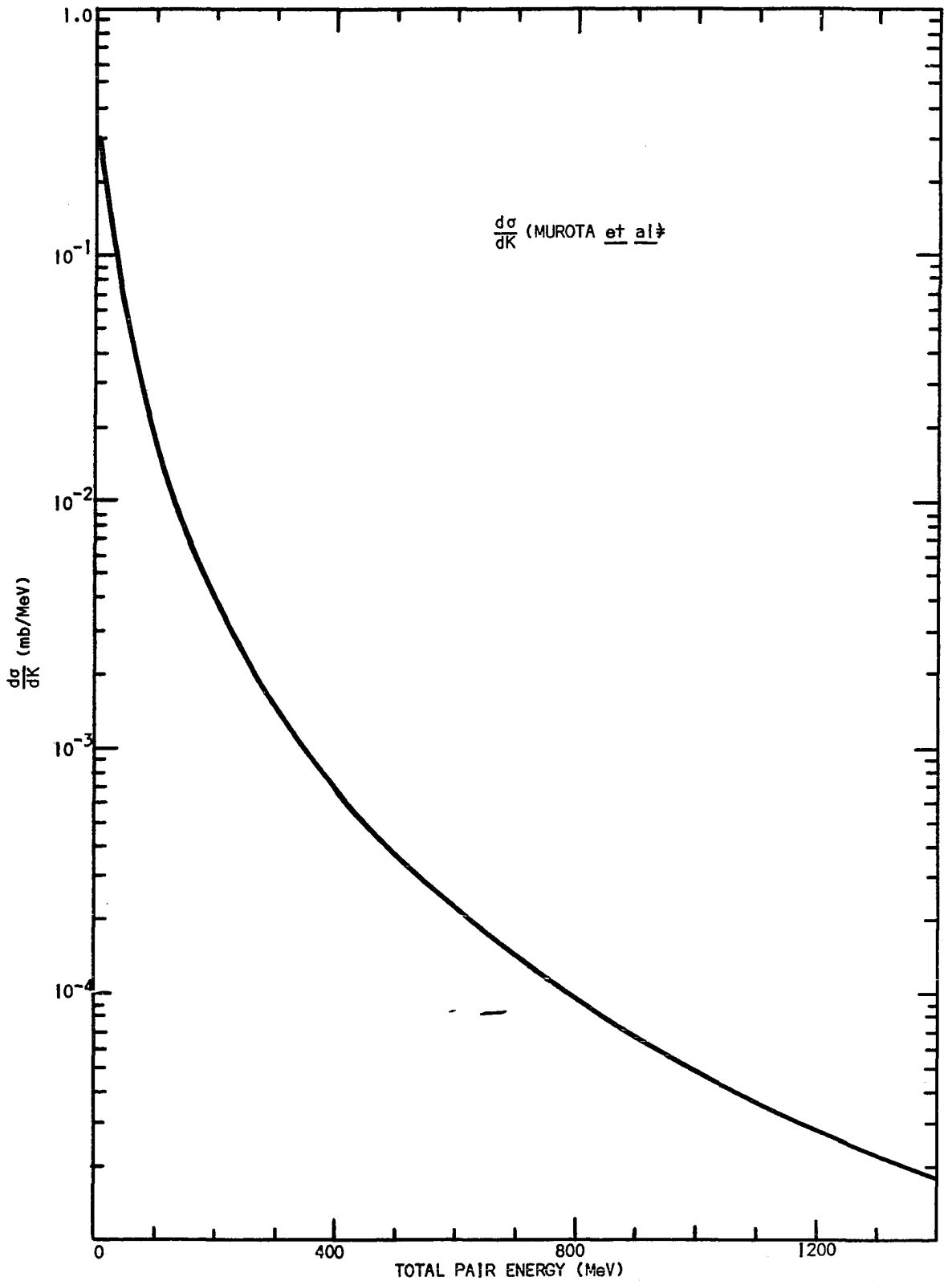

Fig. 28. Murota cross section, differential in K, plotted against K, the total pair energy.

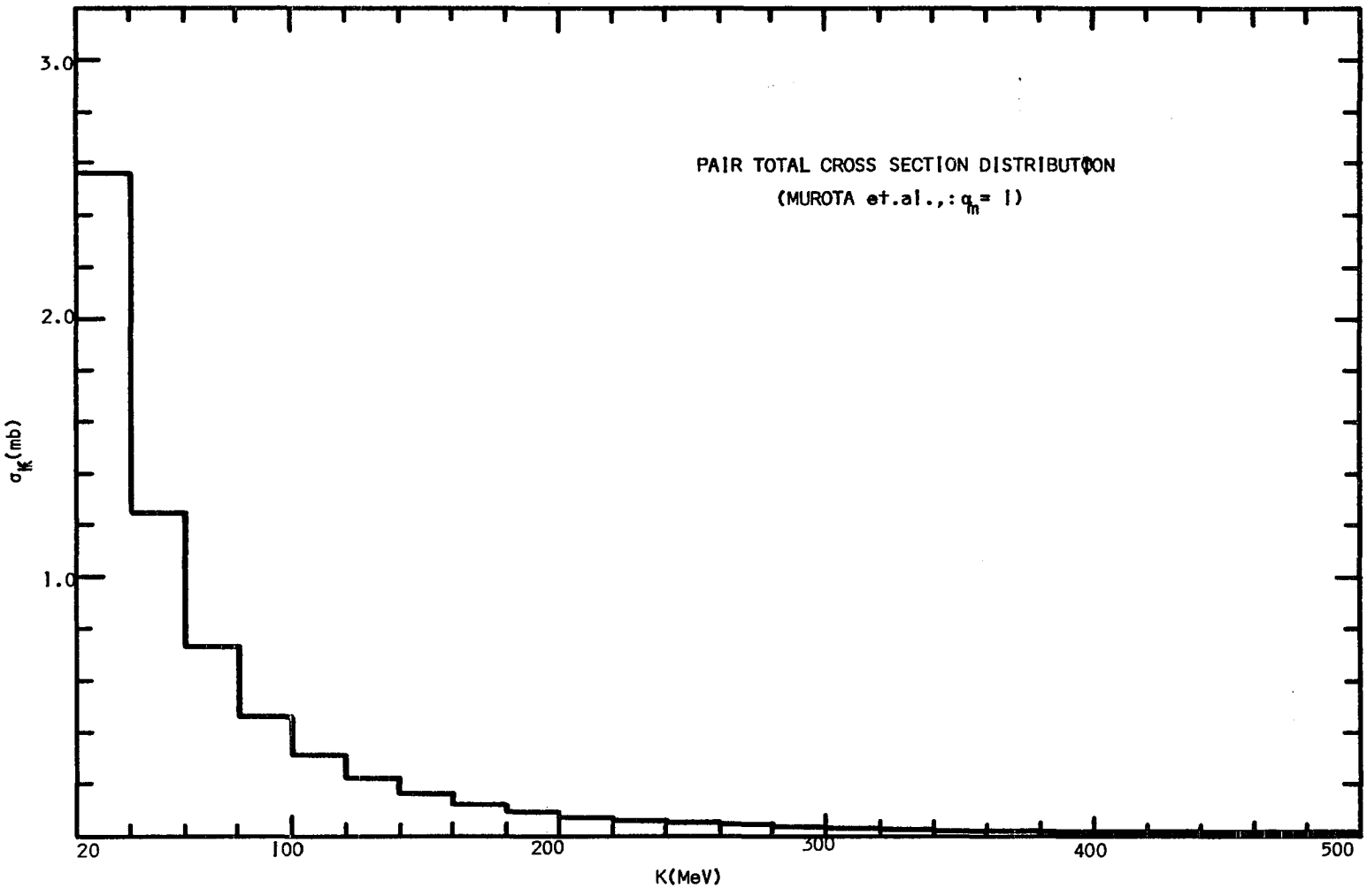

Fig. 29. Distribution of Murota's total cross section for pair production by 16 BeV pions, per 20 MeV energy interval.

The final theoretical treatment which will be considered in this work is the one by Zapolsky (1962). He showed, for heavy incident particles, that only diagrams A and A' are important. Using a Weizacker-Williams type approach, he calculated the differential cross section, valid in the low pair energy region, to be (neglecting screening of the atomic electrons)

$$\frac{d^2\sigma(E_+,E_-)}{dE_+dE_-} = \frac{Z^2e^8}{8(2\pi)^6E^2}\{E_a[4\pi A_3 \ln Q + 4\pi A_4 + 4\pi A_1 - 8\pi A_2]$$
$$+ E_b[16\pi A_5 \ln Q + 16\pi A_6 - 16\pi A_7]$$
$$- E_c[32\pi A_1] - E_d[32\pi A_5] - E_e[8\pi A_3]\}$$

where

$$E_a = \frac{(E^2+E'^2)(E_+^2+E_-^2)}{K^4} ,$$

$$E_b = \frac{E_+E_-(E^2+E'^2)}{K} m_e^2 ,$$

$$E_c = \frac{EE'E_+E_-}{K^4} ,$$

$$E_d = m_e^2E_c ,$$

$$E_e = \frac{EE'(E_+^2+E_-^2)}{K^4}$$

$$E_f = \frac{E_+^2E_-^2}{K^4} m_e^2m_\pi^2 ,$$

$$E_g = \frac{E_+E_-(E_+^2+E_-^2)}{K^4} m_\pi^2 ,$$

E, m_π = incident particle energy, mass (pion),

$$A_1 = -\frac{1}{m_e^2}\left[\frac{1}{3}\log(m_e/\delta) - \frac{2}{9}\right],$$

$$A_2 = \frac{1}{2m_e^2}\left[\log(m_e/\delta) - 0.734\right],$$

$$A_3 = \frac{1}{m_e^2}\left[\log(m_e/\delta) - \frac{1}{2}\right],$$

$$A_4 = \frac{1}{m_e^2}\left[\log(m_e/\delta) - 0.9\right],$$

$$A_5 = \frac{1}{m_e^4}\left[\frac{1}{6}\log(m_e/\delta) - \frac{1}{12}\right],$$

$$A_6 = \frac{1}{m_e^4}\left[\frac{5}{36}\log(m_e/\delta) - 0.12\right],$$

$$A_7 = \frac{11}{6m_e^4}\left[\frac{1}{6}\log(m_e/\delta) - 0.086\right],$$

$$\delta = \frac{m_e^2(E_+ + E_-)}{2E_+E_-} + \frac{(E_+ + E_-)m_\pi^2}{2EE'},$$

$$Q = \frac{EE'}{E_+E_-}\left(\frac{m_e}{m_\pi}\right)^2,$$

$$K = E_+ + E_-.$$

Approximations made in this calculation limit the region of expected validity of this expression to

$$2m_e < K << 2m_e E/m_\pi .$$

For the higher energy region an asymptotic approximation was employed. The result obtained is the same as the equation given above by Bhabha in the high energy region.

After changing variables to μ and K, the expression for the cross section remains the same, but the variables become

$$E_a = \frac{(E+E'^2)(1+\mu^2)}{K^2} ,$$

$$E_b = \frac{(1-\mu^2)(E^2+E'^2)m_e^2}{4K^2} ,$$

$$E_c = \frac{(1-\mu^2)EE'}{4K^2} ,$$

$$E_d = m_e^2 E_c ,$$

$$E_e = \frac{EE'(1+\mu^2)}{2K^2}$$

$$E_f = \frac{1}{16}(1-\mu^2)^2 m_e^2 m_\pi^2 ,$$

$$E_g = \frac{1}{8}(1-\mu^2)(1+\mu^2)m_\pi^2 ,$$

$$Q = \frac{4EE'}{K^2(1-\mu^2)}\left(\frac{m_e}{m_\pi}\right)^2 ,$$

$$\delta = \frac{2m_e^2}{K(1-\mu^2)} + \frac{Km_\pi^2}{2EE'} .$$

If we now specialize this cross section to 16.2 BeV incident fermions with pion mass, the differential cross section, $d\sigma/dK$, thus obtained is plotted in Figure 30. A histogram of the total cross section for 20 MeV intervals is given in Figure 31. For this special case, the region of validity of the above calculation is $2m_e < K < 60$ MeV. Above this energy the asymptotic approximation is used.

It should be noted that, in all of the above calculations, screening of the atomic electrons was considered. The screened cross section is meaningful only when it is less than the corresponding

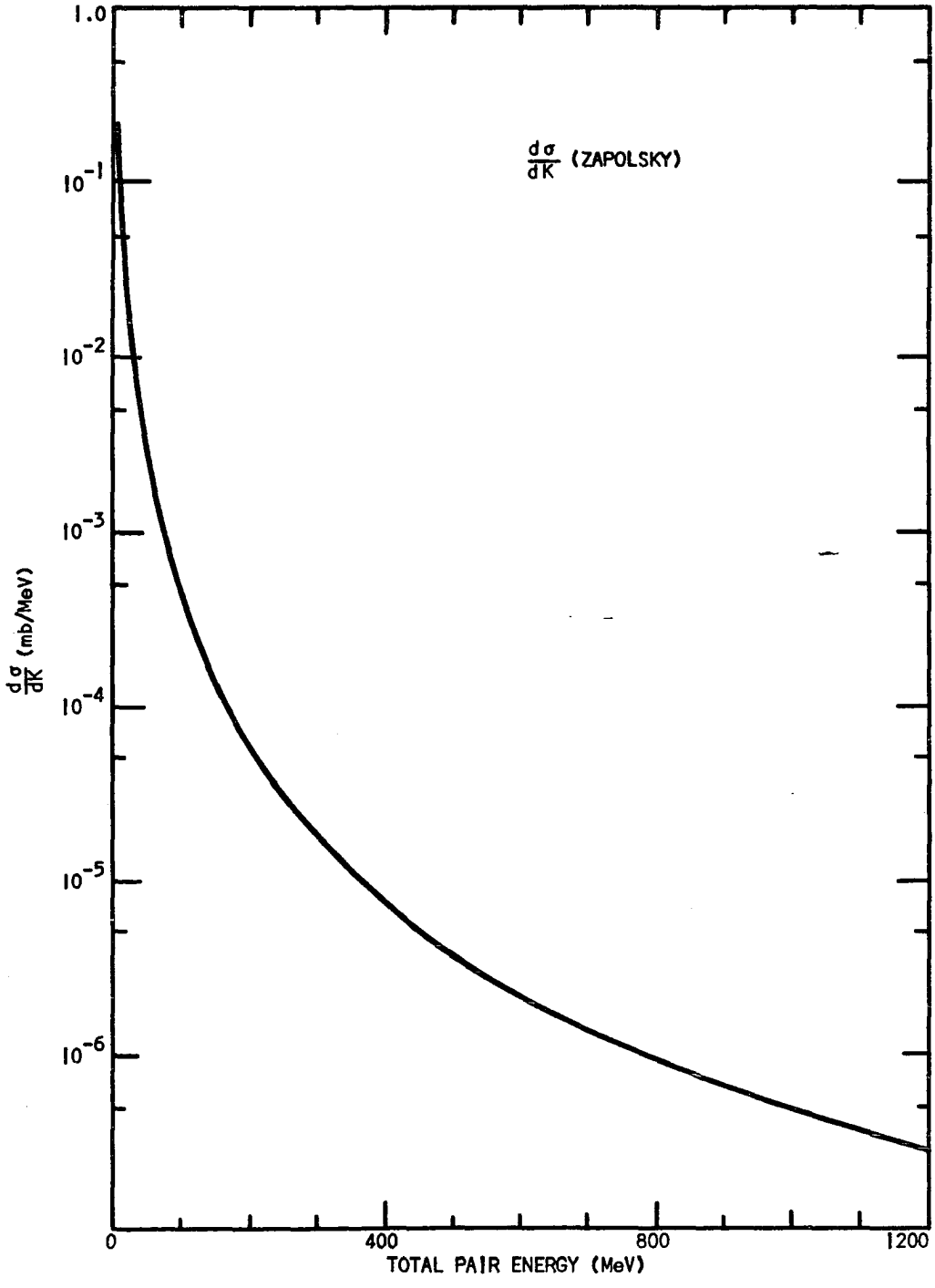

Fig. 30. Zapolsky cross section, differential in K, for the production of electron pairs by pions vs. K, the total pair energy.

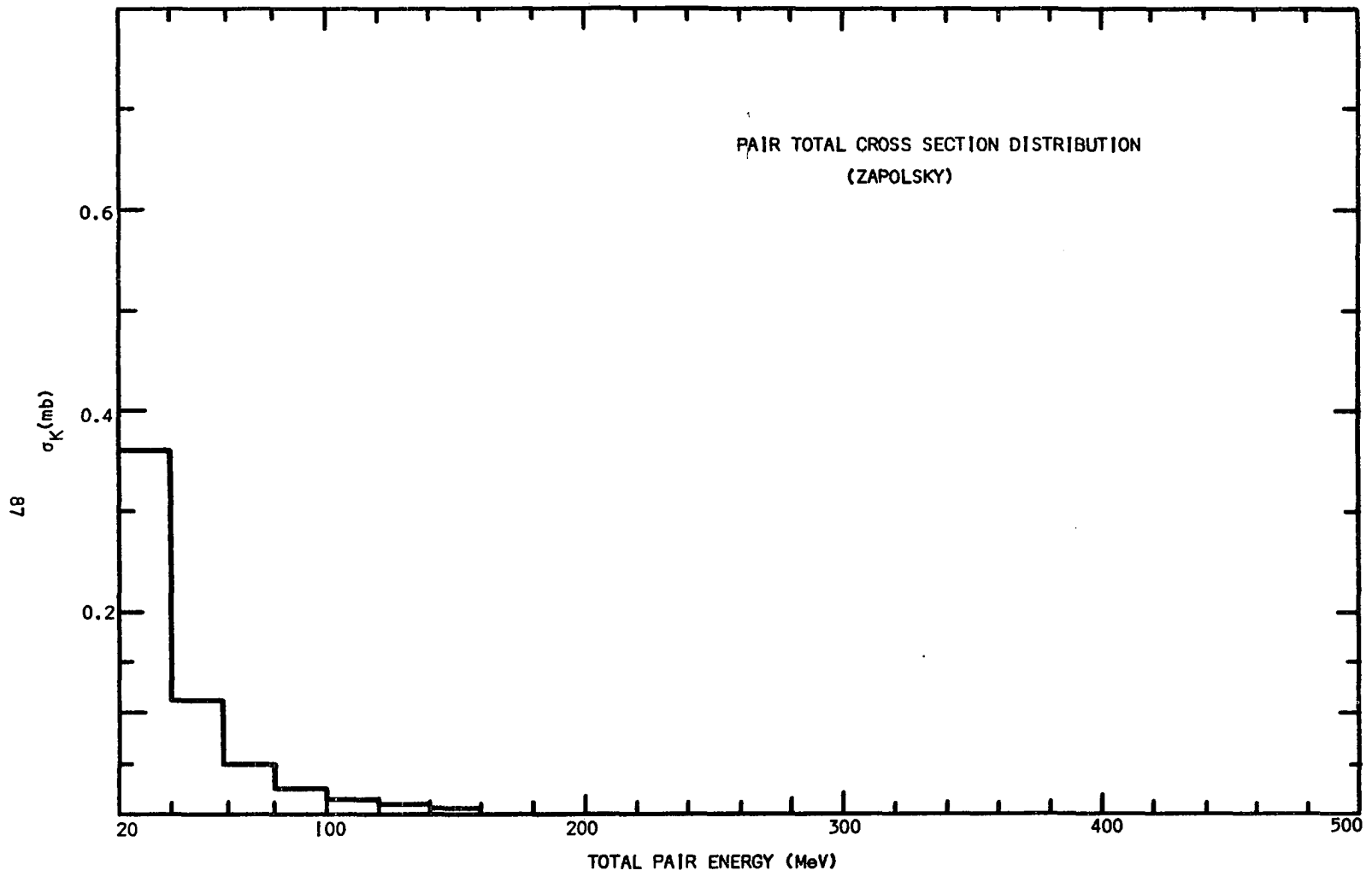

Fig. 31. Distribution of Zapolsky's total cross section for pair production by 16 BeV pions, per 20 MeV total pair energy interval.

unscreened cross section. In every case above, the screened cross section was greater than the unscreened value over the entire region of interest. This implies that, at least for the type screening considered by these authors, the non-screened cross sections should be used.

Electron Pair Experimental Procedure

Introduction

In scanning 16 BeV pion emulsion tracks, events with three prongs, two of which were electrons, were found. These events, electron pairs produced by the incident pions, occur with a lower frequency than do knock-on electrons, one such pair being found on the average for approximately each nine meters of track. These events frequently are distinguishable from knock-on electrons only after careful energy-angle investigations because one of the tracks is of low energy (<5 MeV) or at a large plane angle and hence difficult to see. However, in general these events look like stars with three minimum ionizing secondary tracks, one of which is in approximately the same direction as the incident pion. This is, the pion seldom changes direction noticeably. Two examples of such pairs are given by the photomicrographs in Figure 32.

Event Identification

All events located in scanning which had three minimum ionizing secondary tracks and no other visible tracks were carefully analyzed. Such interactions can be true electron pairs produced directly by the pion, nuclear interactions (white stars) with three high energy secondaries, gamma conversion electron pairs produced on or near the pion track, or nuclear interactions with 2 secondaries,

EVENT 1

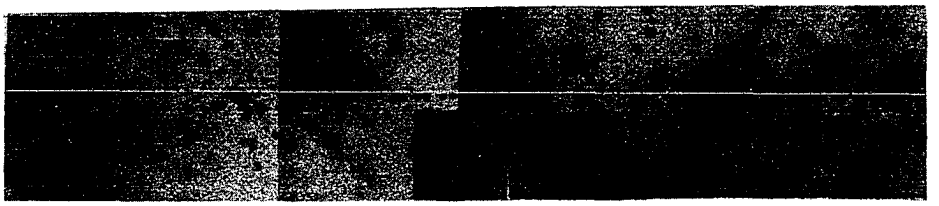

EVENT 114

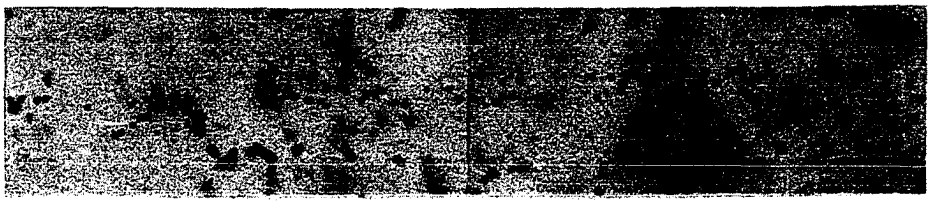

Fig. 32. Electron pair photomicrographs.

one of which is a π^{o} which decays immediately into an electron pair (Dalitz pair).

For 16.2 BeV incident pions there is a very small probability for pion deflection greater than 1° in direct pair production. In fact, none of the interactions which were finally determined to be true examples of electron pair production by the pion had a pion deflection >22'. Nuclear interactions with only 3 minimum ionizing secondary tracks, one of which makes an angle of less than 1° with the incident pion, are distinguishable from electron pairs only after careful analysis. Due to the fact that the average energy of pion secondaries in such nuclear interactions found in a sample scan of 514 m. is 3.0 BeV while the average energy of electron secondaries in electron pair interactions found in this work is 48 MeV, only a small percentage of the pairs having large energies have a probability of being confused with nuclear interactions. High energy electron tracks can be distinguished from high energy pion tracks by measuring the track energies at their origins and again at a distance greater than or equal to one radiation length from that point. This can be seen by considering the equation for the average fractional energy loss by radiation per radiation length of an electron[20],

$$-\frac{1}{E}\frac{dE}{dt} = 4\alpha X_o \frac{N}{A} Z^2 r_o^2 \ln\left(\frac{2E}{m_e}\cdot\frac{1}{3}\right)$$

when $m_e << E << 137\, m_e Z^{-1/3}$ with $t = \chi/X_o$, where χ = distance traveled, X_o = radiation length. The expression becomes

$$-\frac{1}{E}\frac{dE}{dt} = 4\alpha X_o \frac{N}{A} Z^2 r_o^2 \left[\ln(183\, Z^{-1/3}) + \frac{1}{18}\right]$$

when $E>>137\ m_e Z^{-1/3}$. In these equations, X is defined by

$$\frac{1}{X_o} = 4\alpha \frac{N}{A} Z^2 r_o^2 \ln(183\ Z^{-1/3}) \quad ,$$

N is the number of neutrons in the material, A is the mass number of the material, and E is the energy of the electron. For emulsion, $X_o \simeq 3$ cm. From the above equations it can be seen that on the average electrons of 100 MeV energy theoretically lose ≃90% of their energy in one radiation length, while electrons of $\geq$1 BeV lose on the average >98% of their energy in one radiation length. For electrons >100 MeV, energy loss by collision is negligible relative to radiation energy loss. However, radiation loss for pions is insignificant relative to collision loss in the energy region of interest here. The fractional change of the energy of a pion in one radiation length is thus small relative to that of an equally energetic electron.

From the above equations it is seen that electron secondaries should be easily distinguishable from pions. There were four white stars found during scanning in which one secondary pion direction was between 10' and 3° of the incident pion direction. These events were distinguished from electron pairs by using this approach.

Electron pairs produced by gamma rays can be mistakenly interpreted as directly produced pairs if the point of materialization occurs closer to the primary pion track than the minimum resolvable distance in emulsion. The chief source of gamma rays traveling in the direction of the pion such that pairs produced will have a large probability of being in the close proximity to the pion track is

bremmstrahlung by the pion. Only those bremsstrahlung gamma rays which are produced close to the forward direction are important. There is also a γ ray background coming from the decay of π° mesons produced in strong interactions of beam particles. Since there is no reason for γ conversions from this background to be preferentially located near pion primaries (the distribution should be random), the number of expected pair coincidences from this source can be estimated. This is done by observing the number of coincidence electron pairs originating in a 6 micron cylinder around the pion primaries and from this determining the number of such coincidences which are expected to originate within a 1 micron cylinder around the pion. Such close coincidences would have been called pairs produced directly by the pions since their point of origin would not have been resolvable from the pion track. Actually the minimum resolvable distance is generally less than 1 micron, so that this estimate will provide an upper bound on the number of such coincidence pairs from background gamma conversions.

Gamma conversion of bremmstrahlung photons is considered as a large source of error in the trident process (pair production by electrons) and determines the upper limit of experimental accuracy in such investigations. [10, 24, 25]. Thus it is necessary to investigate this process for the present case of primary pions. This process has been treated theoretically by Piron et al,[26] who calculated the number of coincidence pairs expected per unit length of track using known radiation and materialization cross sections.

Piron et al obtained an expression for the number of coincidence pairs expected per unit track length of a particle of mass m, charge e, and energy E moving in a given medium to be

$$n_f = \int_{2m_e}^{E} \Sigma_p(k)dk \int_{\ell} \int_{\theta} \Sigma_b(E,k,\theta)d\ell \iint_{C(\ell\theta,\rho')} dydz \frac{1}{\pi}\frac{1}{\sigma^2} \exp\left(-\frac{y'^2+z'^2}{\sigma^2}\right)d\theta$$

where $\Sigma_b(E,k,\theta)dkd\theta$ is the macroscopic radiation cross section, differential in the photon energy k and the photon angle of emission θ. $\Sigma_p(k)$ is the total macroscopic cross section for the conversion of a photon of energy k.

$$\sigma^2 = \frac{\theta_s^2{}_{av}}{3} \cdot \ell^2 = \frac{F^2\ell^3}{X_o(E-k)^2}$$

where $\theta_s^2{}_{av}$ is the average angular deflection of the primary particles in the distance ℓ, X_o is the radiation length of the medium, and F is a constant with the units of energy (F = 12.1 MeV)[20].

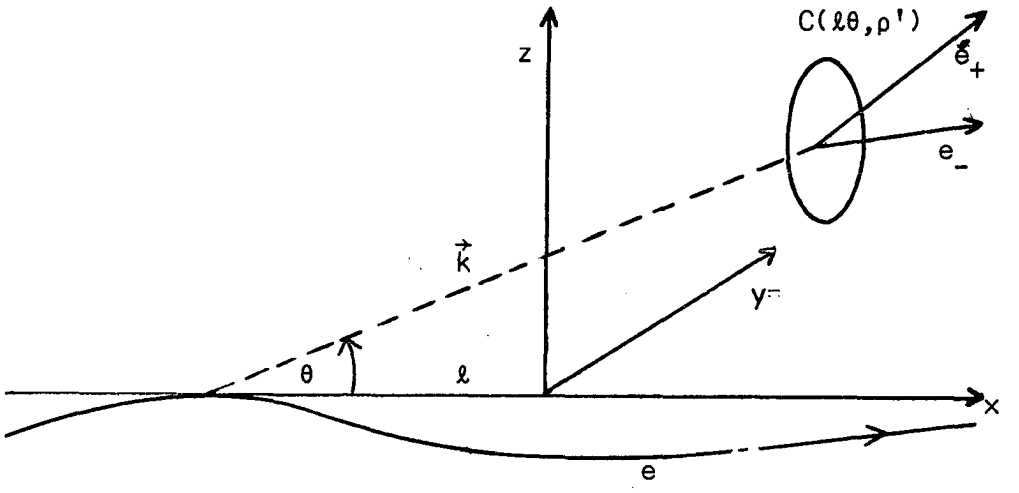

Fig. 33. Coincidence pair production diagram.

The integration over $C(\ell\theta,\rho')$ means that the integration with respect to y' and z' is carried out in a circle of radius ρ' centered at a distance $\ell\theta$ from the tangent to the particle trajectory.

Piron et al. evaluated the above expression approximately and obtained

$$n_f \simeq \frac{1}{X_o}\frac{(m_e)^2}{F^2} P(E,Z)\bar{g}(r_{max})$$

where

$$r_{max} = \rho'/X_o \frac{F^2 E}{m^3} ,$$

ρ' = minimum resolvable distance in emulsion,

$\bar{g}(r_{max})$ = dimensionless function dependent only on r_{max} which was evaluated numerically,

$$P(E,Z) = (\frac{7}{9} - \frac{1}{54}\frac{1}{\ln 183Z^{-1/3}})\ln\frac{E}{2m_e}$$

$$+ \frac{1}{\ln(183Z^{-1/3})}(\frac{28}{9})e^{2/7}(183Z^{-1/3})^{\frac{1}{2}}(\frac{2m_e}{E})^{\frac{1}{2}}$$

$$- \frac{1}{\ln(183Z^{-1/3})}(\frac{151}{54} - \frac{7}{9}\ln 4 + \frac{7}{36}e^{4/7}183Z^{-1/3})\frac{2m_e}{E}$$

$$- \frac{7}{18}\ln(183Z^{-1/3}) - (\frac{1553}{378} - 2\ln 4 + \frac{7}{18} - \ln^2 4)\frac{1}{\ln(183Z^{-1/3})}$$

$$- \frac{25}{9} + \frac{7}{9}\ln 4 .$$

For the present case of 16.2 BeV pions the numerical values for these quantities are

$$F = 12.1 \text{ MeV} ,$$
$$X_o = 2.99 \text{ cm.} ,$$
$$\rho = 1 \text{ micron} ,$$
$$P(E,Z) = 3.62 ,$$
$$\bar{g} \simeq .87\cdot 10^{-4},$$

which yield a value of

$$n_f = 1.88 \cdot 10^{-5}/m \ .$$

Hence, for a total track length of 902.7 m., ≃ .02 coincidence pairs from conversion of Bremsstrahlung photons are expected. For primary pions, this is clearly a negligible source of error. It is of interest to note that, at the same energy, primary electrons would be expected to produce ≃30 coincidence pairs/m. of emulsion track. However, electrons with the same velocity as 16 BeV pions (≃59 MeV electrons) would produce only ≃.006 coincidence pairs per meter. As electron energy increases, coincidence pairs become more and more important, with the number of coincidence pairs equalling the number of direct pairs at about 2 BeV electron energy.

In a sample scan of 258 m. of track in which care was taken to look for such coincidence pairs, twenty-one pairs were found whose origins were within 6μ of the pion, but which could be distinguished from directly produced pairs. Since the actual depth of focus of the microscopes (considering emulsion shrinkage) is only ≃±3 microns, all such pairs will not be seen in scanning. It is difficult to estimate the scanning efficiency for locating such events, but an efficiency of 70% should serve as an underestimate of the actual efficiency. Using this efficiency, thirty coincidence pairs are expected within the 6μ cylinder. For 902 m. of track, 105 such pairs are expected. Thus, considering such coincidence pairs to be randomly distributed within the cylinder, an upper limit of three coincidence pairs are expected to have originated within a one micron cylinder around the pion, and hence to be considered as direct pairs produced by the pion.

It is possible to determine the number of Dalitz pairs expected for the pion track length considered by analyzing the number of π-nucleon interactions with two minimum ionizing pion secondaries. Since the multiplicity of π^+, π^-, or π° mesons should be approximately the same in strong interactions, it is possible to estimate the number of π-nucleon interactions with two pion secondaries, one of which is a π°, to be approximately one-half of the number of such interactions with two charged pion secondaries (neglecting the fraction of these which also have a neutral secondary pion). Five such events were found in a sample scan of 514 m. of track[27]. None of the secondaries from these interactions made an angle of $<1^\circ$ with the primary pion direction, which is an observed feature of all electron pairs located (actually $\theta_{\pi\gamma} \lesssim 22'$). From these considerations alone one would expect no Dalitz pairs in the track length scanned. For greater statistics, it is possible to consider π-nucleon interactions with 2, 3, or 4 secondary pions, determining the number of such events with a direction change of $<1^\circ$ from the primary pion direction for at least one of the secondary tracks. Twenty-nine events of this sort were found, but only three had such a small angle for one of the secondaries. Assuming the same multiplicity for π^+,π^- and π° mesons and that there are equal numbers of 2, 3, and 4 track stars, there are 0.5 events expected in 514 m. of tracks with one neutral pion secondary and one charged pion secondary at an angle of $<1^\circ$ relative to the primary pion. Thus, approximately one such event is expected in 902.7 m. Since there is a probability of about 1% for such neutral pions to decay into an electron pair near the point of interactions,

there is <<1 such Dalitz pair expected in the 902.7 m. of track scanned in this work.

Ninety-nine interactions were located in scanning 902.7 m. of track which were determined to be true examples of direct electron pair production, with total pair energies $\geq$10 MeV. In all of these *interactions the primary pion deflection was small* (<22' *projected* angle), most of the measured deflections being less than 7'. The projected pion deflection was measured using an eyepiece goniometer with measurement accuracy for measuring angles on beam tracks of $\pm$3'.

Measurements

Momentum measurements.

For electron pair events it is necessary to measure directly the momentum of each secondary electron. The only method available for measuring the momenta (or $p\beta$, with $\beta = v/c \approx 1$) for high energy electrons in emulsion is multiple Coulomb scattering. Grain density methods aren't applicable because, even for momenta as low as 5 MeV, the blob density is in the plateau region.

Momentum measurements using scattering methods are based on the fact that charged particles are scattered when they pass through the Coulomb fields in matter (multiple Coulomb scattering), being scattered less the larger their momenta. By measuring the net macroscopic scattering (deviation from a straight line) along the particle's path it is possible to determine its momentum (or $p\beta$).

Momentum calculations were performed using a modified form of Barkas' method[22]. The modifications[28] made concerned noise elimination. They consisted of dropping Barkas' assumption that $\delta_k = 0$ and realizing that difference products $D^r_k D^r_{k+\ell}$ of all orders are not independent of one another. Using mean square averages of the independent second, third, and fourth differences, one obtains the mean square noise-corrected second difference to be

$$\Delta_t^2 = \frac{2}{3}\left[\sum D''^2_k + 2\left(\sum D''_k D''_{k+1} + D''_k D''_{k+2}\right)\right] .$$

The equation used for the mean absolute second difference, D, assumes that second differences have a Gaussian distribution, so that

$$D = \left[\frac{2}{\pi}\Delta_t^2\right]^{\frac{1}{2}} .$$

The standard cut-off at four times the average absolute second difference was used. $p\beta$ was then determined from

$$p\beta = \frac{K_c\, t^{3/2}}{573\, D} ,$$

where K_c is a dimensionless scattering factor corresponding to cell length t, in microns. The factor 573 gives units of MeV for $p\beta$ when D is measured in microns.

By considering that two-thirds of the scattering measurements used were independent[22] and using the statistical estimation of error, the error in $p\beta$ was calculated as

$$\Delta p\beta = p\beta\sqrt{2N/3} ,$$

where N is the number of measurements used for the calculation.

As was shown above, fast electrons in matter tend to lose energy rapidly with distance traveled, causing considerable difficulty in measuring the momentum of a given electron. Due to this loss of energy and to the small mass of the electron, electrons tend to scatter more than other particles, frequently undergoing relatively large angle single scatters. For these reasons the portion of each electron track used for scattering measurements was that between the track origin and the point where it appeared to have lost a significant fraction of its energy -- i.e., to the point where it was possible to visually detect the scattering to be larger than it was near the origin of the track. The measurements were made at a base cell length small enough that, using only the segment of track between the event origin and this point, an average of seventy measurements could be made on each track. However, a minimum cell length of 10 microns was used for all tracks, including those on which this caused less than seventy measurements to be obtained. Exceptions were made for some low energy (<10 MeV) tracks whose large scattering required the use of a 5 micron cell.

Using the set of N points measured at a basic cell length t, the momentum of each electron was calculated with the method of overlapping cells, using multiples of this cell length, M x t, ranging in length from t to M_{max} x t, where M_{max} was determined by the requirement that $N/M_{max} \geq 10$ in order to use at least ten measured points in any calculation. Each cell multiple, M x t, will yield M estimates for the momentum of the electron, one estimate corresponding to the choice of each of the first M measured points as the first point used

in calculating the differences described above. The average of the M estimates for the particular cell length should give a good estimate of the momentum measured at that cell length. The standard deviation among these M estimates was also calculated. In this manner a single value for the momentum is obtained for each cell length. The final value for the momentum of the particle was chosen from these M_{max} estimates to be the one with the smallest standard deviation. For most electrons, several different cell lengths yielded quite similar results, tending to imply a range of cell lengths which give reliable momentum estimates for a given electron track.

Thus, if a cell multiple M was chosen as the one which gave the best estimate, $\overline{p\beta}$ was given by

$$\overline{p\beta} = \frac{\sum_{i=1}^{M} (p\beta)_i}{M}$$

while the error was calculated from

$$\Delta(\overline{p\beta}) = \frac{\left[\sum_{i=1}^{M} (\Delta p\beta)_i^2\right]^{\frac{1}{2}}}{M} \quad .$$

In order to determine experimentally the reliability of the scattering method for high energy electrons, the momenta of twenty-seven knock-on electrons were measured by scattering. Since the energies of these electrons had been measured in a different and more accurate manner, it was possible to check the scattering method for electrons which had energies representative of those measured for pairs. Exactly the same criteria were used in measuring these energies as were used for pair electrons. Agreement was found for the electrons measured, the energies obtained by scattering being, in every case

Table 2: Data for Scattering Check

Event	Energy by Angle (MeV)	Energy by Scattering (MeV)
297	13±.5	22±5
1340	15±1.5	12±2
334	16±2	17±3
310	16±2	10±2
3209	19±1	22±4
10	22±1	23±4
1211	22±1	25±5.6
311	23±1	20±4
689	24±1	21±4
564	36±1	26±5
122	36±1	43±7
592	38±1	29±5
1709	40±1	36±6
1636	43±1	32±5
333	43±1	27±5
305	54±1	25±6
631	66±3	68±16
381	78±2	58±10
140	86±3	100±16
2948	163±5	127±32
399	170±4	165±27
62	189±5	163±25
126	232±8	251±58
1498	285±35	232±50
2111	350±22	435±74
*319	558±30	585±135
*319	558±30	596±138

*Measured twice by scattering at different cell lengths.

except one, within error of or slightly smaller than the energy determined by angle measurement ("correct" energy). These results are listed in Table 2. From these results it is seen that, for electrons, the energy measured by scattering has a large probability of being equal to or less than the actual energy, within the error limits.

Since high energy electrons have a large probability of losing energy while passing through matter, it was necessary to check for energy losses over the region of track measured. A detectable energy loss would have indicated that the originally measured energy needed to be corrected to compensate for this loss. This was done by calculating the momentum of each track in the manner described above using different groups of measured points. The four groupings were made up of all of the measured points, the first half of the measured points (nearest the origin), the last half of the measured points, and the points measured up to the first scatter of the track which was large enough that the electron might have lost a measurable fraction of its energy. Each group of points gives an estimate of the electron momentum. Using these four different measurements of each momentum (two of which were completely independent), it should have been possible to determine the energy loss with distance for each electron and hence to correct the measured momentum value for this loss. However, the errors in each measurement were large enough that the ranges of the different measurements overlapped, preventing any definite conclusions concerning energy loss. However, in most cases a decrease was found in the energy calculated from the first half of the measured points to that calculated using the last half of the measured points. These four calculations of the momentum provide a reliable estimate of the momentum of each electron.

Angle measurements.

The projected angles of emission, θ, of the secondary pion and the pair electrons with respect to the primary pion direction were measured with an eyepiece goniometer. Dip angles, ϕ, were measured in the same manner as for knock-on electrons -- i.e., by measuring the vertical (z) distance between the pion and the secondary tracks at ≈100 microns (distance depending on electron energy) from the origin of the event using the fine focus micrometer on the microscope. The final measurement was chosen as the average of ≈5 repeated measurements. For low energy electrons ($\leq$20 MeV) there is a large probability for large angle changes in the track directions, making their measured angle unreliable. In the cases where low energy tracks make small angles (<2°) with the primary pion direction it is difficult to accurately determine the relative magnitudes of dip and projected angle. This fact is important in determining the plane angle, ρ, for low energy, small angle electrons, since an uncertainty in either the projected or dip angle for such small angles produces a correspondingly much larger uncertainty in the plane angle ($\sin\rho = \sin\phi/\sin\omega$, $\cos\omega = \cos\theta\cos\phi$). For such electrons the plane angle was considered to be unmeasurable and was disregarded in plotting plane angle distributions. Histograms of the projected pion deflection and the electron and positron scattering angles are given in Figures 34 and 35.

Data

Data used for the electron pair experiment is given in Table 3. Included are three pairs which were found in a manner not suitable for cross section determination and which are therefore not used in the

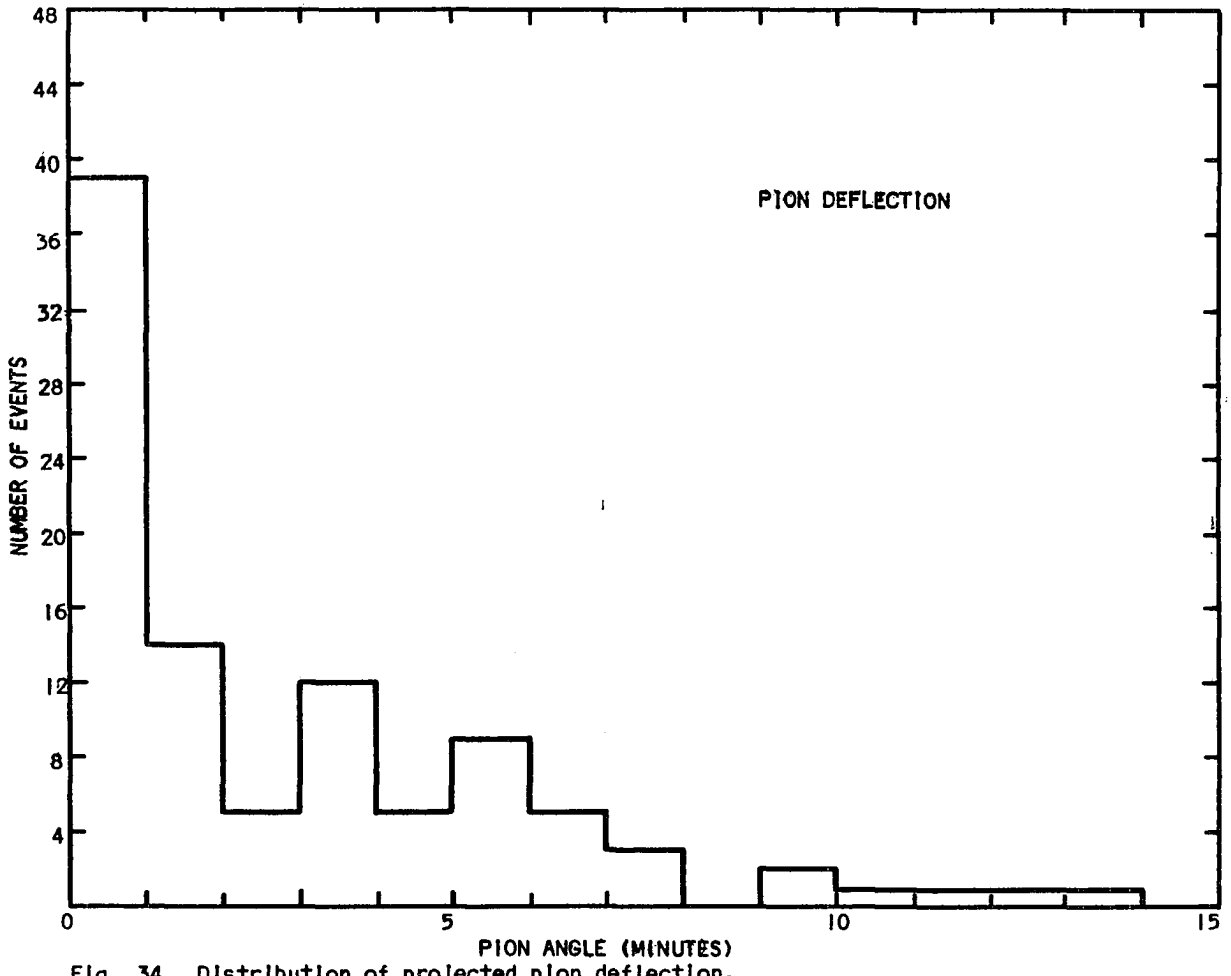

Fig. 34. Distribution of projected pion deflection.

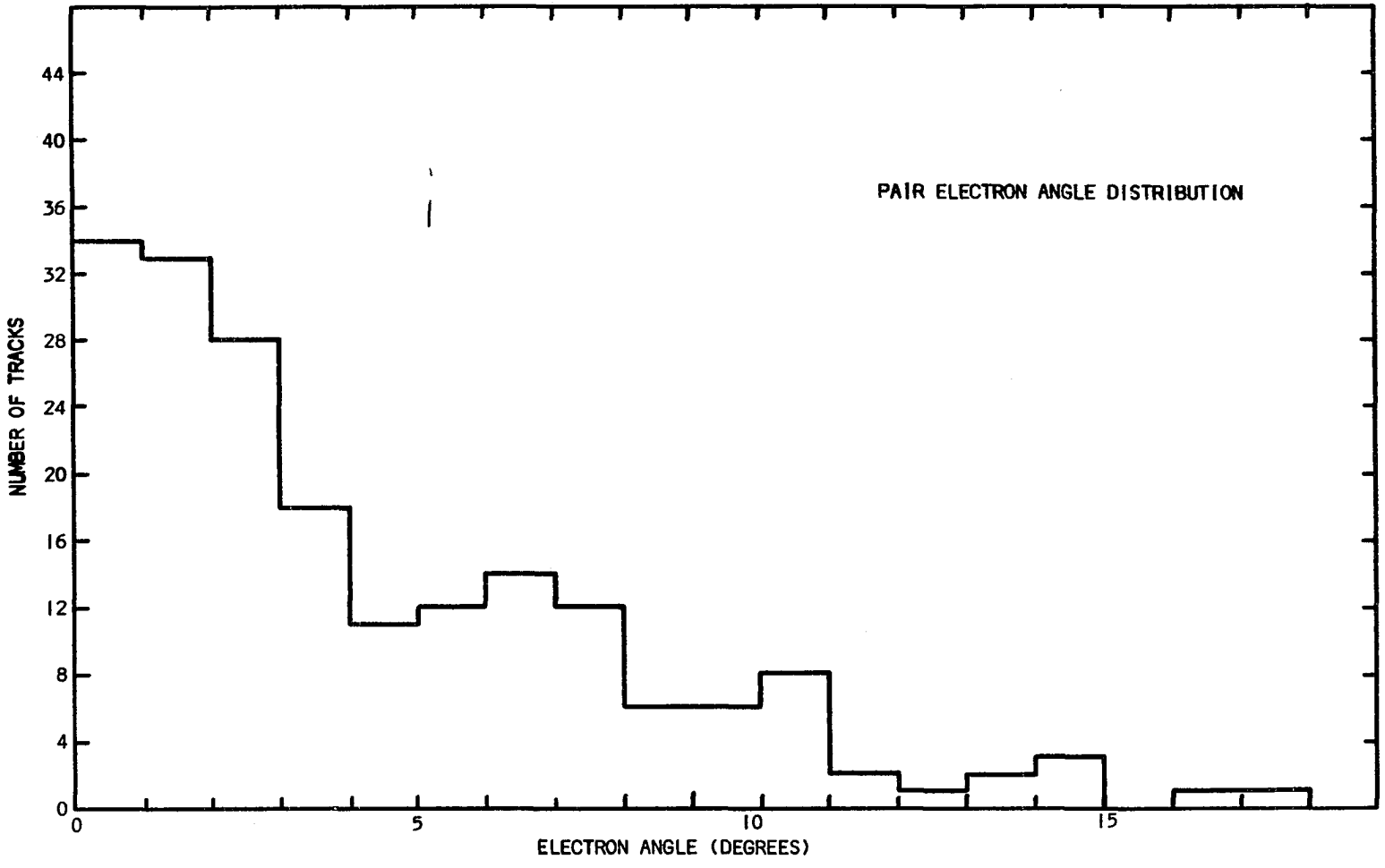

Fig. 35. Distribution of secondary electron and positron angles of emission per degree.

Table 3. Electron Pair Data

Event	E_+(MeV)	ΔE_+	ω_+(°)	ρ_+(°)	E_-(MeV)	ΔE_-	ω_-(°)	ρ_-(°)	ω_π(min.)	E_{total}(MeV)
1771	5.4	1.7	6.63	34.63	4.8	1.2	10.43	15.6	3	10.2
1878	9.8	3.5	4.06	37.3	1.2	.6			0	11.0
846	10.9	2.1	36.0		.5				0	11.4
2657	6.0	3.0	0.0		5.8	2.5	13.15	29.63	0	11.8
1614	14.0	3.3	3.0		1.0	0.5			0	15.0
3285	8.0	1.6	3.55	50.71	7.5	2.1	6.71	55.31	1	15.5
2411	8.3	1.7	1.56	90.0	7.5	2.5	9.66	0.0	0	15.8
1052	7.6	1.3	4.06	66.40	9.7	2.6	8.23	53.90	1	17.3
2039	11.9	2.1	5.95	78.95	6.0	1.5	7.38	73.56	0	17.9
1689	9.9	3.3	.10		11.2	2.8	9.33	70.93	0	21.1
3328	8.8	2.1			14.0	3.0	8.83	9.96	3	22.8
2715	16.1	3.9	10.18	33.18	7.2	2.7	10.90	28.63	0	23.3
2003	23.4	4.7	6.41	71.63	0.5				0	23.9
1682	23.7	7.3	2.75	35.63	1.0	0.5			0	24.7
2429	18.8	3.3	14.66	28.03	7.3	2.1	13.41	13.96	0	26.1
1563	18.1	3.9	0.0		8.1	3.5	0.0		0	26.2
698	25.5	5.2	5.43	81.01	1.0	0.5	71.76		7	26.5
533	11.3	2.8	10.45	81.41	15.6	3.5	6.83	60.60	11	26.9
817	11.6	3.6	5.06	73.83	15.7	3.2	7.78	80.00	12	27.4
1564	27.9	8.6	2.88	0.0	0.5				0	28.4
2416	14.3	2.6	1.61	76.96	14.3	3.2	2.53	64.58	0	28.6
1930	25.0	3.9	5.30	0.0	4.0	1.3	7.01	90.00	1	29.0
2087	12.3	2.0	7.48	80.36	17.0	4.0	5.41	83.88	0	29.3
1487	29.1	4.7	3.25	77.01	0.8	0.3			1	29.9
2274	19.5	4.0			10.7	3.1			0	30.2

Table 3. (Continued)

Event	E_+(MeV)	ΔE_+	ω_+(°)	ρ_+(°)	E_-(MeV)	ΔE_-	ω_-(°)	ρ_-(°)	ω_π(min.)	E_{total}(MeV)
3125	24.2	3.8	2.15	89.83	8.4	1.7	1.46	49.21	3	32.6
1065	16.8	5.0	1.25	0.0	16.0	4.0	.36		5	32.8
2152	32.2	7.0	1.25	78.13	.6	.1			3	32.8
1821	10.4	1.6	3.73	65.36	22.8	3.9	7.70	0.0	0	33.2
436	28.9	4.6	2.21	67.63	5.8	1.4	3.81	49.08	6	34.7
687	5.5	1.7	14.90	19.20	31.2	6.9	3.73	9.00	2	36.7
1516	22.8	5.5	.76	70.46	14.0	2.6	1.63	90.00	0	36.8
1793	7.2	2.3	10.76	60.78	30.6	5.0	2.05	75.56	0	37.8
1929	24.9	4.1	1.18	72.53	13.5	3.2	2.43	64.41	0	38.4
2007	8.2	2.1	5.10	22.50	30.4	6.0	1.40	0.0	0	38.6
146	22.3	7.1	10.91	26.71	16.9	5.2	9.18	63.58	1	39.2
3194	32.0	8.6	6.73	55.75	12.9	2.5	6.96	32.66	0	44.9
1906	24.6	6.2	5.43	43.98	21.0	4.5	6.56	14.80	4	45.6
*1016	6.1	1.2	7.10	10.30	40.9	5.6	4.28	43.86	8	47.0
3132	20.3	5.6	11.45	23.61	28.8	8.8	2.40	21.25	0	49.1
160	31.3	7.0	1.00	68.81	18.0	3.9	2.25	61.83	1	49.3
1908	26.3	5.9	5.31	53.83	23.6	4.1	3.88	51.08	5	49.9
346	22.9	4.6	2.01	71.90	28.7	4.5	.38		0	51.6
461	33.8	5.4	6.45	25.31	18.6	3.2	3.93	28.35	3	52.4
2468	30.8	5.7	5.78	57.50	21.7	4.1	18.11	26.13	4	52.5
2198	27.5	5.5	1.00	21.91	26.6	5.8	2.95	46.91	0	54.1
114	16.0	4.3	3.38	23.03	38.1	11.9	1.78	0.0	2	54.1
1736	46.0	11.6	1.51		9.3	1.9	3.61		3	55.3
1604	24.0	5.2	3.91	40.00	32.5	5.6	9.30	31.68	0	56.5
2953	7.7	1.3	5.15	82.20	54.4	9.6	0.0		1	62.1
1971	36.6	6.1	2.83	77.20	30.4	9.3	6.00	27.41	2	67.0
3310	66.3	11.7	1.26	36.36	1.0	0.5			1	67.3

Table 3. (Continued)

Event	E_+(MeV)	ΔE_+	ω_+(°)	ρ_+(°)	E_-(MeV)	ΔE_-	ω_-(°)	ρ_-(°)	ω_π(min.)	E_{total}(MeV)
1263	41.6	6.6	2.21	0.00	26.0	5.3	4.50	44.20	0	67.6
3142	47.1	11.8	7.01	55.93	22.7	5.9	7.25	19.31	0	69.8
2509	35.4	6.9	1.98	33.16	34.7	6.7	3.86	72.38	6'	70.1
999	56.9	11.9	2.15	18.53	15.9	4.6	8.03	22.38	0	71.5
2072	70.8	19.4	2.11	27.35	1.0	.5			0	71.8
664	10.8	2.3	3.30		65.0	8.9	2.05		5	75.8
2113	75.9	14.2	1.45	35.53	1.0	.5			1	76.9
3277	37.2	6.6	7.18	9.81	42.1	7.1	6.76	0.00	1	79.3
2478	41.5	9.6	.63	0.0	37.9	6.00	0.00		1	79.4
931	71.7	16.6	1.53	0.0	8.2	1.2	9.01	58.95	1	79.9
331	18.0	3.2	6.01	45.21	64.1	10.3	9.81	48.43	3	82.1
805	58.2	14.8	1.25	0.0	24.0	6.0	2.01		5	82.2
1281	67.1	11.4	.73		19.7	3.3	2.98		0	86.8
505	73.9	18.0	.70	0.0	13.0	3.2	8.16		0	86.9
1450	28.8	8.3	8.20	86.38	61.6	10.3	.88	66.76	0	90.4
349	60.8	13.2	6.41	57.66	31.9	5.2	11.63	82.63	22	92.7
3207	69.0	11.7	4.78	8.48	23.9	4.0	7.33	39.98	6	92.9
1813	89.3	22.3	1.90	50.78	27.2	7.1	3.08	44.51	1	116.5
2963	93.9	19.0	.25	0.0	23.8	8.8	4.76	41.28	3	117.7
1	105.0	22.7	1.98	0.0	13.7	3.1	4.18	45.55	7	118.7
2086	112.1	25.9	2.65	59.91	7.7	3.3	7.05	13.51	0	119.8
345	56.2	10.2	2.05	50.56	65.2	11.4	1.33	54.35	5	121.4
443	126.6	31.9	.66	6.00	0.5				0	127.1
830	8.5	1.6	12.06	90.00	121.9	27.9	2.63	60.30	1	130.4
841	73.0	13.7	.95		62.7	11.1	.50		9	135.7

Table 3. (Continued)

Event	E_+(MeV)	ΔE_+	ω_+(°)	ρ_+(°)	E_-(MeV)	ΔE_-	ω_-(°)	ρ_-(°)	ω_π(min.)	E_{total}(MeV)
*1015	79.5	12.0	4.20	36.26	57.6	8.7	2.68	37.05	0	137.2
2112	57.6	10.5	0.00		79.7	12.9	0.00		0	137.3
824	127.6	16.8	1.95	26.50	14.0	2.2	3.66	0.00	9	141.6
603	90.0	22.9	1.31		52.8	10.0	.96		6	142.8
*1014	139.0	34.8	1.35	90.00	10.1	2.2	4.25	30.41	2	149.1
930	1.2	.6	21.45	71.33	153.3	22.1	0.00		0	154.5
1785	21.3	3.7	10.55	10.46	133.4	20.6	1.41	0.00	1	154.7
1672	94.9	16.4	1.21	29.55	68.5	19.8	1.83	52.95	5	163.4
1995	25.6	4.9	1.35	21.08	139.2	24.1	.78	0.00	3	164.8
2215	42.9	7.2	4.60	29.35	132.3	20.4	1.58	26.40	4	175.2
141	51.9	13.0	3.23	22.11	135.5	24.5	3.25	14.16	4	187.4
3056	140.7	22.6	.96	89.83	50.0	8.6	0.00		3	190.7
1677	140.2	33.7	.85	90.00	57.9	11.9	1.71	6.18	2	198.1
487	170.6	55.0	1.66	62.91	29.7	4.2	1.90	0.00	10	200.3
829	130.6	20.0	1.43	45.86	72.9	10.9	1.01	0.00	3	203.5
148	52.1	13.9	6.08	80.10	167.9	29.8	1.11	28.86	5	220.0
531	98.9	16.2	2.73	47.76	126.5	22.4	3.75	36.01	7	225.4
2724	203.0	31.1	0.00		22.5	4.1	0.00		4	225.5
3175	51.6	8.8	1.68	41.43	182.6	45.7	0.00		5	234.2
1583	136.3	29.1	2.11	56.60	111.1	24.9	17.56	67.38	2	247.4
1870	94.3	21.1	5.53	18.53	200.1	40.9	6.70	30.90	21	294.4
1205	96.5	19.6	3.81	63.66	266.9	38.5	.33	0.00	3	363.4
130	65.5	12.1	10.01	60.05	315.6	61.3	2.83	79.23	6	381.1
473	307.2	49.6	4.20	36.76	152.0	25.3	2.68	37.05	0	459.2
1236	418.5	74.2	.70	0.00	51.6	8.8	2.81	24.48	5	470.1

*Events not used in cross section calcualtion.

cross section determinations. Angle nomenclature for each electron is the same as in the knock-on electron case (Figure 11) with subscripts added to distinguish the two tracks. It should be noted that there is no way of distinguishing the positron track from the electron track, so that the assignments of + and - have no significance except in distinguishing one track from the other.

Scanning Efficiency

The scanning efficiency for electron pairs is much higher than that for knock-on electrons because two tracks are generally much easier than one to see. In addition, in most cases, both tracks make small angles to the incident pion track direction. Although some events had electron angles >8°, the majority of the electron angles were <4° (Figure 35). The average electron angle is 4.7°. Small angle secondaries are detected with a greater efficiency than are large angle secondaries, as was demonstrated in the scanning efficiency tests in the knock-on electron case. This is partially due to smaller dip angles.

A method similar to that used in checking knock-on electron scanning efficiencies was used in checking electron pair scanning efficiencies. Tracks on which pairs had been found, in addition to about three times that number of tracks on which different types of events or no events had been found, were rescanned by the scanners. In this manner a total of 22.1 m. of track was rescanned by each scanner being checked.

This method does not provide a good quantitative estimate of the percentage scanning efficiency, but it does give an indication of the scanning efficiency. In addition, it provides a good method for determining the relative scanning efficiencies of the different scanners. The results of this rescanning implied an initial scanning efficiency of approximately 88% for relocating events. This is probably an overestimate of the scanning efficiency since it gives no check of the number of pairs missed in the original scanning.

It is instructive to plot the plane angle (ρ) distribution for pairs, where the plane angle is the angle between the plane of the emulsion and the plane formed by the pion and either electron. This distribution provides for a further check on the scanning efficiency, although not as directly as in the knock-on electron case due to the presence of two tracks, either of which could have served to locate the event in scanning. If all pairs have been found, an isotropic distribution of plane angles is expected. This distribution for the pair electrons, excluding electrons with very low energies together with very small angles due to the large uncertainty of their actual plane angle, is given in Figure 36. It is instructive to investigate the plane angle distribution for the tracks having the smallest plane angle in each pair since there is a large probability that the flattest track in each pair was the one which caused the event to be seen. This distribution is also given in Figure 36. The decrease in number of events seen here for events with plane angle between 30° and 90° is expected, but this graph does indicate that many of the pairs found were located by seeing dipping tracks. This indicates a high scanning efficiency.

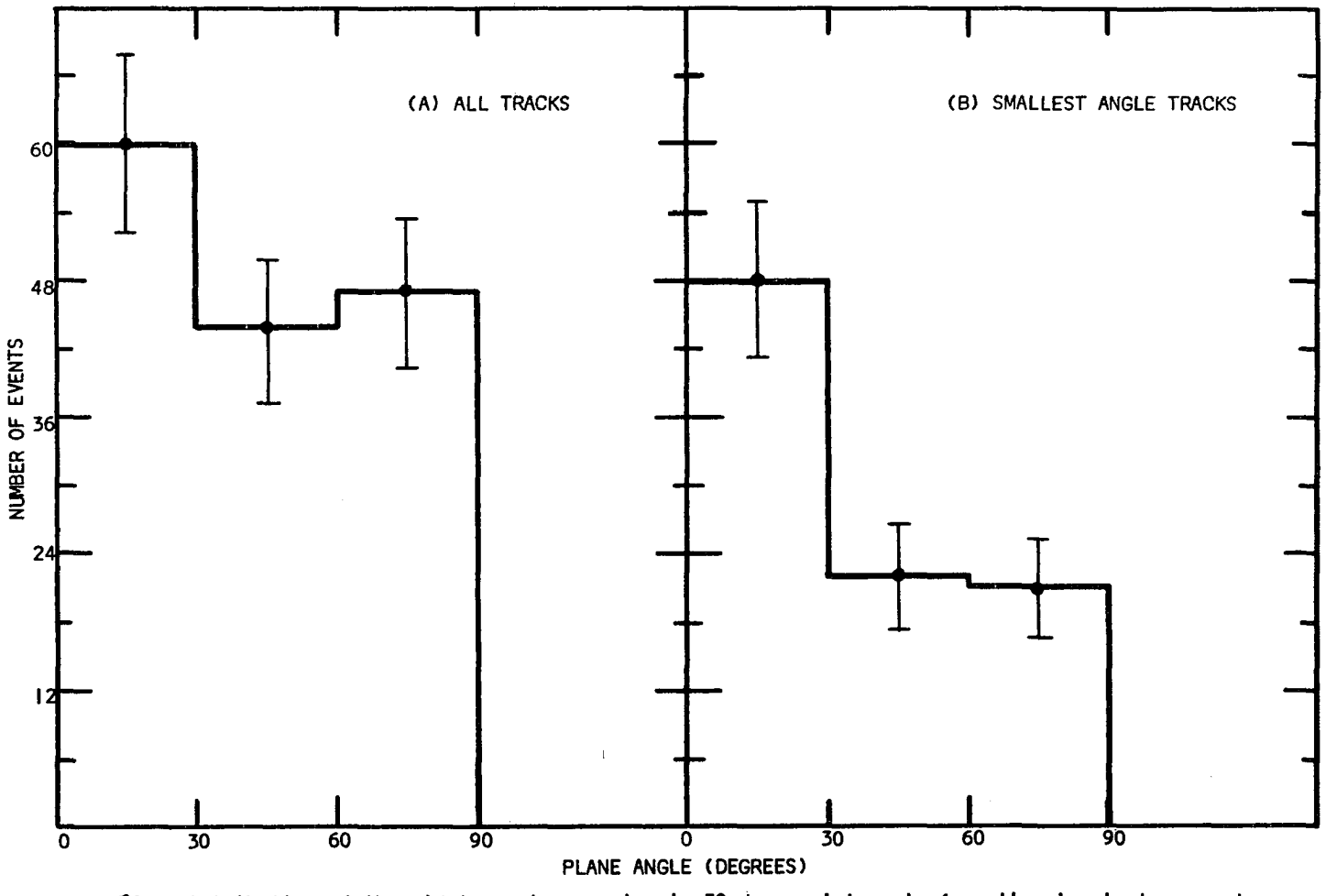

Fig. 36. Distribution of the electron plane angles in 30 degree intervals for all pair electrons and positrons (A), and for the tracks, one from each pair, with the smallest plane angle in (B).

Conclusions which can be made using the plane angle distributions are limited since the statistical errors overlap. However, the distribution for all tracks indicates that there is a probability of having missed events with tracks having large dip angles. This decrease in scanning efficiency is uncertain, but is estimated to be approximately 5%. This estimate is made by determining the number of tracks needed to make the distribution isotropic.

Results

The relative number of pairs expected, according to Ternovskii, as a function of the disparity, $\mu = |E_+ - E_-|/(E_+ + E_-)$, in the secondary electron energies is plotted in Figures 37, 38, 39 and 40 at fixed values of K. This relative probability is proportional to $d^2\sigma/dKd\mu$ at constant K, with μ ranging from 0.0 to 1.0. Due to small statistics it is impossible to obtain an experimental curve for $d^2\sigma/dKd\mu$ at a constant value of K. However, since the theoretical curve has a slowly changing shape with increasing values of K, an experimental comparison is made by plotting the number N of pairs with $K = 50 \pm^{25}_{40}$ MeV, K>75 MeV, and all K in Figure 41, as a function of μ. By comparing the experimental results with the theoretical curves it can be seen that the large expected probability for pair production with $\mu \simeq 1$ (i.e., pairs with one very high energy track and one low energy track) doesn't occur experimentally. In fact, no increased probability is observed. All values of μ appear to have equal probability of occurring, within statistical error, for any value of K.

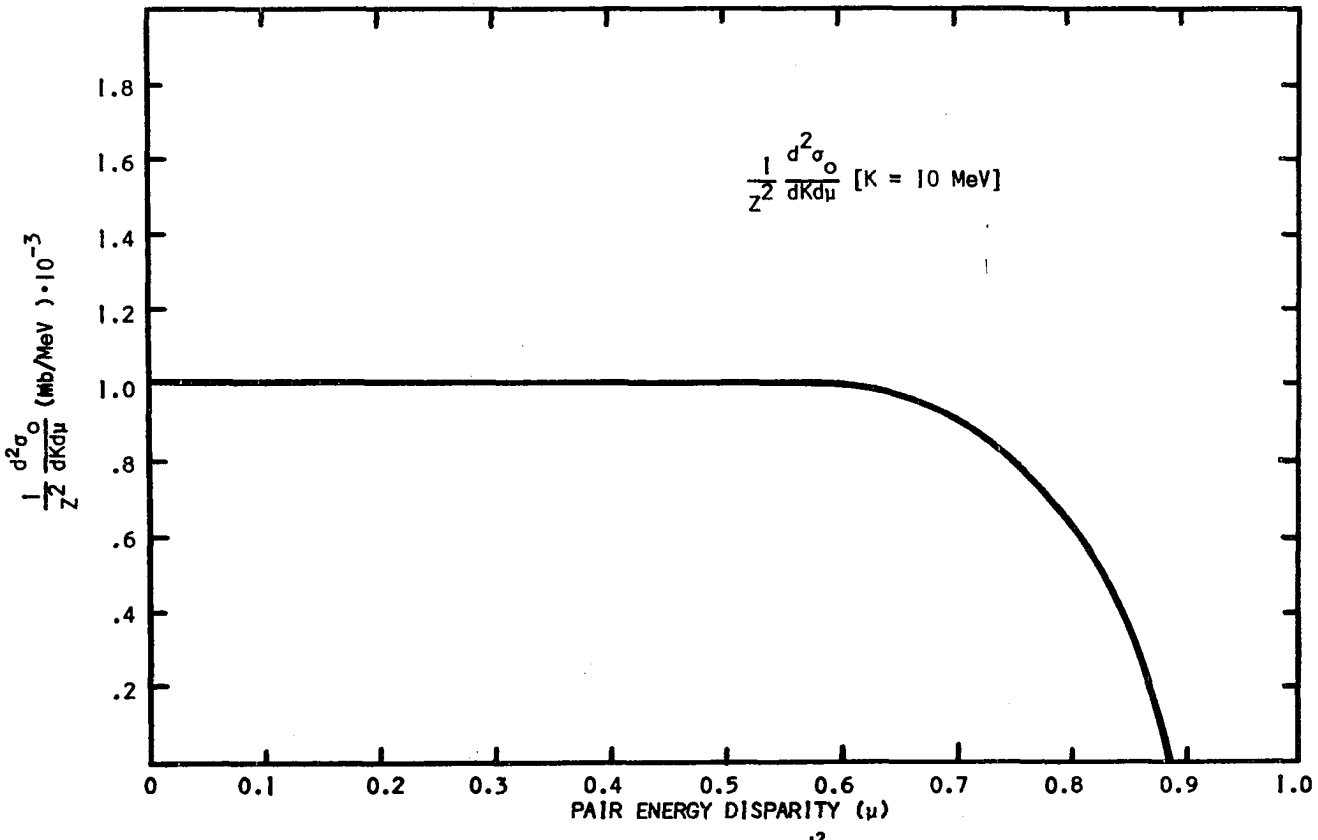

Fig. 37. Ternovskii's differential cross section, $\frac{d^2\sigma_o}{d\mu dK}$, for pair production by pions plotted against μ, the pair energy disparity, at a fixed K = 10 MeV.

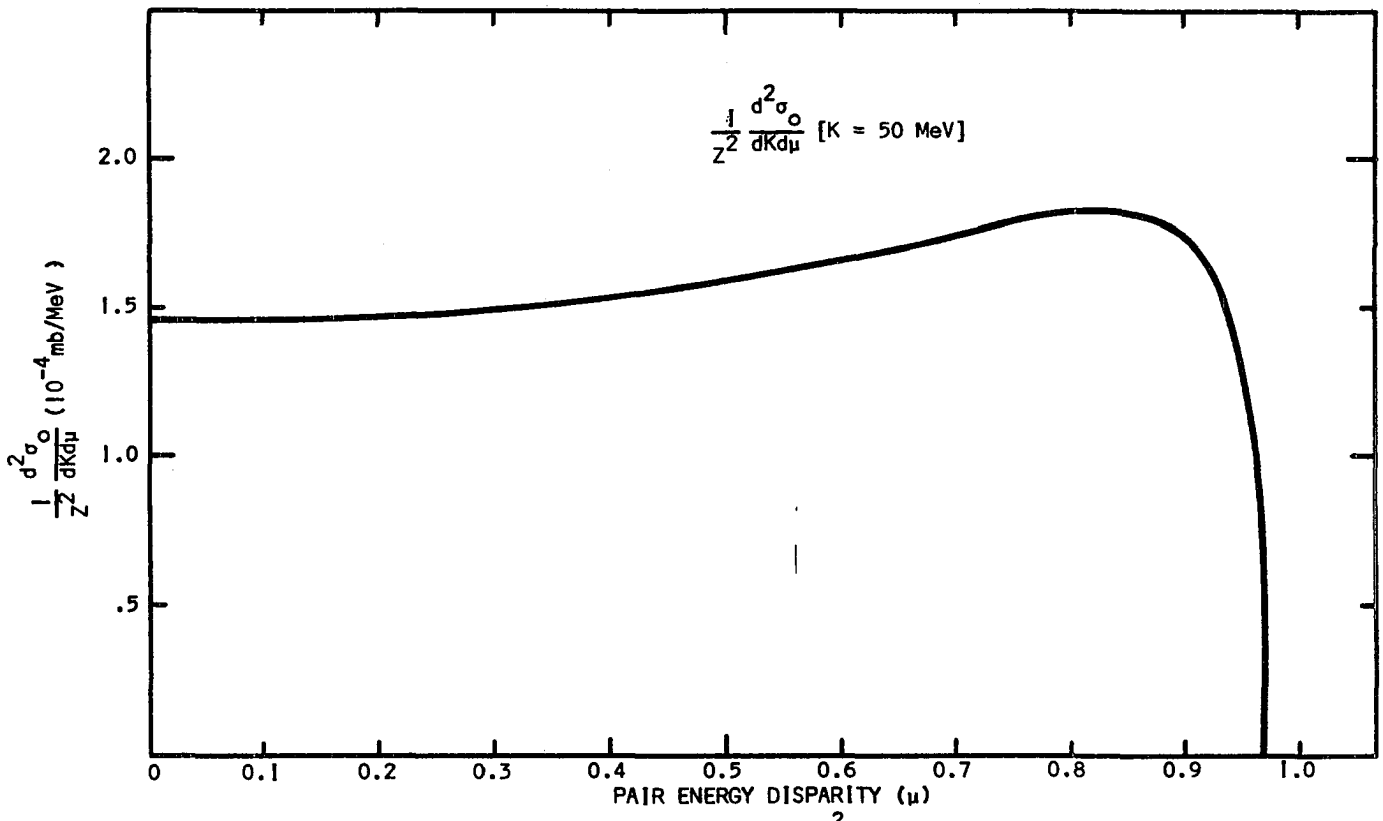

Fig. 38. Ternovskii's differential cross sections, $\frac{d^2\sigma_o}{dKd\mu}$, for pair production by pions vs. μ at a total pair energy of 50 MeV.

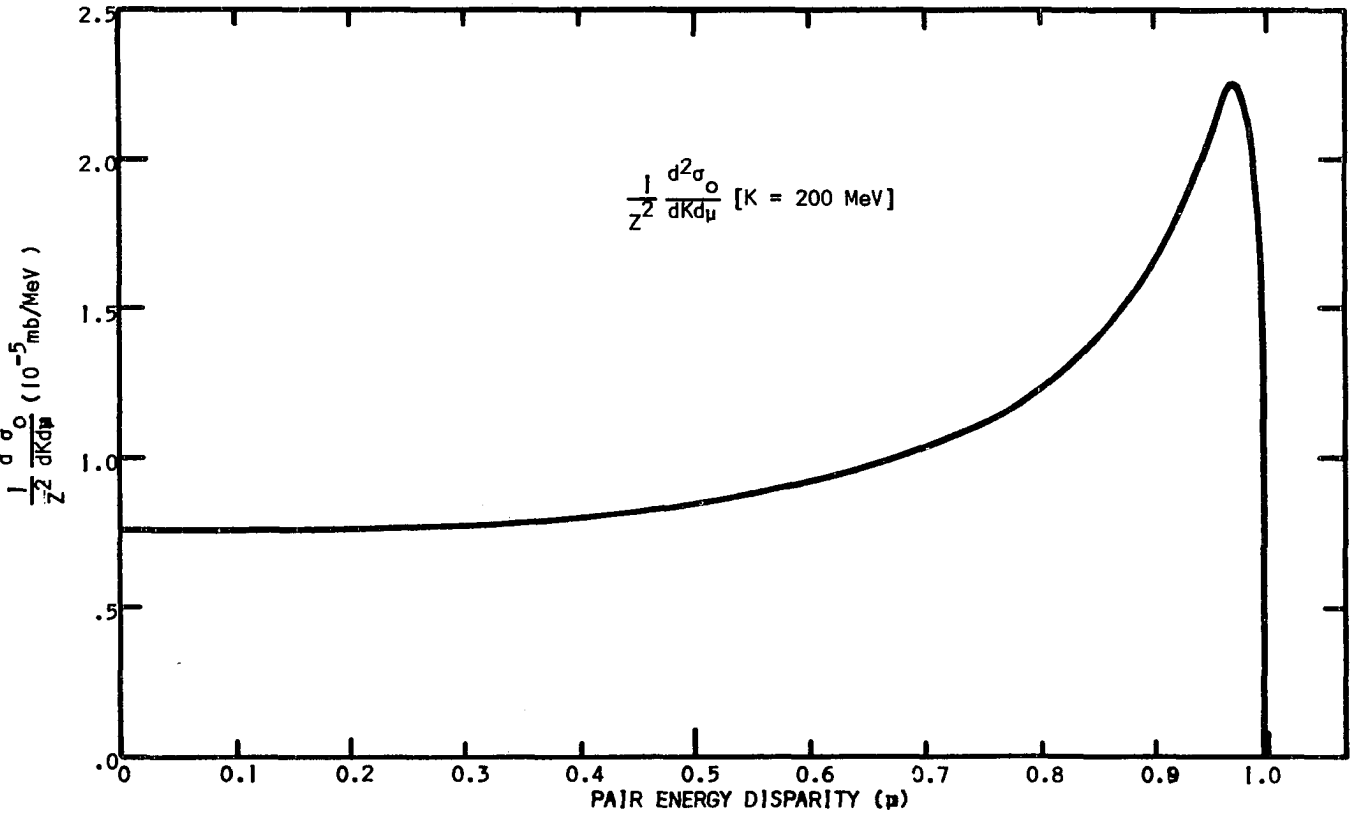

Fig. 39. Ternovskii's cross section, differential in K and μ, for pair production by pions plotted against the pair energy disparity for the case of a total pair energy of 200 MeV

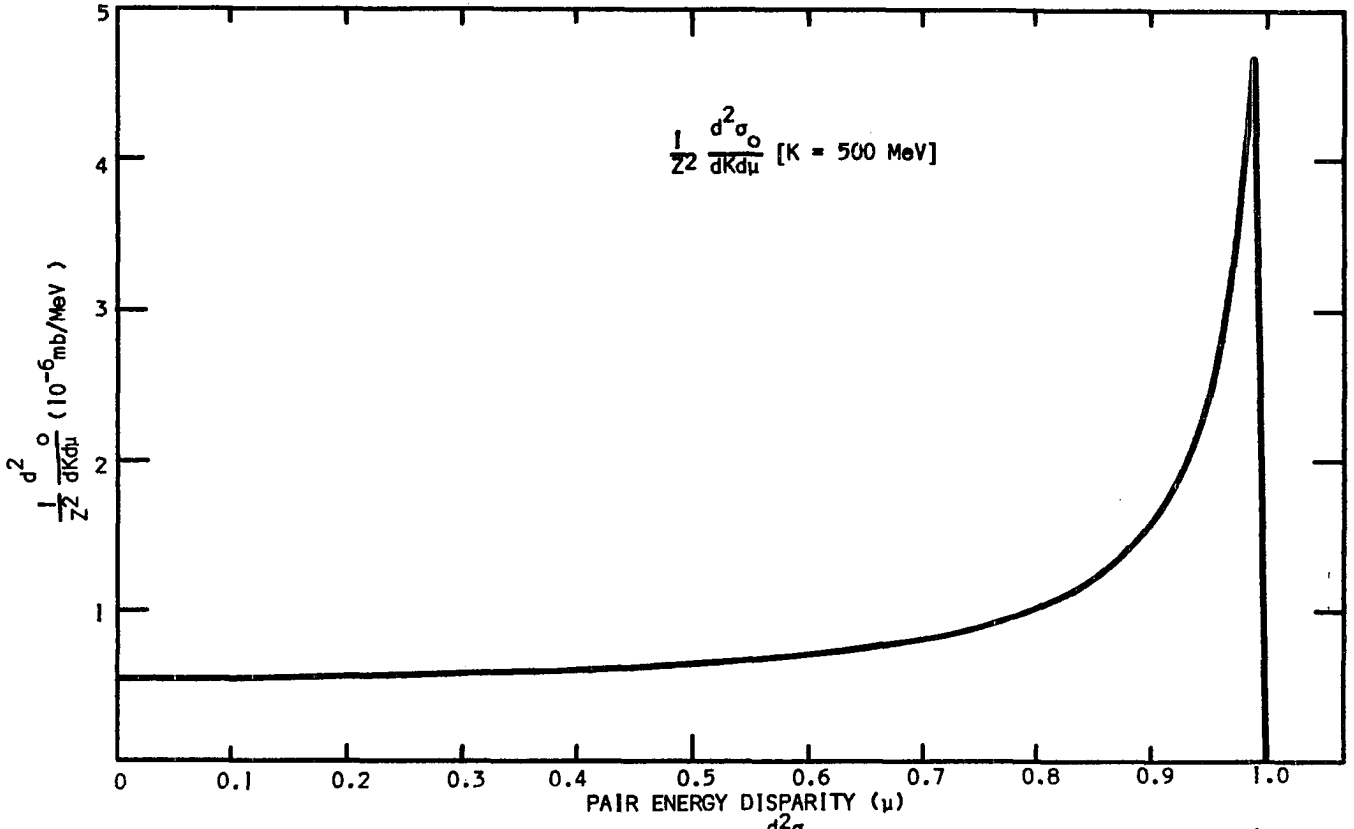

Fig. 40. Ternovskii's differential cross section, $\frac{d^2\sigma_o}{dKd\mu}$, for the production of pairs by 16 BeV pions plotted against the pair energy disparity (μ) for the case of K = 500 MeV.

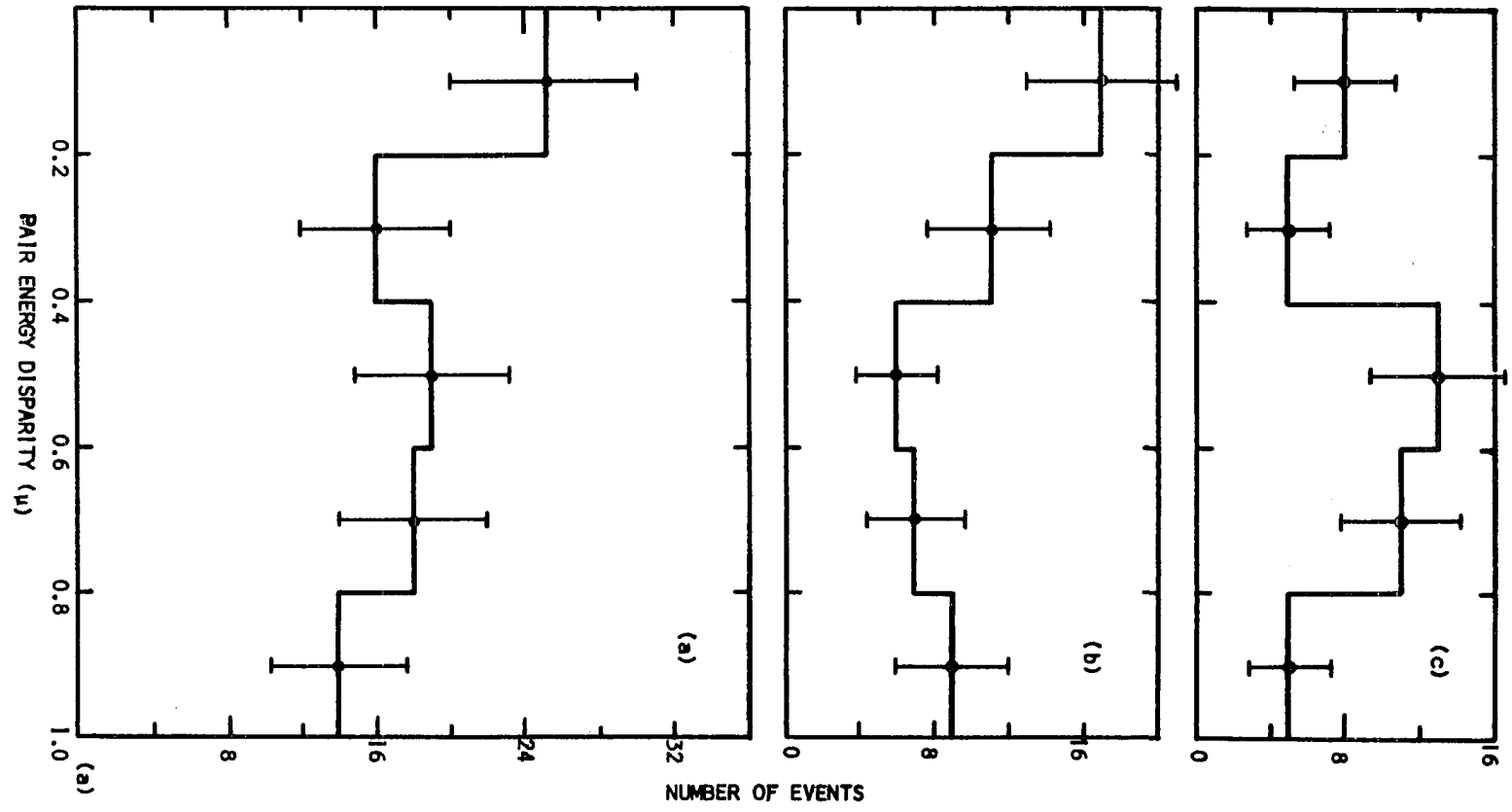

Fig. 41. The number of events ($\propto \frac{d^2\sigma}{dK d\mu}$) vs. μ, at intervals $\Delta\mu = 0.2$, for events with total pair energy >75 MeV in (c), $= 50^{+25}_{-30}$ MeV in (b) and for all energies in (a).

It is more instructive to compare the number of events predicted theoretically with the number found than to compare theoretical and experimental cross sections. The number of events, N, with total pair energies between K and K + ΔK is related to the total cross section, σ_K, for the production of a pair with total energy in this range by

$$N = Ln\sigma_K ,$$

where L = total track length scanned and $n = 7.898 \cdot 10^{22}$ atoms/cm^3 = number of emulsion nuclei per unit volume[22].

Experimentally it appears that the cutoff of 20 MeV, rather than 10 MeV, should be employed due to the relatively small number of events located with total energies between 10 and 20 MeV compared to the number predicted by theory. In addition, fewer events were found with energies between 10 and 20 MeV than were found between 20 and 30 MeV, in contradiction to the theoretically expected results. As was discussed above, this is not surprising due to the increasing difficulty in event location with decreasing pair energy (below $\approx$20 MeV total pair energy).

Histograms of the number of pairs per 20 MeV total energy interval are given in Figure 42 for a cutoff energy of 20 MeV. A similar distribution is given in Figure 43 for this data corrected for approximately 83% scanning efficiency and 3% coincidence pair effects. The number of pairs expected per energy interval as predicted by Ternovskii (calculated in the manner described above), using Ternovskii's suggested value for y_{min}, is superposed. The parameter D (related to

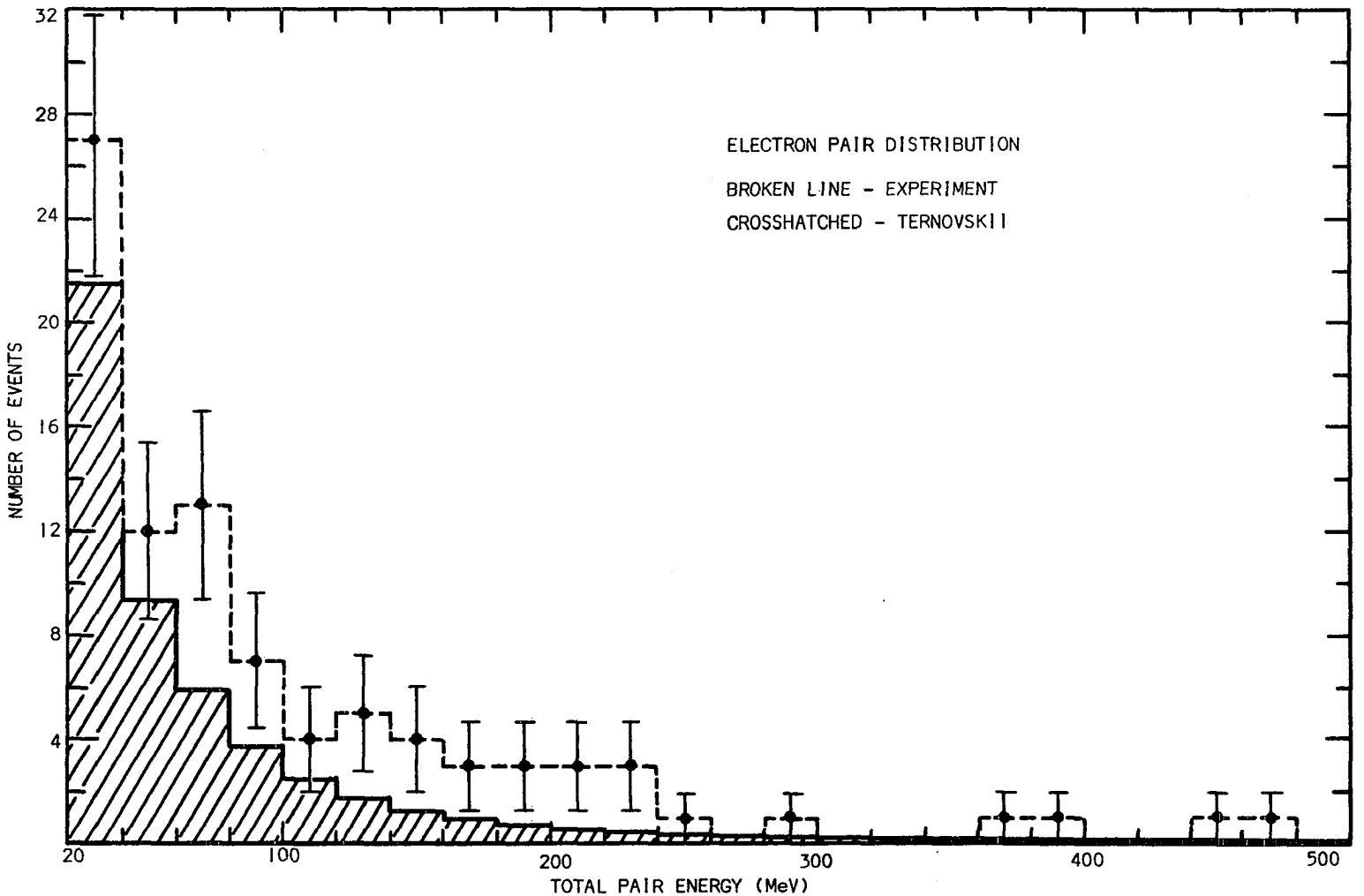

Fig. 42. Distribution of the total number of electron pairs per 20 MeV total pair energy found in 902.7 m. of track, with the number predicted by Ternovskii superposed (D = 1).

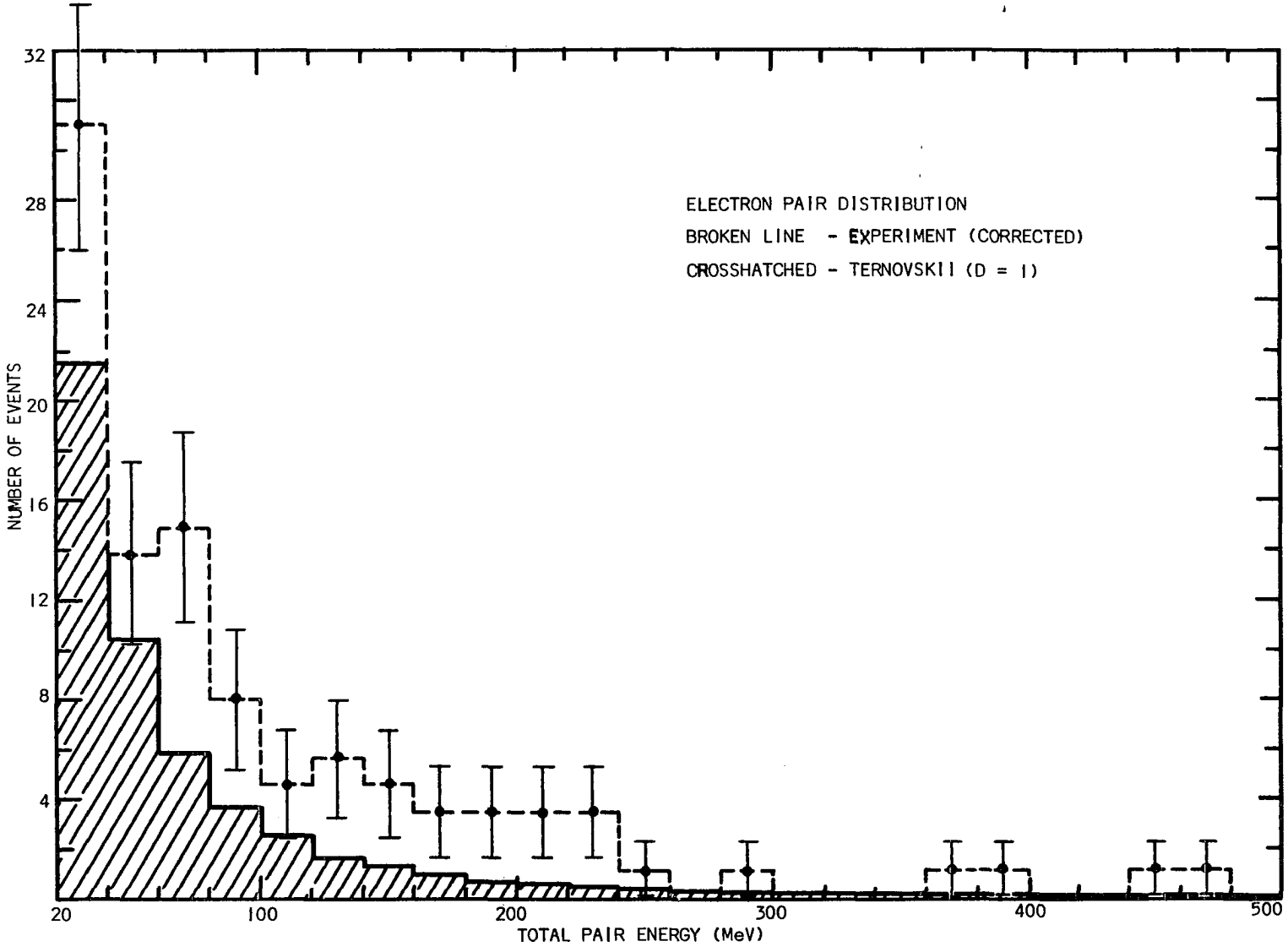

Fig. 43. Experimental pair production cross section results corrected for scanning efficiency, with Ternovskii's predicted results (not normalized at low energies) superposed.

the choice of y_{min}) in the theoretical result was then adjusted to give a good fit of the theoretical result with experiment at low pair energies, the value chosen being D = 1.48, corresponding to $y_{min} = \frac{K\ H}{1.48\ p_+p_-}$. This result is plotted in Figure 44. This normalization procedure is justified by the fact that the choice of y_{min} is not exactly defined, as was discussed above. Changing y_{min} has a smaller fractional effect on the theoretical predictions for total pair energies greater than 100 MeV than in the lower energy region.

As was shown above, due to the tendency for the scattering method to give values for measured energy smaller than the actual value, the energies measured for the electrons should be increased. However, since the fractional increase expected is smaller than the error in measurement, this effect will be neglected.

From Figure 44 it is seen that the experimental cross section is above the normalized theoretical one at energies greater than 60 MeV. The above mentioned probability for measuring energies to be smaller than the actual values tends to give better agreement between theory and experiment in this region. That is, the discrepancy between theory and experiment would be larger if the measured energies were increased.

The experimental total cross sections for the production of electron pairs with total energy greater than 10 MeV were measured. Experimental results for total cross sections, mean free paths, and number of events found are listed in Tables 4 and 5 for various cutoff energies and energy intervals. Corrected and uncorrected

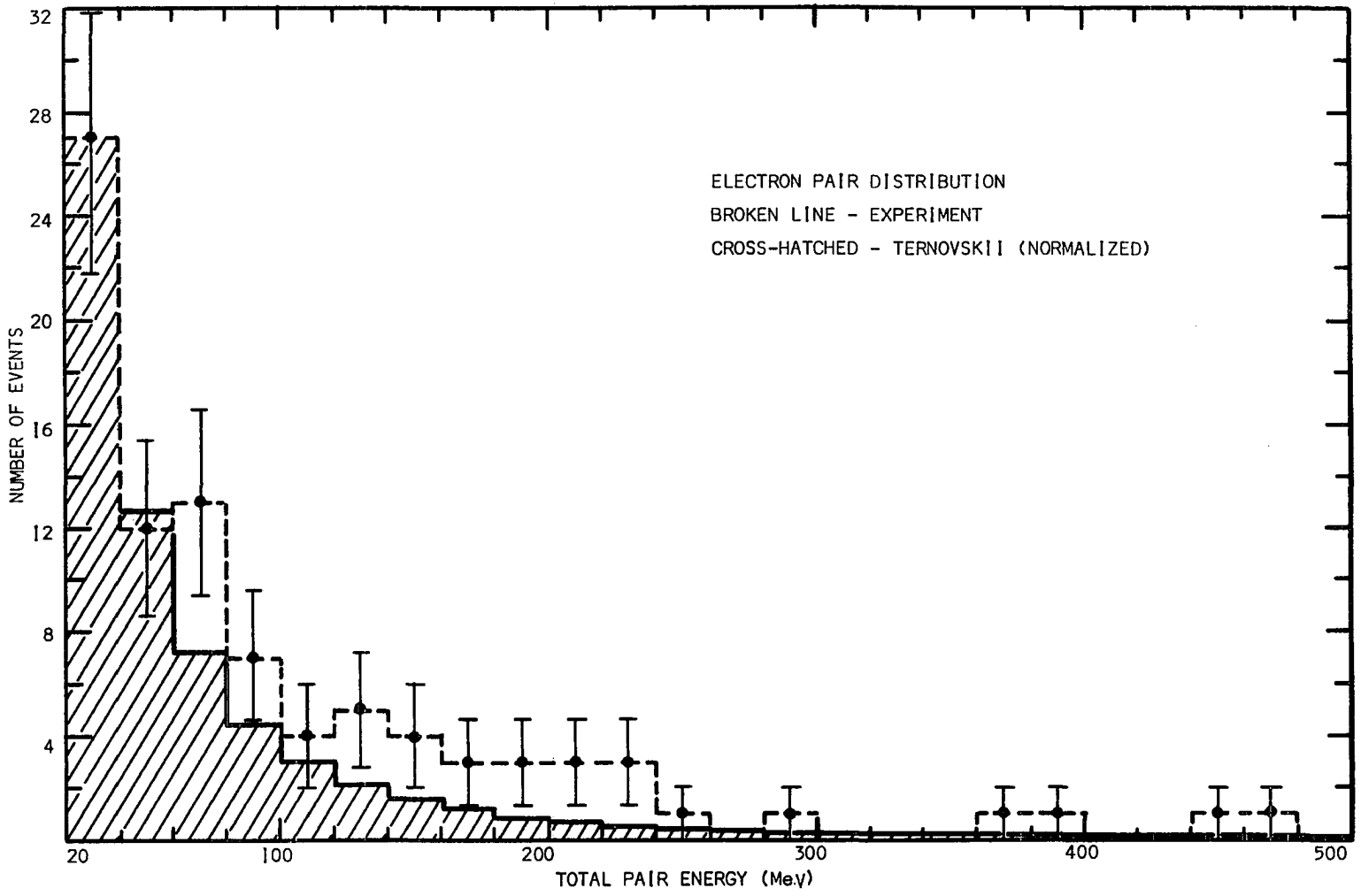

Fig. 44. Distribution of the total Number of electron pairs per 20 MeV total pair energy found in 902.7 m. of track, with the theoretical result of Ternovskii, normalized to fit at low energies, superposed (D = 1.5)

Table 4. Total Number of Pairs with Total Energies $\geq K_{min}$

K_{min}	20	40	60	80	100	120	140	160	180	200	220	300
N (Experiment)	90	63	51	38	31	27	22	18	15	12	9	4
N (Experiment Corrected)	105.9	74.1	60.0	44.7	36.5	31.8	25.9	21.2	17.6	14.1	10.6	4.7
N (Ternovskii)	52.4	31.0	20.6	14.7	11.0	8.5	6.7	5.4	4.4	3.7	3.1	1.7
N (Ternovskii Normalized)	64.5	37.5	24.9	17.7	13.1	10.1	7.9	6.3	5.2	4.3	3.5	1.9
N (Murota)	45.3	27.3	18.4	13.2	9.9	7.7	6.1	5.0	4.1	3.4	2.9	1.7
N (Murota Normalized)	62.7	35.7	23.4	16.4	12.0	9.3	7.4	6.0	5.0	4.1	3.5	2.1
N (Bhabha)	16.4	3.0	.45	.25	.16	.11	.08	.06	.05	.04	.03	.02
N (Bhabha Normalized)	33.4	6.4	.94	.51	.18	.13	.09	.06	.05	.04	.03	.02

Table 5. Comparison of Experiment and Theory for Various Energy Intervals*

Pair Energy nterval (MeV)	Experiment			Ternovskii			Ternovskii (Normalized)			Murota (Normalized)		
	N	σ	λ	N	σ	λ	N	σ	λ	N	σ	λ
20-60	39	5.5± .9	23.1±3.7	31.8	4.6	28.4	39.6	5.6	22.8	39.9	5.6	22.6
60-1000	51	7.2±1.0	17.7±2.5	20.6	2.9	43.8	24.9	3.5	36.3	25.1	3.5	36.0
20-80	52	7.3±1.0	17.4±2.4	37.7	5.3	23.9	46.8	6.6	19.3	47.4	6.7	19.0
80-1000	38	5.3± .9	23.8±3.9	14.7	2.1	61.4	17.7	2.5	51.0	17.6	2.5	51.3
20-100	59	8.3±1.1	15.3±2.0	41.6	5.8	21.7	51.4	7.2	17.6	52.0	7.3	17.4
100-1000	31	4.4± .8	29.1±5.2	11.0	1.5	82.0	13.1	1.8	68.9	13.0	1.8	69.4
20-120	63	8.9±1.1	14.3±1.8	44.0	6.2	20.5	54.4	7.6	16.6	55.1	7.7	16.4
120-1000	27	3.7± .7	33.4±6.4	8.5	1.2	106.2	10.1	1.4	89.4	9.9	1.4	91.2
20-140	68	9.5±1.1	13.3±1.6	46.2	6.5	19.5	52.2	7.3	17.3	57.3	8.0	15.8
140-1000	22	3.1± .7	41.0±8.7	6.3	.9	143.2	7.9	1.1	114.3	7.7	1.1	117.2

N = number of electron pairs,

λ = mean free path (meters),

σ = total cross section in each energy interval.

results are given. The corresponding theoretical results as predicted by Ternovskii, using his suggested value for y_{min} as well as the value of y_{min} which gave the best fit at low pair energies (normalized to uncorrected experimental results), are also listed in the Tables.

A comparison of the experimental results with the theoretical results for spin one-half incident particles (with pion mass, 16 BeV energy) will not be made. Bhabha's result is plotted along with the experimental results in Figure 45, with $\alpha_B = 1$, $\alpha' = 1$ and in Figure 46, with $\alpha_B = 6$, $\alpha' = 1$ to give a good fit at low energies. The number of pairs predicted by Murota's cross section is superposed on the experimental results in Figures 47 and 48, with the variable $\alpha_m = 1$ and $\alpha_m = 2.1$, respectively. $\alpha_m = 2.1$ gives good agreement at low energies. In Figure 49 the experimental results are plotted with the results predicted by Zapolsky's cross section superposed. No adjustable parameter was given in this calculation.

The total numbers of pairs predicted by these calculations, along with the experimental results for different lower cutoff energies are also listed in Tables 4 and 5. Corresponding mean free paths (λ) and total cross sections are listed.

Results of Previous Experiments

Similar experiments considering pair production by high energy pions have been attempted before[15,16]. The results of these experiments give agreement, within experimental and statistical error,

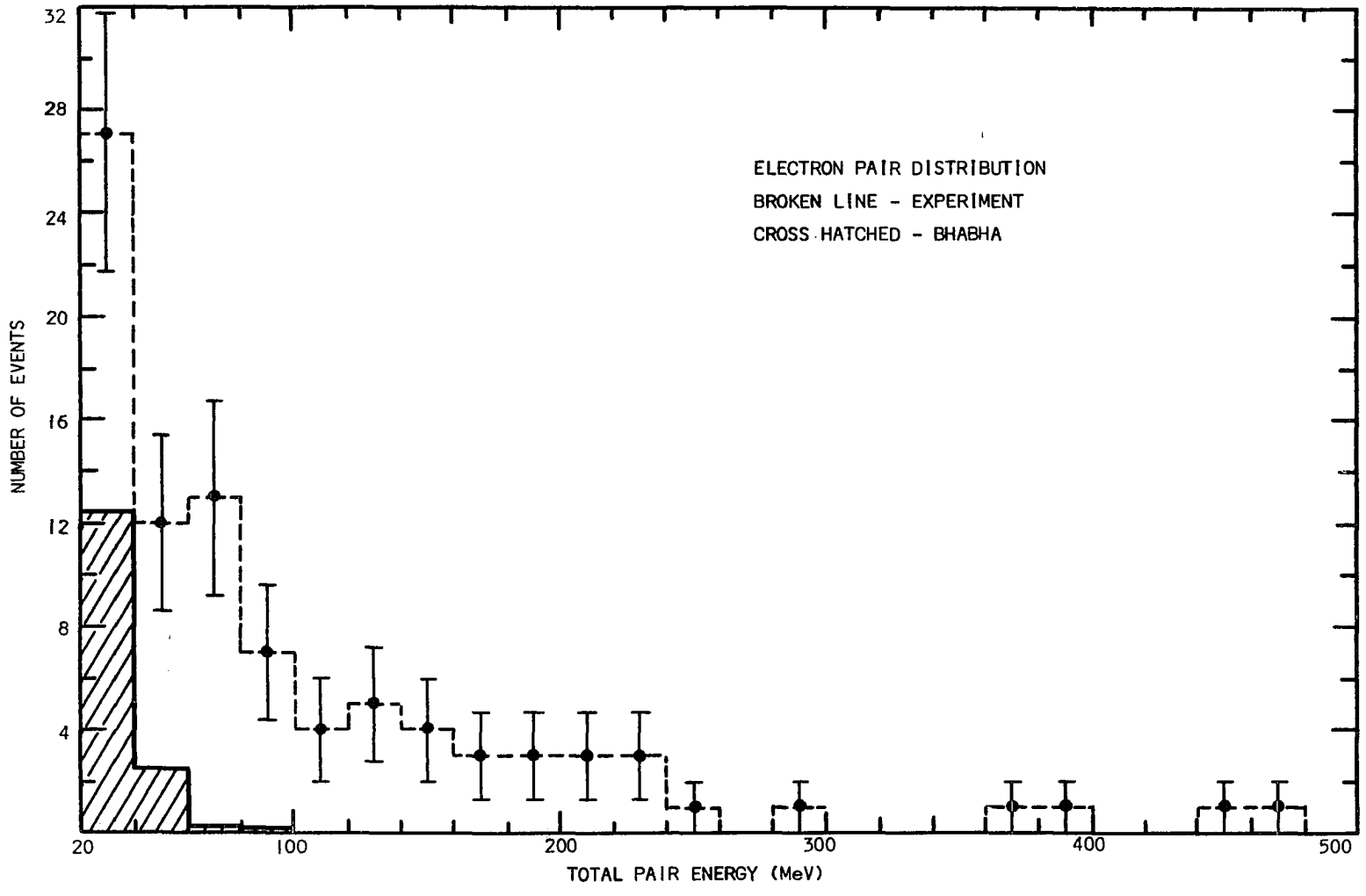

Fig. 45. Distribution of the total number of electron pairs per 20 MeV total pair energy found in 902.7 m. of track, with the number as predicted by Bhabha superposed ($\alpha_B = 1$).

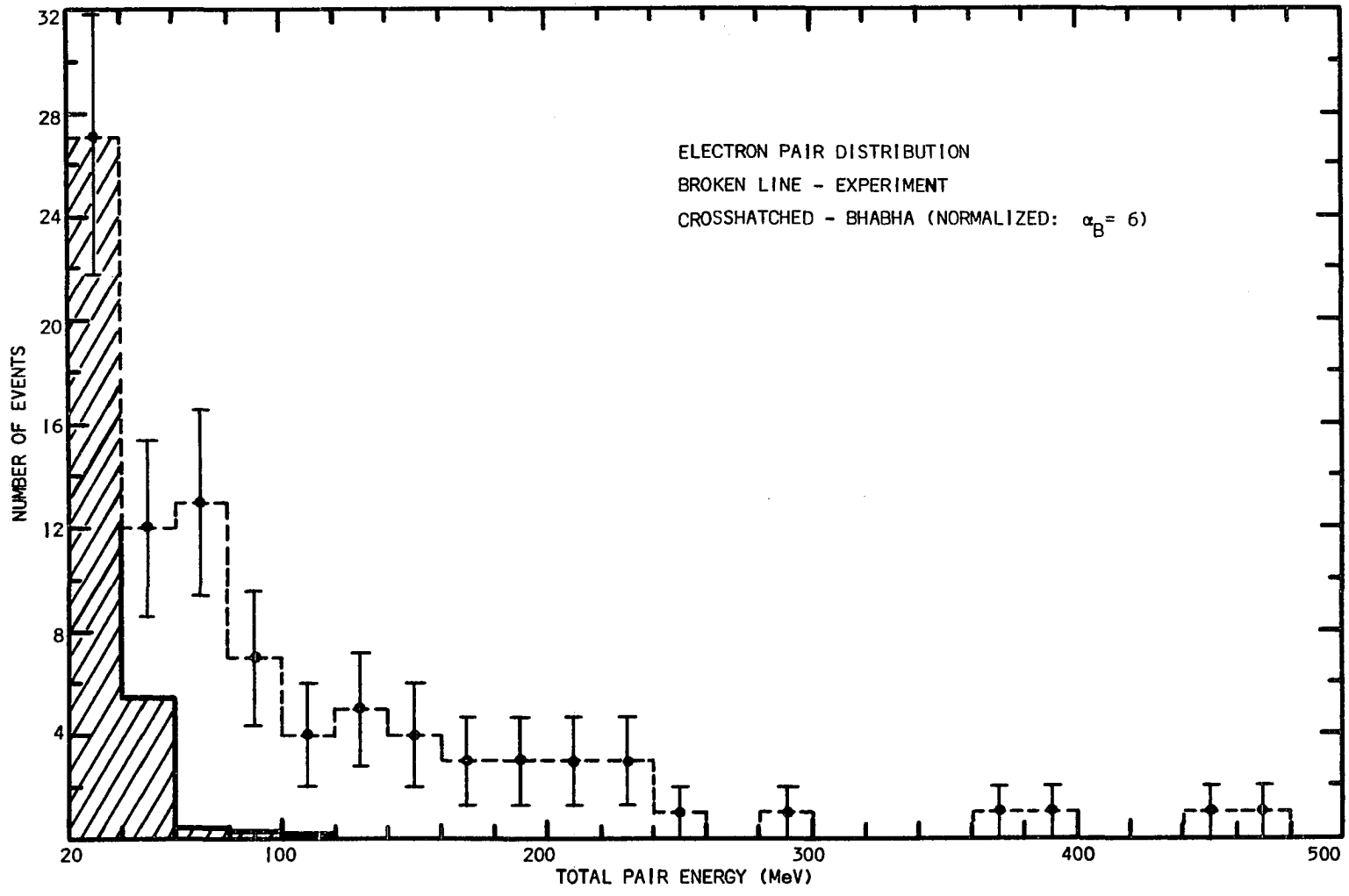

Fig. 46. Distribution of the total number of electron pairs per 20 MeV total pair energy found in 902.7 m. of track with the theoretical results of Bhabha, normalized to fit at low energies, superposed (α_B = 6).

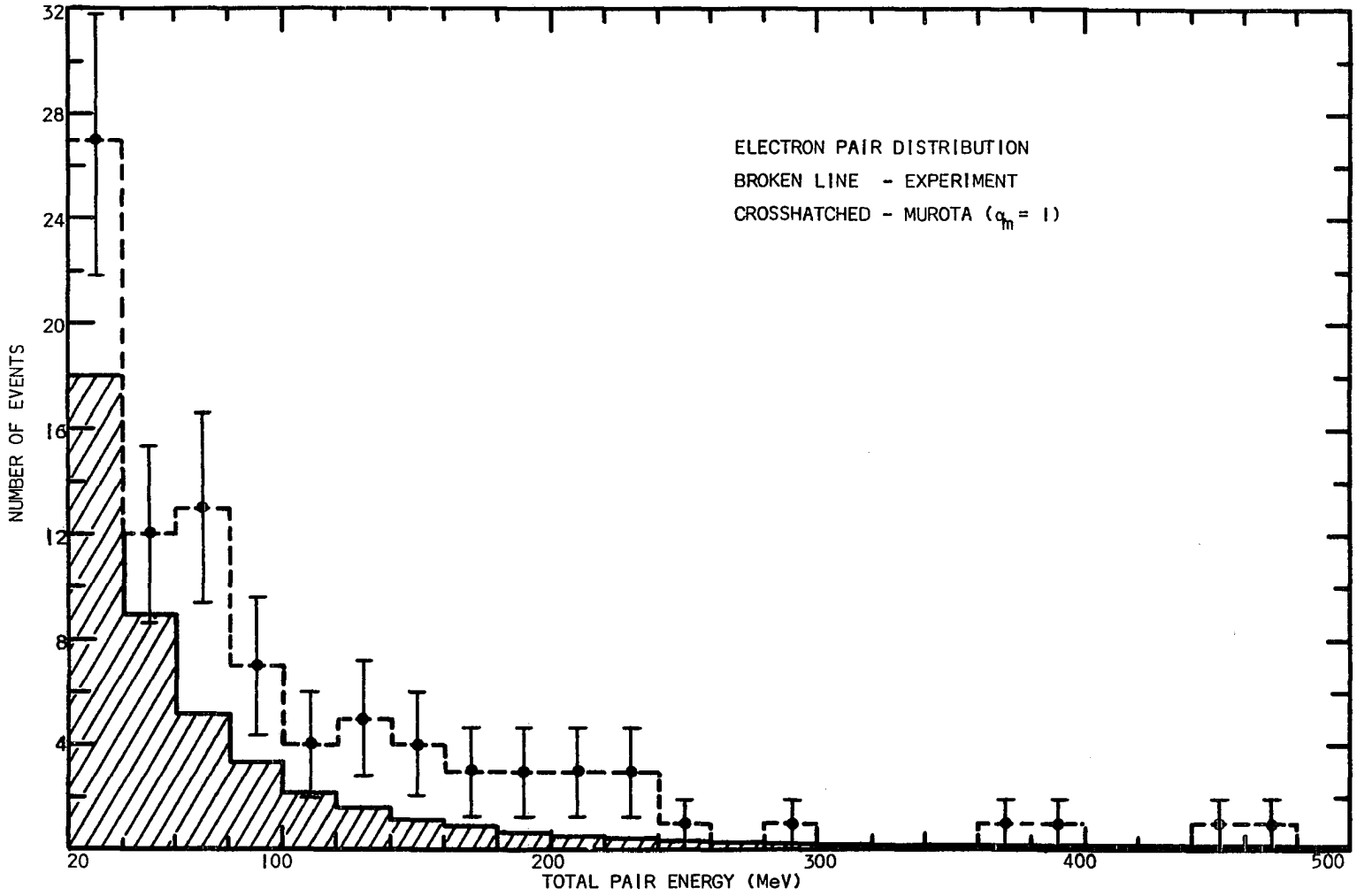

Fig. 47. Distribution of the total number of electron pairs per 20 MeV total pair energy found in 902.7 m. of track with the number predicted by Murota superposed (α_m = 1).

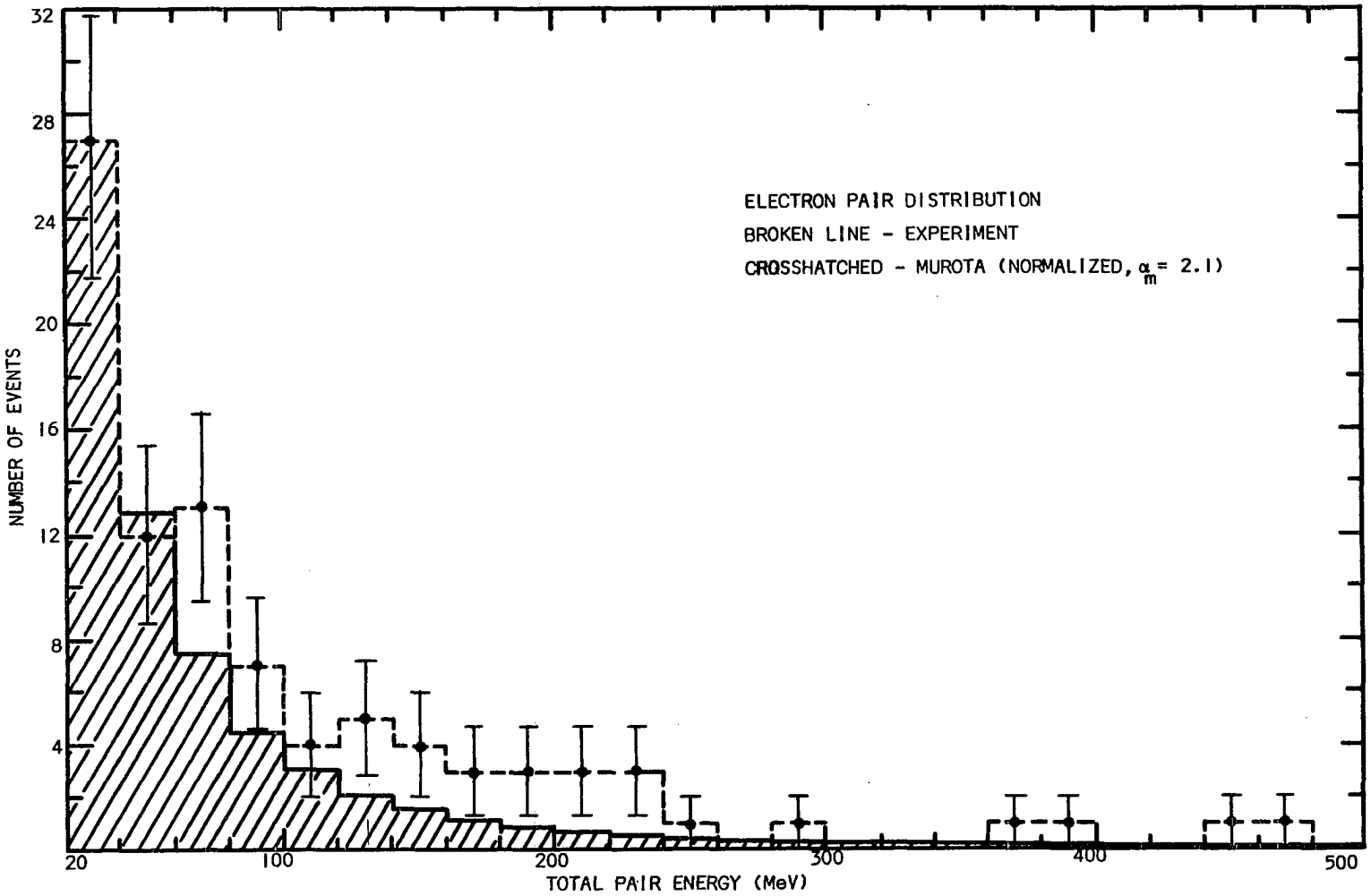

Fig. 48. Distribution of the total number of electron pairs per 20 MeV total pair energy found in 902.7 m. of track, with the theoretical result of Murota, normalized to fit at low energies, superposed (α_m = 2.1)

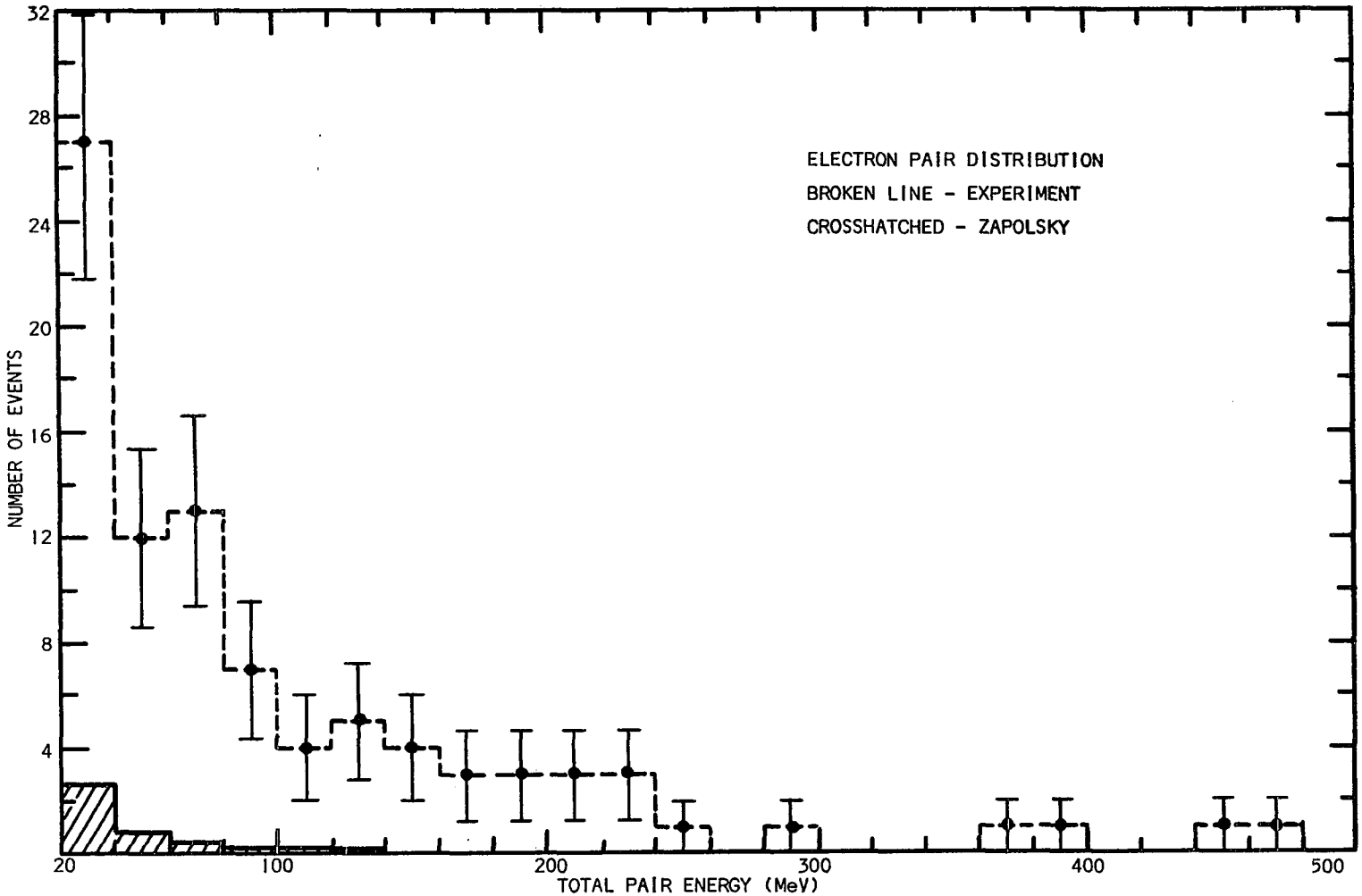

Fig. 49. Distribution of the total number of electron pairs per 20 MeV total pair energy found in 902.7 m. of track, with the number predicted by Zapolsky superposed.

the cross section for the direct production of high energy electron pairs as obtained theoretically by Ternovskii, explaining why the theory has been accepted as correct to this point. In Figures 50 and 51 are given the results of Evans et al. obtained in scanning a total of 393 m. of 16 BeV pion track in emulsion, with the theoretically expected results superposed (crosshatched). Cutoffs of K = K = 10 MeV and K = 20 MeV are used in these Figures. The value for y_{min} as suggested by Ternovskii (D = 1) was used in these Figures, as well as by Evans et al. in making the theoretical comparison. In Figure 52 are given the results of Mora, for a total of 244.5 m. of 16 BeV pion track, again with the results as predicted by Ternovskii superposed. It should be noted that the results of these two experiments are similar, having essentially all of the interactions with total energy less than 100 MeV.

The total cross sections for the production of electron pairs as obtained by Evans and by Mora, considering different values of the cutoff energy, are listed in Table 6. The total cross sections for various energy intervals are also listed. Corresponding theoretical results as predicted by Ternovskii and experimental results found in the present experiment, are also given in the Table. The corresponding mean free paths are tabulated. The value of $\langle Z^2 \rangle^{\frac{1}{2}}$ used in this work is 21.42, whereas the value used by Evans and Mora was 22.1. This causes ≈6.5% difference in the theoretical predictions since the cross section is proportional to $\langle Z^2 \rangle$.

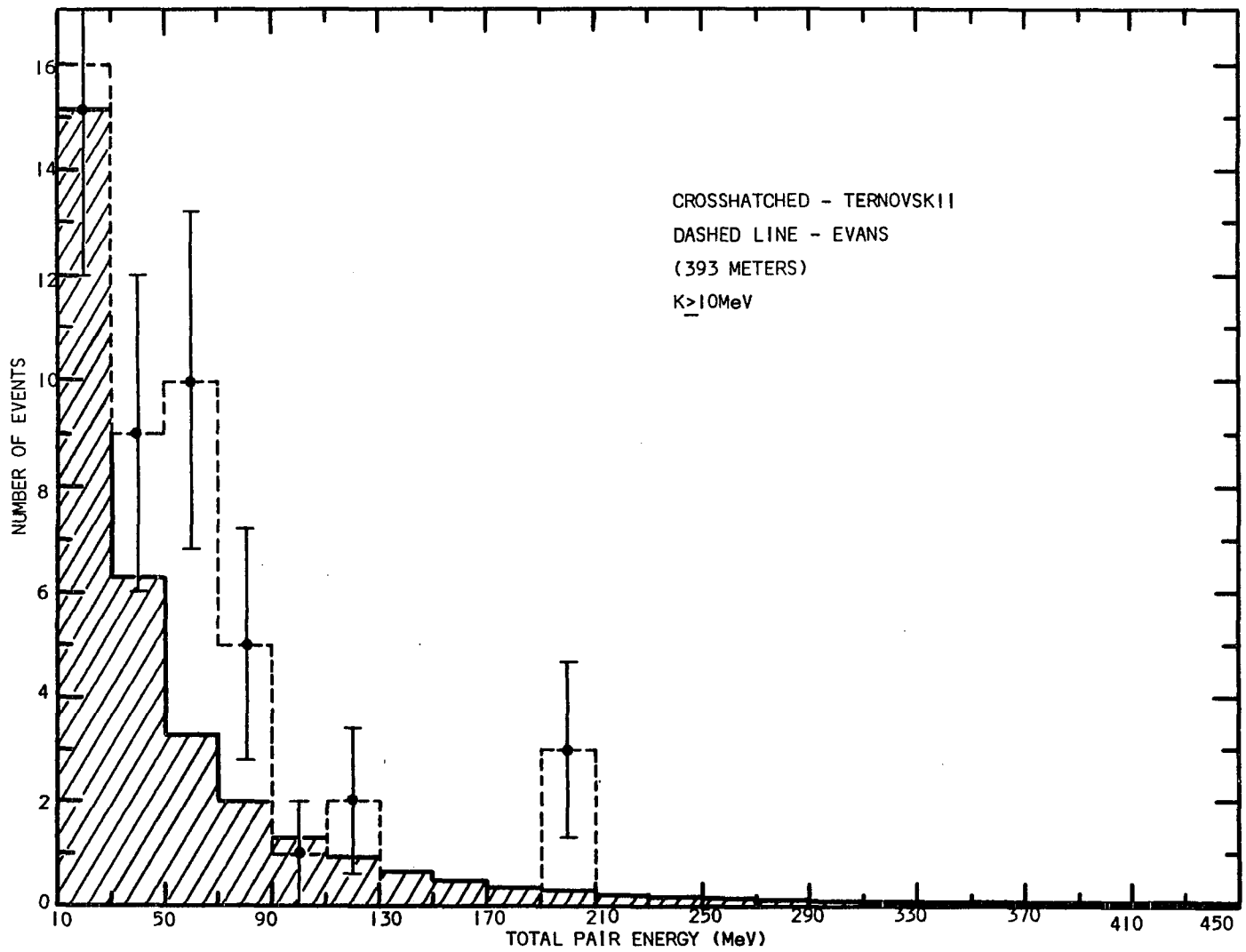

Fig. 50. Number of pairs predicted by Ternovskii per 20 MeV interval, cutoff at K = 10 MeV, superposed on the experimental results of Evans et al, found using 393 m. of 16 BeV pion track in emulsion.

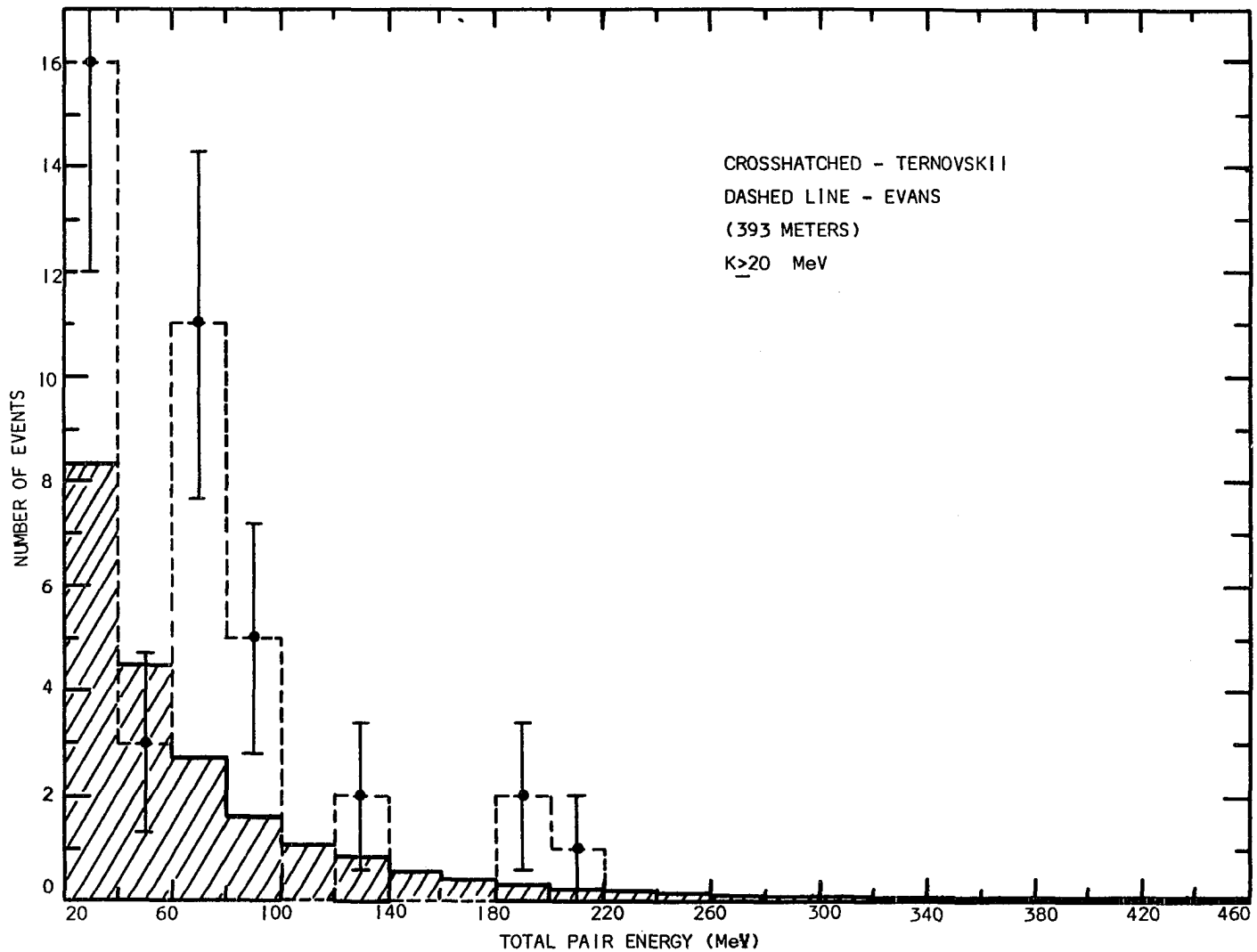

Fig. 51. Number of pairs predicted by Ternovskii per 20 MeV interval, cutoff at K = 20 MeV, superposed on the experimental results of Evans et al, for 393 m. of 16 BeV pion track in emulsion.

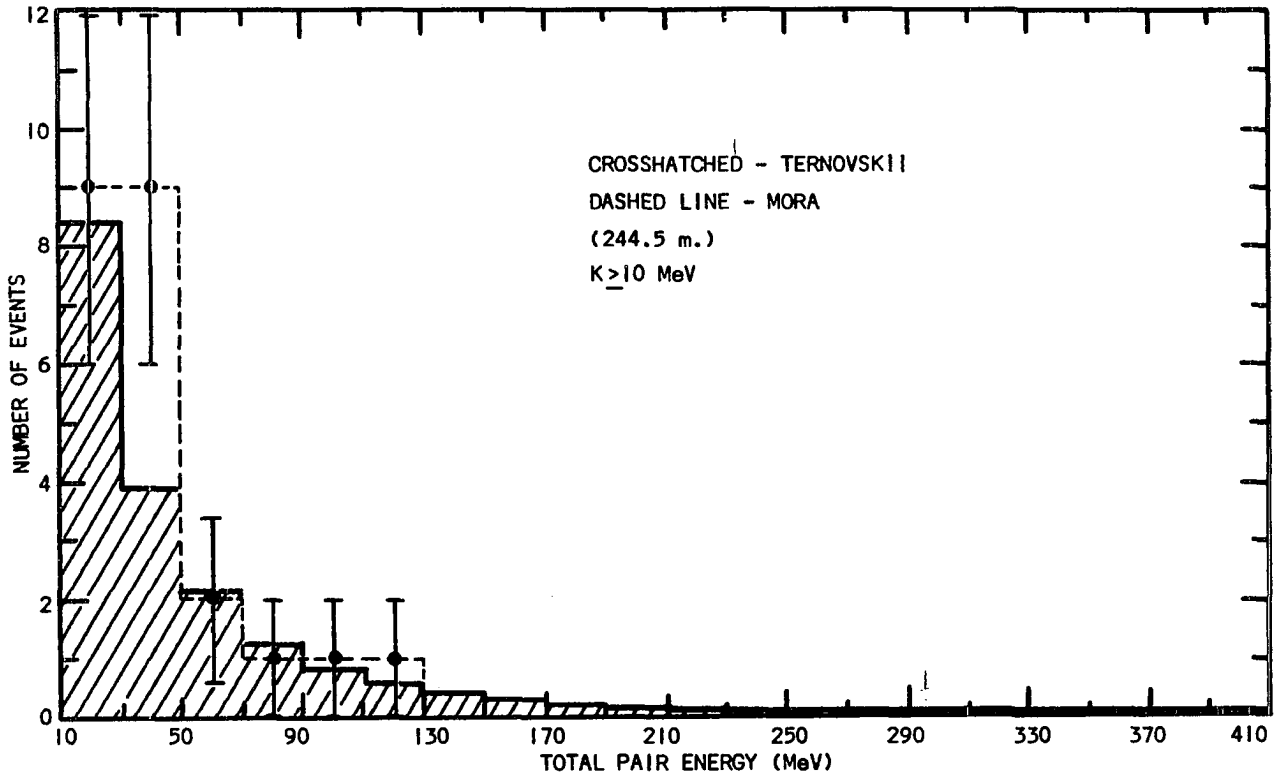

Fig. 52. Distribution of the number of pairs per 20 MeV interval found by Mora in 244.5 m. of tracks, with the number predicted by Ternovskii superposed.

Table 6 . Comparison of the present experiment with the previous experiments and theory.

Pair Energy Interval (MeV)	Ternovskii			Evans (393 m.)			Mora (244.5 m.)			Present Experiment (902.7 m.)	
	λ	σ	N	λ	σ	N	λ	σ	N	λ	σ
10-1000	12.2	10.4	47	8.4 ± 1.2	15.1±2.2	23	10.6± 2.2	12.0±2.5	99	9.1± .9	13.9±1.4
20-1000	17.3	7.3	40	9.8 ± 1.6	12.9±2.1				90	10.0±1.1	12.7±1.4
30-1000	22.9	5.5	31	12.7 ± 2.3	10.0±1.8	14	17.5± 4.7	7.2±1.9	75	12.0±1.4	10.6±1.2
40-1000	29.2	4.3	24	16.4 ± 3.3	7.7±1.6				63	14.3±1.8	8.9±1.1
50-1000	36.2	3.5	23	17.1 ± 3.6	7.4±1.6	5	48.9±21.9	2.6±1.2	58	15.6±2.0	8.1±1.0
60-1000	43.8	2.9	21	18.7 ± 4.1	6.9±1.5				51	17.7±2.5	7.2±1.0
80-1000	61.4	2.1	10	39.3 ±12.4	3.2±1.0				38	23.8±3.9	5.3± .87
100-1000	82.4	1.5	6	65.5 ±26.7	1.9± .8	2	122.3±86.4	1.0± .7	31	29.1±5.2	4.4± .8
120-1000	106.7	1.2	6	65.5 ±26.7	1.9± .8				27	33.4±6.4	3.9± .7
140-1000	134.9	.94	4	98.25±49.1	1.3± .6				24	37.6±7.7	3.4± .7

Conclusions

The experimental result for the total cross section for the production of electron pairs is th disagreement with the theoretical predictions. At low energies (<60 MeV total pair energy) theory and experiment agree, within statistical error. The discrepancy between predicted and experimental results increases as the total pair energy increases and becomes particularly large at high energies.

Of all the theoretical calculations considered, Ternovskii's result for pair production by high energy charged spin 0 particles agrees best with this experiment over the entire range of pair energies considered. The second type cross section of Ternovskii, σ_o, gives good agreement with experiment in region I (K<<60 MeV) as defined by Ternovskii, where it is expected to make the main cross section contribution (Figures 42, 43, and 44). In region II (K>>60 MeV), σ_o continues to make the main contribution to the cross section for all energies of interest. σ_c and σ_d remain negligible relative to σ_o over the entire energy range considered. Between regions I and II is the most interesting energy region experimentally. It is this region where experiment and theory disagree most strongly, as can be seen in Figures 42, 43, and 44 and in Tables 4 and 5.

As can be seen in these tables, there is reasonable agreement between Ternovskii's unnormalized result and experiment between 20 and 60 MeV total pair energies. Above 60 MeV there is a increasing fractional discrepancy with increasing K. The experimental total cross section is approximately a factor of three larger than the

theoretical results for $K \geq 80$ MeV. Normalization of this theoretical result (D = 1.48) to give a good fit at low energies (Figure 44) improves experimental agreement between 20 and 60 MeV, as is expected, but the disagreement at higher energies is largely unchanged. Due to the nature of the logarithmic term in which the normalization factor occurs, normalization has a decreasing fractional effect as K increases. It would be possible to normalize the theoretical results to give good agreement at a higher energy interval, but this would cause the theoretical cross section to be very much larger than experiment at low energies where the theory is expected to be most reliable. It should be noted again that Ternovskii does not actually include the possibility of normalization, although his arguments do not exclude the possibility of such normalization.

It is interesting to note that the rates of decrease of σ_d and σ_c are more comparable to the experimentally observed rate of decrease of the cross section than is that of σ_o. It is possible that cross section contributions from cross terms between the σ_o and the σ_d and σ_c matrix elements would be important in the lower energy region where theory and experiment disagree. Such cross terms have not been considered due to extreme calculational difficulties.

The cross section calculation of Murota *et al* for pair production by spin one-half charged particles is quite similar in shape to that of Ternovskii, but it is slightly smaller over the entire energy region of interest (Figures 42 and 47). However, this result includes an arbitrary constant to be determined by experiment but

which is thought to be approximately unity. As a result, this cross section can be made larger or smaller and is thus not necessarily different from that of Ternovskii. This constant occurs in a term quite similar to the term in Ternovskii's result in which the normalizing constant D was inserted. It should be noted again that the results for spin one-half particles are expected to give reliable predictions for spin 0 incident particles since the numerical cross sections for spin 0 and spin one-half particles are calcualted by Ternovskii are identical except at very low pair energies (<<20 MeV). Murota et al claim validity for this calculation in any energy region where the energies of the participating particles are all extremely relativistic. Thus, this result should be valid over the entire region of interest in this work if the calculation is correct. As can be seen from Figures 47 and 48, the unnormalized (α_m = 1) result gives a cross section which is lower than the experimental one over the entire energy region, but the normalized (α_m = 2.1) result gives a fit quite similar to that of the Ternovskii result. Tables 4 and 5 show the differences in the total cross sections for different energy intervals as predicted by Murota et al, and as determined experimentally. Again there is approximately a factor of three difference at energies $\geq$80 MeV. The normalized results of Murota et al, and of Ternovskii are seen to give almost the same results.

Bhabha's cross section for spin one-half primary particles is much smaller than the experimental results at all energies >40 MeV, as is seen from Figures 45 and 46. The normalized cross section

($\alpha_B = 6$, $\alpha' = 1$) gives agreement only in the energy interval used for normalization.

The cross section result of Zapolsky (Figure 49) gives no agreement with experiment.

It is of interest to compare the results of this experiment with those of the other two experiments which used high energy negative pions. All three were carried out in emulsion. The first such experiment was by Evans et al.[15] using 393 m. of 16.2 BeV pion track. Mora[16] later performed a similar experiment using 244.5 m. of 16.2 BeV pion track. Both employed a lower cutoff of 10 MeV total pair energy. As is mentioned above, it is felt that the cross section results in the present experiment aren't good below K = 20 MeV. The same reasoning probably applies to the other two experiments since Evans et al found fewer pairs between 10 and 20 MeV than between 20 and 30 MeV. Nevertheless, comparison will be made using this 10 MeV cutoff as well as higher cutoffs. The results of Evans et al and of Mora are given in Figures 50, 51, and 52, where they are compared to the unnormalized results of Ternovskii. Table 6 lists the experimental mean free paths and cross sections for all three experiments, along with the predicted mean free paths of Murota et al and of Ternovskii. From this table it is seen that the mean free paths for K≈10 MeV are comparable for all three experiments. However, considerable differences occur at larger values of K_{min}. Most of the events found by Evans et al, and by Mora seem to cluster below K = 100 MeV. The results of the present experiment show no such tendency.

Results of this experiment may be in error due to systematic errors in energy measurement. As was discussed above, careful analysis of possible errors and methods of energy measurement implied that there is a large probability for having measured energies of electrons to be within the error limits of or below their actual energies. All energies were also calculated using a different scattering equation as given by Barkas[22], with comparable results. Great care was taken in assuring the reliability of energy measurements. This tendency toward measured energies being lower than the actual energies produces better agreement between theory and experiment than would be obtained if the energies were increased. Thus, there is a possibility that the discrepancy between theory and experiment shown above should be larger.

The scanning efficiency corrections produce an even larger discrepancy between theory and experiment. Experimental results, corrected for 83% scanning efficiency and 3% error from coincidence pair effects, are given in Figure 43 where they are compared to the unnormalized results of Ternovskii.

These results indicate a definite need for a better theoretical calculation of the cross section for pair production by charged particles. Such a calculation should be made starting from first principles, with only necessary approximations being made. The approximations must be valid in the entire energy region of interest. Both types of Feynman diagrams (A + A' and B + B' in Figure 19), as well as cross terms between these diagrams, should be considered.

Only when a more reliable theoretical calculation is made can these results, or those of any other charged particle - pair production experiment, be used to say anything fundamental about the validity of quantum electrodynamics at extremely relativistic energies such as are involved in this experiment.

All theoretical calculations of the pair production cross section to date use assumptions about angular deflection of the primary particle, angles of emission of the pair particles, and transverse momenta of the particles involved. The coordinate systems used in calculations frequently involve unmeasurable angles and transverse momenta. The experimental distributions of these quantities, relative to the incident pion, are given in Figures 34, 35, and 53 (lab system). In order for these experimental results to be of assistance in making theoretical approximations, it will be necessary to make calculations in coordinate systems simply related to the lab system. Such approximations will probably always be made in any such calculation due to the extreme complexity of the task.

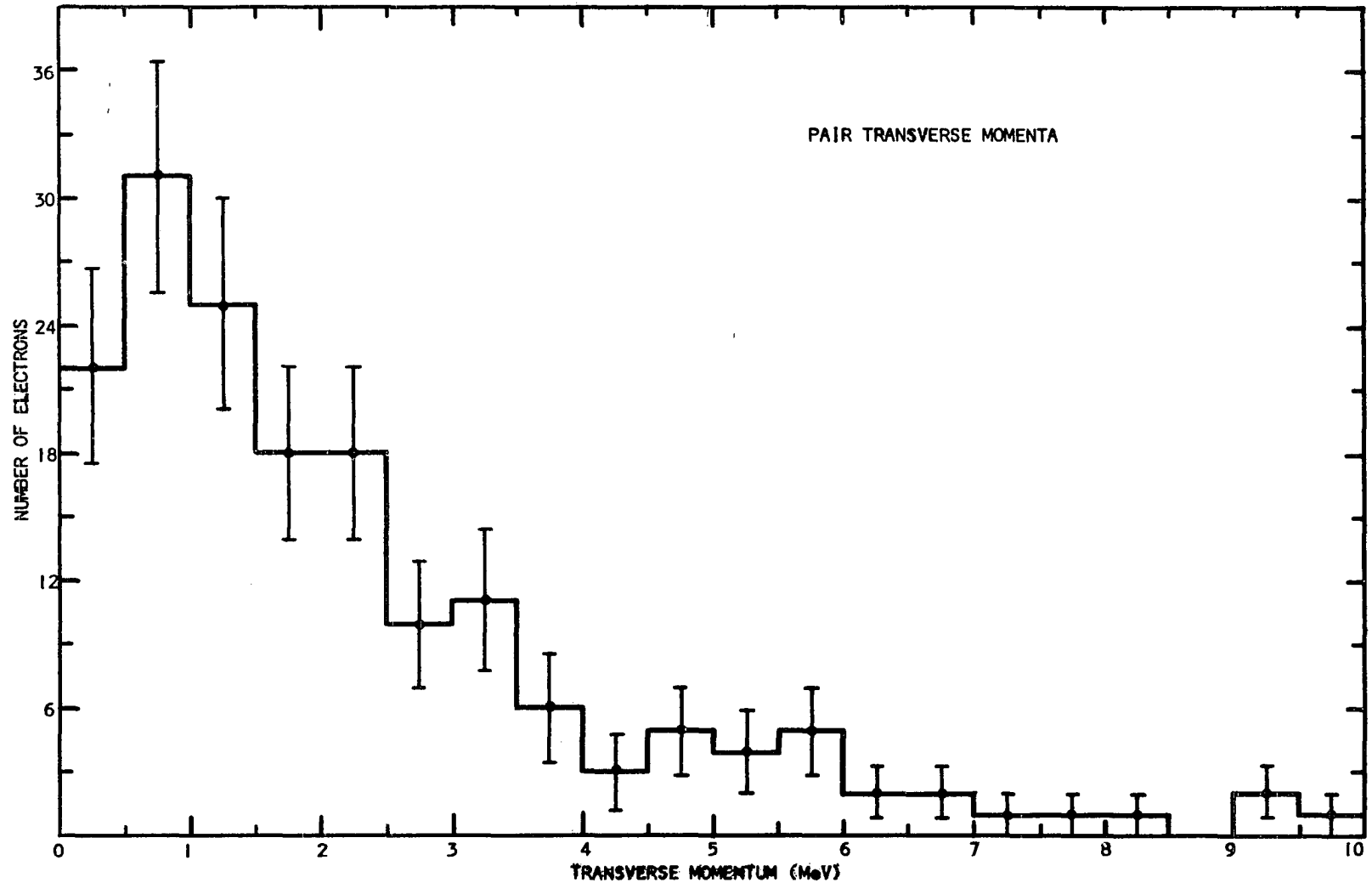

Fig. 53. Distribution of transverse momenta of secondary pair electrons and positrons per 0.5 MeV.

LIST OF REFERENCES

1. H. J. Bhabha, Proc. Roy. Soc. A164, 257 (1938).
2. H. Salecker, Z. Naturforschung 15a #12, 1023 (1960).
3. J. Allan, G. Ekspong, P. Sallstrom, and K. Fischer, N. Cim. 32, 1144 (1964).
4. L. Landau and E. Lifshitz, Phys. Zs. Sov. Un. 6, 244 (1934).
5. H. J. Bhabha, Proc. Roy. Soc. A152, 559 (1935).
6. E. J. Williams, Kgl. Dansk, Vid. Selskab 13 #4, (1935).
7. Y. Nishima, S. Tomanaga, and M. Kobayashi, Sci. Pap, Inst. Phys. Chem. Res. Tokyo 27, 137 (1935).
8. E. Stueckelberg, Helv. Acta, Phys. 8, 325 (1935).
9. G. Racah, N. Cim. 13, 66 (1936), 14, 93 (1937).
10. M. M. Block, D. T. King, and W. W. Wada, P. Rev. 96 #6, 1627 (1954).
11. T. Murota, A. Ueda, and H. Tanaka, Prog. Theor. Phys. 16 #5, 482 (1956).
12. J. D. Bjorken and S. D. Drell, P. Rev. 114, 1368 (1959).
13. F. F. Ternovskii, JETP 10 #3, 565 (1960).
14. H. S. Zapolsky, On the Theory of Pair Creation by Extremely Relativistic Charged Fermions: The Trident Process, Ph.D. Dissertation, Cornell U. (1962)
15. D. Evans, A. Hossain, F. M. Votruba, A. Wataghin, C. M. Fischer, A. Mason, W. Venus, V. Pelosi, L. Tallone, I. Ahmed, A. Ghani, M. M. Kasim, M. A. Shaukat, F. Baldassare, A. Caforio, and D. Ferraro, Aix-en-Provence Int. Conf. on Elem. Part. Vol. #1, 79 (1961).

16. S. Mora, C. Rendus. 256 #22, 4650 (1963).

17. N. N. Bogoliubov and D. V. Shirkov, Introduction to the Theory of Quantized Fields, (Interscience Publishers, Inc., New York, 1959).

18. J. D. Bjorken and S. D. Drell, Relativistic Quantum Mechanics (McGraw-Hill, New York, 1964).

19. K. E. Eriksson, N. Cim. 19 #15, 999, 1010, 1044 (1961).

20. B. Rossi, High Energy Particles (Prentice-Hall, New York, 1962).

21. Koshiba and Kaplon, P. Rev. 97, 193 (1955);

22. W. H. Barkas, Nuclear Research Emulsions (Academic Press, New York, 1963).

23. A. I. Achiezer and I. J. Pomerancuk, Fortschritte der Phys. 7, 102 (1959).

24. M. Avan and L. Avan, N. Cim. 6, 1590 (1957); Roe and Ozaki, P. Rev. 116, 1022 (1959).

25. J. Hooper, D. King and A. Moorish, Phil. Mag. 42, 304 (1951).

26. C. Piron, M. Gailloud, P. Rosselet and M. Biasutti, Helv. Phys. Acta. 33, 945 (1960).

27. C. A. Oleson, Effective Target Mass in Pion-Proton Interactions, (Master's Thesis, Oklahoma University, 1966).

28. J. R. Burwell, Proceedings of the VI International Conference on Corpuscular Photography, 1966 (to be published)